HEINRICH HEINE
UNIVERSITÄT DÜSSELDORF

NMR solution structures of the MloK1 cyclic nucleotide-gated ion channel binding domain

Inaugural-Dissertation

zur

Erlangung des Doktorgrades

der Mathematisch-Naturwissenschaftlichen Fakultät

der Heinrich-Heine-Universität Düsseldorf

vorgelegt von

Sven Schünke

aus Solingen

Juni 2010

Aus dem Institute of Complex Systems (ICS)
Strukturbiochemie (ICS-6) im Forschungszentrum Jülich
und dem Institut für Physikalische Biologie
der Heinrich-Heine-Universität Düsseldorf

Gedruckt mit der Genehmigung der
Mathematisch-Naturwissenschaftlichen Fakultät
der Heinrich-Heine-Universität Düsseldorf

Referent: Prof. Dr. Dieter Willbold
Koreferent: Prof. Dr. Lutz Schmitt
Tag der mündlichen Prüfung: 25.06.2010

Contents

List of Figures

List of Tables

Chapter 1

Introduction

1.1 First structural insights about cyclic nucleotide-binding domains

Cyclic nucleotides, like cAMP and cGMP, have prominent roles in the fields of physiology and cellular signal transduction. Cyclic nucleotides mediate cellular responses to hormones and other stimuli and many receptor proteins of cyclic nucleotides have been identified. The first structure of a cyclic nucleotide-binding domain (CNBD) was solved in 1981 when the crystal structure of the catabolic gene activator protein (CAP) was reported (McKay & Steitz 1981). The structure revealed a β roll topology comprised of eight antiparallel aligned β strands and six α helices, whereas one of these helices covered the cAMP-binding site. The catabolic activated protein serves as a bacterial transcription factor and was identified due to the capability to bind cAMP. CAP binds DNA in the presence of cAMP and is involved in *lac operon* regulation.

The first crystal structure of a regulatory subunit of protein kinase A (PKA) was obtained by Susan Taylor and co-workers (Su et al. 1995). The binding of cAMP stimulates PKA, that controls the activity of proteins through phosphorylation. PKA is one of the most important signaling component in the cell. This structure, as well as further resolved structures of PKA (Diller et al. 2001; Kim et al. 2005), guanine nucleotide-exchange factor that is directly activated by cAMP (Epac; Rehmann et al. 2003; Rehmann et al. 2006), and cyclic nucleotide-activated ion channels (Zagotta et al. 2003; Clayton et al. 2004) confirmed that the β roll topology is highly conserved. In addition, a short α helical region of conserved residues, designated as phosphate binding cassette (PBC), could be observed. This PBC helix is directly involved in the binding of cyclic-nucleotides. Furthermore, in all CNBD structures an α helix, designated as hinge helix, was observed, which changes its position relative to the α roll upon

binding of cyclic nucleotides. The hinge helix is followed by another C-terminal helix. In particular, this helix region shows the greatest variation between individual CNBDs. Thus, it provides a conserved function and interacts with the base of the bound cyclic nucleotide, thereby covering the binding pocket like a 'lid', stabilizing the bound cyclic nucleotide and shielding it from the solvent. Even though these proteins mediate diverse biological functions, they all harbour a conserved cyclic nucleotide-binding domain, that binds cAMP or cGMP, and mediates the activity of these proteins.

1.2 Cyclic nucleotide-activated ion channels

Ion channels activated by cyclic nucleotides play key roles in neuronal excitability and sensory signaling. They belong to two subfamilies: Cyclic nucleotide-gated (CNG) channels, and hyperpolarization-activated and cyclic nucleotide-gated (HCN) channels (Kaupp & Seifert 2001; Kaupp & Seifert 2002; Robinson & Siegelbaum 2003). Both channel types belong to the superfamily of voltage-gated channels. CNG channels require cyclic nucleotides to open and are only weakly voltage dependent, whereas HCN channels are activated by hyperpolarization and their activity is modulated by cyclic nucleotides (Kaupp et al. 1989; DiFrancesco & Tortora 1991). Both HCN and CNG channels consist of four subunits, arranged as tetrameric structures (**Fig. 1.1**). In mammalian CNG channels four different A and two different B subunits have been identified (Kaupp & Seifert 2002). The CNG channel from rod photoreceptor cells is composed of three A1 subunits and one B1a subunit (Weitz et al. 2002); the channel from cone photoreceptor cells consists of two A3 and B3 subunits (Peng et al. 2004), and the channel from olfactory sensory neurons consists of two A2 subunits, one A4, and one B1b subunit (Zheng & Zagotta 2004). Four homologous HCN channel subunits have been identified in mammals, forming four different homotetramers with distinct biophysical properties (HCN1-4). However, it is commonly believed that the number of potential HCN channel types is increased by the formation of heterotetramers *in vivo* (Chen et al. 2001; Altomare et al. 2003; Much et al. 2003; Ulens & Tytgat 2001; Whitaker et al. 2007). Each of the four subunits consists of six transmembrane-spanning regions (S1-S6), followed by a C-linker region, and a C-terminal cyclic nucleotide-binding domain (CNBD). The CNBD is directly connected to S6 by the C-linker ($\sim$80 amino acids). The C-linker regions of CNG and HCN channels show sequence homology to each other. Furthermore, functional and structural studies suggest that the C-linker contributes to the contacts between channel subunits and promotes tetramerization (Zagotta et al. 2003; Zhou et al. 2004; Craven & Zagotta 2006). In the crystal structure of the mammalian HCN2 channel CNBD, the C-linker consists of six α helices (designated A' to F') and virtually all of the contacts between the tetrameric arrangement of the CNBDs

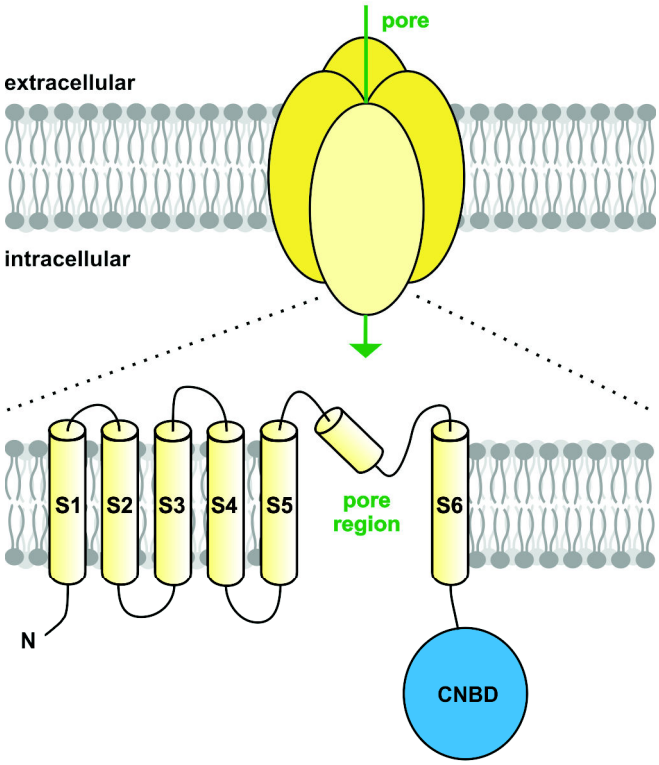

Figure 1.1: Subunit topology of a cyclic nucleotide-regulated ion channel. The channel consists of four subunits and each subunit encompasses six transmembrane segments S1-S6 (yellow). The intracellular cyclic nucleotide-binding domain (CNBD) is connected by a C-linker to the last transmembrane segments S6.

occur due to C-linker regions A' and B' of one with C' and D' of the neighbouring subunit (Zagotta et al. 2003). Thus, the C-linker seems to be an important part for the allosteric mechanism of HCN and CNG channel activation. HCN and CNG channels are activated by binding of cyclic nucleotides to their intracellular cyclic nucleotide-binding domain (CNBD). In both channels ligand binding to the CNBD promotes the opening of the channel, probably by propagating a conformational change from the CNBD to the pore. However, the mechanism that is underlying activation is only poorly understood.

1.3 The MloK1 cyclic nucleotide-gated ion channel

In addition to HCN and CNG channels, several members of prokaryotic channels activated by cyclic nucleotides have been identified so far. One member represents the prokaryotic K^+ selective CNG channel, designated MloK1, and has been identified in *Mesorhizobium loti* (Nimigean et al. 2004; Nimigean & Pagel 2007). The prokaryotic channels share several key

features with classical CNG channels: The MloK1 channel forms homotetramers, each subunit encompasses six transmembrane segments, a 'GYGD' signature sequence for K^+ selectivity (Heginbotham et al. 1994), and a C-terminal CNBD. Moreover, unlike the mammalian CNG channels, the CNBD is connected via a short C-linker ($\sim$20 residues) to transmembrane helix S6 (Nimigean et al. 2004). Crystal structures of the MloK1 CNBD revealed a dimeric arrangement and the dimer interface formed by the short C-linker has been proposed to be involved in channel gating (Clayton et al. 2004; Altieri et al. 2008). However, in a structure revealed by electron microscopy of the full-length MloK1 channel in presence of cAMP the CNBDs appear as independent domains separated by discrete gaps, suggesting that CNBDs are not interacting with each other (Chiu et al. 2007). Four isolated CNBDs could be modelled into the electron density map. Furthermore, ligand-binding studies show that the MloK1 channel as well as the monomeric CNBD bind to cAMP with similar affinity in a non-cooperative manner (Cukkemane et al. 2007), suggesting that the MloK1 CNBDs are functionally independent of each other. The fourfold symmetry of the MloK1 channel was confirmed by a high-resolution structure of the transmembrane domains (Clayton et al. 2008). However, the CNBD could not be resolved in that structure.

Chapter 2

Aims

To elucidate the mechanism of cyclic nucleotide-channel gating, knowledge of the structure of ligand-free and ligand-bound cyclic nucleotide-binding domains is required. The key objective of this study is to determine the solution structures of wildtype MloK1 cyclic nucleotide-binding domain with and without cAMP by nuclear magnetic resonance (NMR) spectroscopy. The structural differences between the liganded and unliganded state of the CNBD should be characterized. The cAMP molecule shows high affinity ($K_D = 107$ nM) to the CNBD protein (Cukkemane et al. 2007). This, in turn, results in co-purification of cAMP with the protein, and even extensive dialysis fails to remove cAMP to obtain pure cAMP-free protein samples in previous studies (Clayton et al. 2004; Cukkemane et al. 2007; Altieri et al. 2008). In this context an appropriate procedure needed to be established to prepare cAMP-free CNBD protein samples in quantities sufficient for structure determination by NMR spectroscopy.

Chapter 3

Scientific publications

In the following scientific publications that have emerged in the context of this thesis I have the following share:

3.1. Schünke S., Novak K., Stoldt M., Kaupp U.B., and Willbold D.
Resonance assignment of the cyclic nucleotide binding domain from a cyclic nucleotide-gated K^+ channel in complex with cAMP.
Biomol NMR Assign (2007), **1**: 179-181.
Complete execution of experimental procedures, data evaluation and 95 % of the manuscript

3.2. Schünke S., Stoldt M., Novak K., Kaupp U.B., and Willbold D.
Solution structure of the *Mesorhizobium loti* K1 channel cyclic nucleotide-binding domain in complex with cAMP.
EMBO reports (2009), **10**: 729 - 735.
Complete execution of experimental procedures, data evaluation and 90 % of the manuscript

3.3. Schünke S., Lecher J., Stoldt M., Kaupp U.B., and Willbold D.
Resonance assigments of the nucleotide-free wildtype MloK1 cyclic nucleotide-binding domain.
Biomol NMR Assign (2010), **4**: 147-150.
Complete execution of experimental procedures, data evaluation and 95 % of the manuscript

3.4. Schünke S., Stoldt M., Lecher J., Kaupp U.B., and Willbold D.
Structural insights into conformational changes of *Mesorhizobium loti* K1 channel cyclic nucleotide-binding domain in solution.
Proc Natl Acad Sci U S A (2011), **108**: 6121-6126.
Complete execution of experimental procedures, data evaluation and 90 % of the manuscript

3.1 Resonance assignment of the cyclic nucleotide binding domain from a cyclic nucleotide-gated K^+ channel in complex with cAMP

published in: ***Biomolecular NMR Assignments***
Vol. 1, Issue 2, December 2007, Pages: 179-181

Sven Schünke[1,3], Kerstin Novak[2], Matthias Stoldt[1,3], U. Benjamin Kaupp[2] and Dieter Willbold[1,3]

[1,2]Institut für Neurowissenschaften und Biophysik [1](INB-2), [2](INB-1),
Forschungszentrum Jülich,
52425 Jülich,
Germany

[3]Institut für Physikalische Biologie,
Heinrich-Heine-Universität,
40225 Düsseldorf,
Germany

Biomol NMR Assign (2007) 1:179–181
DOI 10.1007/s12104-007-9049-5

ARTICLE

Resonance assignment of the cyclic nucleotide binding domain from a cyclic nucleotide-gated K^+ channel in complex with cAMP

Sven Schünke · Kerstin Novak · Matthias Stoldt · U. Benjamin Kaupp · Dieter Willbold

Received: 1 July 2007 / Accepted: 27 August 2007 / Published online: 8 September 2007

Abstract In order to determine the structure of the 15 kDa cyclic nucleotide binding domain of a cyclic nucleotide-activated K^+ channel from *Mesorhizobium loti* and its interaction with cAMP, nearly complete ^1H, ^{13}C, and ^{15}N chemical shifts were assigned.

Keywords Ion channel · Cyclic nucleotide binding domain · Heteronuclear NMR · Resonance assignment · cAMP

Biological context

Ion channels activated by cyclic nucleotides are widely distributed throughout eukaryotes, play key roles in signal transduction of sensory neurons and neuronal excitability and belong to two subfamilies: Cyclic nucleotide-gated (CNG) channels and hyperpolarization-activated and cyclic nucleotide-gated (HCN) channels (Kaupp and Seifert 2002). Whereas HCN channels are activated by voltage and CNG channels are virtually voltage independent, both channels are activated by cyclic nucleotide binding (cAMP and cGMP) to an intracellular cyclic nucleotide binding domain (CNBD), which is connected by a C-linker to the transmembrane core. Ligand binding favors the open state in both channels, potentially owing to a conformational change in the CNBD, which may be conferred to the pore. The mechanistic details that underlie nucleotide activation of CNBDs are not fully understood.

We have initiated the structural characterization in solution of an isolated cyclic nucleotide binding domain from *Mesorhizobium loti* which is homologous to eukaryotic CNBDs. The CNBD is a 15 kDa (142 aa) monomeric single-chain protein. Here, we report the ^1H, ^{13}C, ^{15}N sequence-specific backbone and side chain resonance assignment of the CNBD in complex with cAMP.

Methods and experiments

For protein expression of recombinant *M. loti* CNBD as a GST-fusion protein, DNA encoding the whole CNG-channel (*ml*CNG) was amplified from genomic DNA. The coding region for residues 216–355 of *ml*CNG protein was cloned into pGEX-2T (Amersham Biosciences) and verified by DNA sequencing. DNA was transformed into *E. coli* (BL21 (DE3) pLysE) cells, which were grown in M9 media at 37°C ([^{15}N]-ammonium chloride and [^{13}C]-glucose were used as isotope sources). Overnight expression (25°C) was induced at an A_{600} of about 0.6 with 0.5 mM IPTG. Cells were lysed by sonication in 1× PBS lysis buffer containing DNaseI (30 μg/ml) and protease inhibitor cocktail tablets ("Complete Mini," Roche, Germany). After centrifugation, supernatant was prepurified by affinity-chromatography on glutathione-Sepharose 4B column (Amersham Biosciences), followed by incubation with thrombin for cleavage of the CNBD from the GST-tag overnight. Cleaved protein was eluted and subsequently

S. Schünke · M. Stoldt · D. Willbold (✉)
Institut für Neurowissenschaften und Biophysik (INB-2), Forschungszentrum Jülich, 52425 Jülich, Germany
e-mail: d.willbold@fz-juelich.de

K. Novak · U. B. Kaupp
Institut für Neurowissenschaften und Biophysik (INB-1), Forschungszentrum Jülich, 52425 Jülich, Germany

M. Stoldt · D. Willbold
Institut für Physikalische Biologie, Heinrich–Heine-Universität, 40225 Düsseldorf, Germany

purified by size-exclusion chromatography on a Superdex-75 column (Amersham Biosciences). The CNBD is reported to show high affinity (K_D = 107 nM) for cAMP (Cukkemane et al. 2007). Therefore, the saturation of CNBD with cAMP was close to 100%. Resonances arising from cAMP-free CNBD were not observed.

The NMR sample contained 0.5 mM uniformly [*U*-^{15}N, ^{13}C] labeled CNBD with an equivalent amount of cAMP in aqueous solution (10 mM potassium phosphate (pH 7), 100 mM potassium chloride, 100 µM EDTA, 5% (v/v) $^{2}H_2O$, and 0.02% (v/v) sodium azide).

NMR experiments were performed at 25°C on a Varian ^{Unity}INOVA instrument, equipped with a cryogenic Z-axis PFG triple resonance probe at a proton frequency of 800 MHz. Resonance assignment was accomplished using the following experiments: 2D (^{1}H-^{15}N)-HSQC, 2D ct-(^{1}H-^{13}C)-HSQC, 3D HNCACB, HNCO, HNHA, H(C)CH-COSY, H(C)CH-TOCSY (14 ms mixing time), (^{1}H-^{13}C-^{1}H)-HSQC-NOESY (100 ms mixing time) and (^{1}H-^{1}H-^{15}N)-NOESY-HSQC (120 ms mixing time). Aromatic side chain resonances were assigned using aromatic 2D (^{1}H-^{13}C)-HSQC and 3D (^{1}H-^{13}C-^{1}H)-HSQC-NOESY (140 ms mixing time) experiments. Decoupling of ^{15}N and ^{13}C nuclei during proton acquisition has been performed by application of GARP and adiabatically by WURST sequences. DIPSI-2 isotropic mixing scheme was used during TOCSY-^{13}C spin lock periods. Solvent suppression was achieved by WATERGATE technique. ^{1}H chemical shifts were referenced directly to DSS at 0 ppm and ^{13}C and ^{15}N shifts were referenced indirectly to DSS, using the absolute frequency ratios.

All NMR data were processed using NMRPipe (Delaglio et al. 1995) and evaluated with CARA (Keller 2004) software.

Assignments and data deposition

Interpretation of the triple resonance spectra lead to sequence-specific assignments of 99% of the backbone (excluding ^{15}N resonances and ^{13}C′ resonances of the predecessor residues correlated with the 9 proline residues)

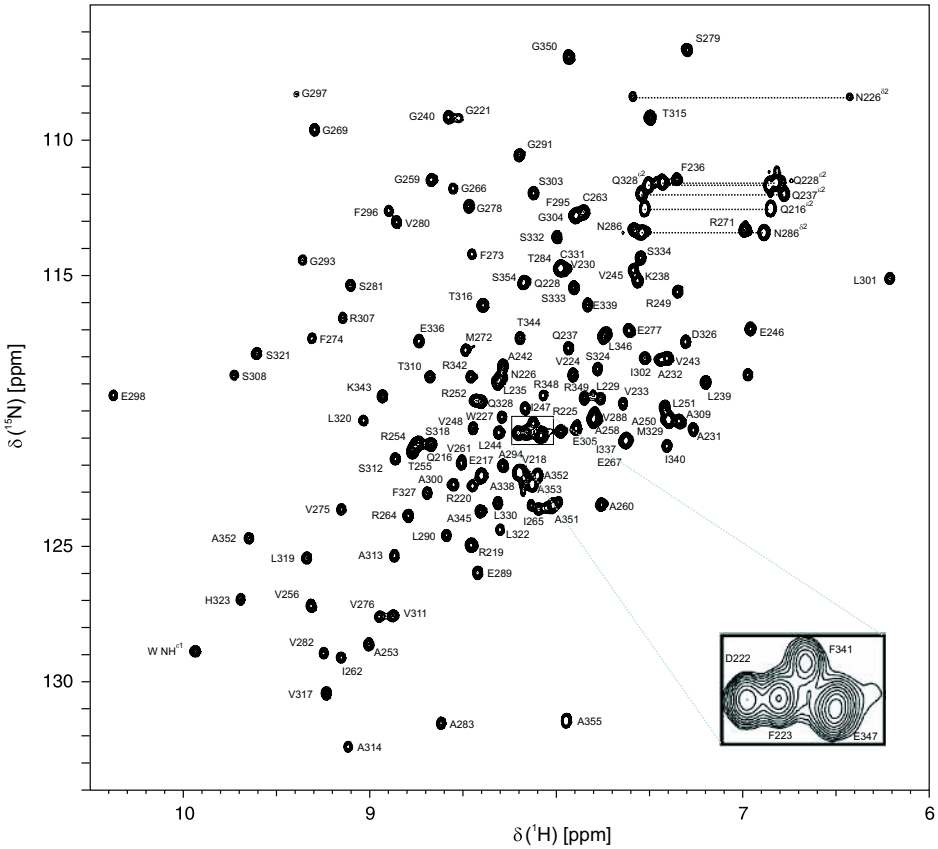

Fig. 1 2D (^{1}H-^{15}N)-HSQC spectrum of [*U*-^{15}N, ^{13}C]-labeled cyclic nucleotide binding domain from *M. loti* in complex with cAMP (protein concentration = 0.5 mM, T = 298 K, pH 7, 95% H_2O/5% $^{2}H_2O$) recorded at 800 MHz. Backbone resonance assignments are indicated by one-letter amino acid code and the sequence number. The side chain amide groups of asparagine and glutamine residues are connected by horizontal lines. Amide resonances of the residues S215 and D270 could not be found in the 2D (^{1}H-^{15}N)-HSQC spectrum

and 94% of the aliphatic and aromatic side chain amide, carbon and proton resonances (excluding ^{1}H-^{15}N and ^{15}N of Lys and Arg, OH, side chain ^{13}C′, $^{13}C^{\zeta}$, and aromatic quaternary ^{13}C), respectively. In particular, amide resonances of the residues S215 and D270 were not found in the 2D (^{1}H-^{15}N)-HSQC (Fig. 1). Secondary structure prediction based on obtained C^{α}, C^{β}, C′, and H^{α} chemical shifts by chemical shift index (Wishart and Sykes 1994) lead to the prediction of five α-helical and six β-strand segments longer than three residues. The resonance assignment of ^{1}H, ^{13}C, ^{15}N backbone and side chain chemical shifts has been deposited at BioMagResBank (www.bmrb.wisc.edu) under accession number 15249.

References

Cukkemane A, Grüter B, Novak K, Gensch T, Bönigk W, Gerharz T, Kaupp UB, Seifert R (2007) Subunits act independently in a cyclic nucleotide-activated K^{+} channel. EMBO Rep 8:749–755

Delaglio F, Grzesiek S, Vuister GW, Zhu G, Pfeifer J, Bax A (1995) NMRPipe: a multidimensional spectral processing system based on UNIX pipes. J Biomol NMR 6:277–293

Kaupp UB, Seifert R (2002) Cyclic nucleotide-gated ion channels. Physiol Rev 82:769–824

Keller R (2004) The computer aided resonance assignment tutorial. CANTINA, Zurich, Switzerland

Wishart DS, Sykes BD (1994) The 13C chemical-shift index: a simple method for the identification of protein secondary structure using 13C chemical-shift data. J Biomol NMR 4:171–180

3.2 Solution structure of the *Mesorhizobium loti* K1 channel cyclic nucleotide-binding domain in complex with cAMP

published in: ***EMBO reports***
Vol. 10, Issue 7, July 2009, Pages: 729-735

Sven Schünke[1,2], Matthias Stoldt[1,2], Kerstin Novak[3], U. Benjamin Kaupp[3,4] and Dieter Willbold[1,2]

[1]Institut für Strukturbiologie und Biophysik,
Strukturbiochemie (ISB-3),
Forschungszentrum Jülich,
52425 Jülich,
Germany

[2]Institut für Physikalische Biologie,
Heinrich-Heine-Universität,
40225 Düsseldorf,
Germany

[3]Institut für Strukturbiologie und Biophysik,
Zelluläre Biophysik (ISB-1),
Forschungszentrum Jülich,
52425 Jülich,
Germany

[4]Center for Advanced European Studies and Research (caesar),
Molekulare Neurosensorik,
53175 Bonn,
Germany

EMBO reports

scientific report

Solution structure of the *Mesorhizobium loti* K1 channel cyclic nucleotide-binding domain in complex with cAMP

Sven Schünke[1,2], Matthias Stoldt[1,2], Kerstin Novak[3], U. Benjamin Kaupp[3,4] & Dieter Willbold[1,2+]

[1]Institut für Strukturbiologie und Biophysik, Strukturbiochemie (ISB-3), Forschungszentrum Jülich, Jülich, Germany, [2]Institut für Physikalische Biologie, Heinrich-Heine-Universität, Düsseldorf, Germany, [3]Institut für Strukturbiologie und Biophysik, Zelluläre Biophysik (ISB-1), Forschungszentrum Jülich, Jülich, Germany, and [4]Center for Advanced European Studies and Research (caesar), Molekulare Neurosensorik, Bonn, Germany

Cyclic nucleotide-sensitive ion channels, known as HCN and CNG channels, are crucial in neuronal excitability and signal transduction of sensory cells. HCN and CNG channels are activated by binding of cyclic nucleotides to their intracellular cyclic nucleotide-binding domain (CNBD). However, the mechanism by which the binding of cyclic nucleotides opens these channels is not well understood. Here, we report the solution structure of the isolated CNBD of a cyclic nucleotide-sensitive K^+ channel from *Mesorhizobium loti*. The protein consists of a wide anti-parallel β-roll topped by a helical bundle comprising five α-helices and a short 3_{10}-helix. In contrast to the dimeric arrangement ('dimer-of-dimers') in the crystal structure, the solution structure clearly shows a monomeric fold. The monomeric structure of the CNBD supports the hypothesis that the CNBDs transmit the binding signal to the channel pore independently of each other.

Keywords: NMR solution structure; MloK1; ion channels; HCN; CNG

EMBO reports (2009) **10**, 729–735. doi:10.1038/embor.2009.68

INTRODUCTION

Ion channels activated by cyclic nucleotides are crucial in neuronal excitability and the signalling of visual and olfactory neurons. They belong to two sub-families: cyclic nucleotide-gated (CNG) channels, and hyperpolarization-activated and cyclic nucleotide-gated (HCN) channels (Kaupp & Seifert, 2001, 2002; Robinson & Siegelbaum, 2003). Both types of channel share a carboxy-terminal cyclic nucleotide-binding domain (CNBD). HCN channels are activated by hyperpolarization and their activity is modulated by cyclic nucleotides. In contrast, CNG channels are voltage independent and require cyclic nucleotides to open them; binding of cyclic nucleotides promotes the opening of the channel. Thus, a conformational change in the CNBD is likely to be propagated to the pore.

Recently, a prokaryotic cyclic nucleotide-sensitive K^+-channel, designated MloK1, has been identified in *Mesorhizobium loti* (Nimigean *et al*, 2004; Nimigean & Pagel, 2007). MloK1 contains six transmembrane domains (S1–S6), a 'GYG' signature sequence for K^+ selectivity and a conserved CNBD connected through a short, C-linker to S6 (Heginbotham *et al*, 1994; Nimigean *et al*, 2004; Fig 1A). The longer C-linker (~80 residues) of mammalian CNG channels is important for relaying the binding signal to the channel gate (Gordon & Zagotta, 1995; Zong *et al*, 1998; Paoletti *et al*, 1999; Wang *et al*, 2001; Johnson & Zagotta, 2001; Zhou & Siegelbaum, 2007). Crystal structures of mammalian HCN channel CNBDs revealed that neighbouring C-linkers contribute virtually all contacts between subunits in the tetrameric protein (Zagotta *et al*, 2003; Flynn *et al*, 2007). The crystal structure of the isolated CNBD of MloK1 suggested that subunits are organized as dimers. The dimer interface formed by the short linker has been proposed to be involved in channel gating (Clayton *et al*, 2004). However, an electron microscopy structure of the complete channel reveals a fourfold symmetry of subunit arrangement (Chiu *et al*, 2007). The CNBDs appear as independent domains separated by discrete gaps, suggesting that CNBDs are not interacting with each other. Furthermore, the MloK1 channel and the isolated CNBD bind to cyclic AMP (cAMP) with similar affinity in a non-cooperative manner (Cukkemane *et al*, 2007). High-resolution studies of the MloK1 transmembrane regions confirm the fourfold symmetry and reveal a flower-like arrangement of the four subunits, with the pore region at the centre and the S1–S4 domains at the periphery (Clayton *et al*, 2008). Here, we study the solution structure of the

[1]Institut für Strukturbiologie und Biophysik, Strukturbiochemie (ISB-3), Forschungszentrum Jülich, 52425 Jülich, Germany
[2]Institut für Physikalische Biologie, Heinrich-Heine-Universität, 40225 Düsseldorf, Germany
[3]Institut für Strukturbiologie und Biophysik, Zelluläre Biophysik (ISB-1), Forschungszentrum Jülich, 52425 Jülich, Germany
[4]Center for Advanced European Studies and Research (caesar), Molekulare Neurosensorik, 53175 Bonn, Germany
[+]Corresponding author. Tel: +49 2461 612100; Fax: +49 2461 612023; E-mail: dieter.willbold@uni-duesseldorf.de

Received 20 October 2008; revised 18 February 2009; accepted 20 March 2009; published online 22 May 2009

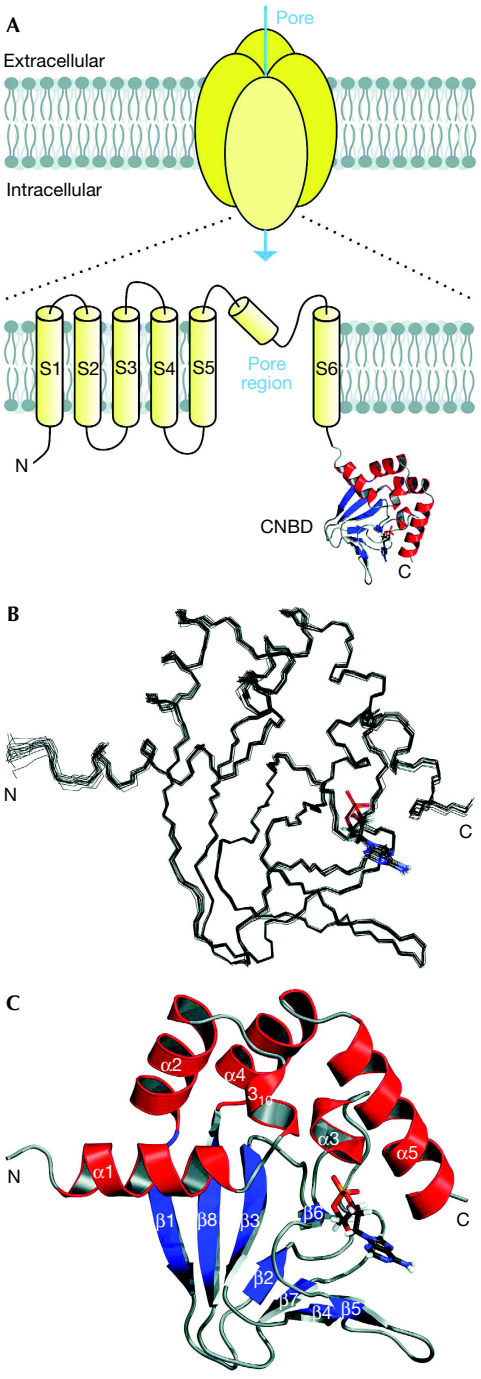

Fig 1 | Solution structure of the isolated cyclic nucleotide-binding domain. (**A**) Subunit topology and assembly of the full-length MloK1 cyclic nucleotide-gated K^+ channel. MloK1 consists of four subunits; each subunit encompasses six transmembrane segments S1–S6 (yellow) and an intracellular cyclic nucleotide-binding domain (CNBD; shown in ribbon representation). (**B**) Superposition of the backbone traces including all cyclic AMP (cAMP) atoms of the family of 15 nuclear magnetic resonance structures with the lowest CYANA target function. Backbone atoms of the amino- and carboxy-terminal ends (residues Q216–V218 and A351–A355) are not shown and were not used for least-square superposition of the structures. (**C**) Ribbon representation of the CNBD structure with the lowest target function. The cAMP ligand is shown as a stick model; secondary structure elements are labelled.

monomeric CNBD in complex with cAMP by using nuclear magnetic resonance (NMR) spectroscopy and compare it with the structure in the dimer.

RESULTS AND DISCUSSION

Solution structure of the cAMP–CNBD complex

All NMR spectra of the CNBD showed a single set of resonance signals. Nitrogen-15 relaxation experiments were performed to characterize the dynamics and the apparent molecular weight of the MloK1 CNBD (supplementary Fig S1 online). From the ^{15}N longitudinal and transverse relaxation rates of $1.03 \pm 0.05\ s^{-1}$ and $14.24 \pm 0.10\ s^{-1}$, respectively, for residues with $[^1H]^{15}N$ nuclear Overhauser effect (NOE) values greater than 0.65, a rotational correlation time of 8.5 ns at 298 K for isotropic rotational diffusion was derived. This value is consistent with the MloK1 CNBD being present as a monomer in solution and is clearly below the value expected for a dimer. The linewidths in the (^1H–^{15}N)-heteronuclear single quantum coherence (HSQC) spectra and transverse relaxation rates suggest that the protein exists in a single conformation, consistent with size-exclusion chromatography, which shows that the protein is monomeric (Clayton *et al*, 2004; Cukkemane *et al*, 2007).

The CNBD of MloK1 shows a high affinity for cAMP ($K_D = 107$ nM; Cukkemane *et al*, 2007). This agrees well with the observation that the CNBD is saturated with [*U*-^{15}N, ^{13}C]-labelled cAMP because resonance signals arising from cAMP-free CNBD were absent. Nearly all of the cAMP hydrogens were assigned using two- and three-dimensional heteronuclear through-bond correlation and heteronuclear-edited nuclear Overhauser enhancement spectroscopy (NOESY) experiments. Only the HN6 resonance signal of the purine amide group could not be assigned owing to proton exchange. The ^1H, ^{13}C and ^{15}N chemical-shift assignments of CNBD were almost complete (99% of the backbone and 94% of the side chain CH) using multidimensional heteronuclear NMR spectroscopy with [*U*-^{15}N, ^{13}C]-labelled CNBD and cAMP (see experimental procedures). Resonance assignments have been published previously (Schünke *et al*, 2007). The NOE cross-peak assignments were obtained by an iterative procedure using a combination of manual and automatic approaches. For the structural calculations, a total of 2,388 intramolecular NOE distance constraints, including 820 long-range NOEs, were evaluated. Another 215 dihedral constraints were derived from chemical-shift data using the program TALOS and included in the calculation of the final structure. A final ensemble of 15 NMR structures with the lowest CYANA target functions were used to characterize the structure of the CNBD–cAMP complex. None of the 15 structures violated NOE distances more than 0.019 nm. No dihedral-angle constraint was violated more than 5°. Most of the residues (86.8%) were found in the most favoured regions of the Ramachandran plot. The root-mean-square (r.m.s.) displacement of the 15 structures compared with the average structure was 0.025 nm for the backbone and 0.068 nm for all heavy atoms (superposition of all residues

except four amino-terminal and five carboxy-terminal residues). This shows that the structure is well defined (Fig 1B). A summary of the experimental constraints and structural statistics is given in the supplementary information (supplementary Table S1 online).

The solution structure of the CNBD–cAMP complex shows a compact fold (Fig 1C), which is similar to the typical fold of other CNBDs (Weber & Steitz, 1987; Su *et al*, 1995; Diller *et al*, 2001; Rehmann *et al*, 2003; Zagotta *et al*, 2003, Flynn *et al*, 2007). The protein core consists of eight antiparallel β-strands (β1: R252–V256; β2: V261–C263; β3: R271–E277; β4: V280–A283; β5: V288–L290; β6: F295–G297; β7: T310–S312; β8: V317–H323), five α-helices (α1: G221–A231; α2: P241–V248; α3: M299–I302; α4: S324–S333; α5: P335–G350) and a short 3_{10}-helix (L235–K238). The eight β-strands form an antiparallel β-roll topped by a helix bundle (α1–α5), whereas the short 3_{10}-helix is located between the α1- and α2-helices of the N-terminus.

Interactions between cAMP and CNBD

The cAMP molecule is bound in a pocket formed by the β-roll, the α3-helix and the α5-helix. The C-terminal α5-helix is placed like a lid above the binding pocket (Fig 2A). A total of 25 intermolecular NOE-distance constraints between CNBD and cAMP were derived. An example of the quality of the NOE spectra used to extract intermolecular distance constraints is shown in Fig 2B. The absence of a strong H1′/H8 NOE, as well as the absence of purine base H2 NOEs to S308, indicates that cAMP is bound in the *anti* conformation.

Residues R307, A300 and S308 interact with the cyclic phosphate through electrostatic and hydrogen-bonding interactions, as seen in all members of the obtained structure ensemble. The amide of G297 and the carboxy group of E298 undergo additional hydrogen-bonding interactions with the 2′-hydroxy group of the ribose. Residues V282, V288, L290, A309 and V311, which are located below the purine base of cAMP, show tight van der Waals contacts with the purine base. The side chain of R348 reaches across the purine base and undergoes close polar contacts with residues F295 and E298. In the crystal structure of the HCN2 channel CNBD, the N6 amine of cAMP forms a hydrogen bond with the backbone carbonyl oxygen of R632. In contrast, the corresponding R348 backbone carbonyl of the MloK1 CNBD is too far away to allow any specific interaction with cAMP.

The CNBD–cAMP complex is rigid

Large values of average local displacement relative to the calculated mean structure indicate either local flexibility of the respective residues or a lack of sufficient experimental data for this region. Only the very N- and C-terminal residues of the MloK1 CNBD (Q216 to R219 and A351 to A355) show increased values of average local displacement and a decreased number of NOE-derived distance constraints (supplementary information S2 online). Heteronuclear $[^1H]$–^{15}N steady-state NOE values are sensitive to the dynamics of the local environment, and values close to 0.8 indicate that residues are highly immobile on the pico- to nanosecond time scale (Kay *et al*, 1989). Rapid internal motion is revealed by lower heteronuclear NOE values that might become negative for residues with large-amplitude motions on a subnanosecond time scale (Yao *et al*, 2001). Most residues of CNBD yielded heteronuclear NOEs close to 0.8, indicating a very rigid compact fold (supplementary information S1 online). Only the very N- and C-terminal residues (Q216–R219 and A351–A355) show lower heteronuclear NOE values indicating increased flexibility.

Comparison with the crystal structure

The solution structure is very similar to the structure of a monomer in the dimer crystal (Clayton *et al*, 2004). A comparison of all CNBD backbone coordinates (residues V218–G350) between solution and crystal structures results in an r.m.s. displacement value of 0.21 nm. The conformations of cAMP in the solution and the crystal structures are also very similar—that is, the glycosyl torsion angles exist in an anti conformation with averaged χ values of -141° and -123° for the NMR and the crystal structure, respectively. However, the coordinates for the N-terminal residues (V218 to P241)—which represent the α1-helix, 3_{10}-helix and associated loop regions—differ remarkably. The α1-helix region (G221–A231) in the solution structure is a straight helix without bending (Fig 3). This is directly supported by the helix-typical NOEs within α1. Their homogeneous intensities are not in agreement with any bending within this helix. In the crystal structure, however, residues R220–N226 of α1 are bent and form the dimer interface. A comparison of backbone coordinates between the solution and crystal structures, excluding these N-terminal residues (V218–P241), results in an r.m.s. displacement value of only 0.12 nm. In addition, the positions of the short 3_{10}-helix (L235–K238) and the associated loop regions between the α1 and α2 helices are displaced towards the top of the helical bundle in the solution structure.

The two most important insights of our study are that (i) the CNBD, even at the high concentration required for NMR measurements, is a monomer, and that (ii) the solution structure, except for the N-terminal C-linker region, is similar to the monomer structure in the dimer crystal structure. The much longer C-linker region of vertebrate CNG and HCN channels is involved in intra- and intersubunit contacts, and contributes virtually all contacts between the subunits in the tetrameric crystal structures of CNBDs from two different HCN channels (for reviews, see Zagotta *et al*, 2003; Craven & Zagotta, 2006; Flynn *et al*, 2007). The formation of dimers and tetramers from monomeric CNBDs requires cAMP (Zagotta *et al*, 2003), suggesting that rearrangement of the C-linker interface represents an important gating event. Thus, the MloK1 channel seems to be set apart from its vertebrate counterparts by the lack of a full-blown C-linker that coordinates intersubunit contacts. This conclusion is supported by an electron microscopic study of the complete MloK1 channel (Chiu *et al*, 2007; Taraska & Zagotta, 2007). An important feature of the electron microscopic structure is that the four CNBDs are separated by discrete gaps and that four isolated CNBDs could be modelled into the electron density map. This structure predicts that binding sites act independently. The C-linker contact observed in the crystal structure (Clayton *et al*, 2004) was possibly enforced by the packing of dimers in the crystal, and these contacts seem to be functionally irrelevant. In fact, cAMP and several analogues bind non-cooperatively to the monomeric CNBD and the tetrameric full-length MloK1 with a high affinity that is virtually identical (Cukkemane *et al*, 2007). Together with the presented solution structure, this shows that the MloK1 cyclic nucleotide binding sites are functionally independent of each other.

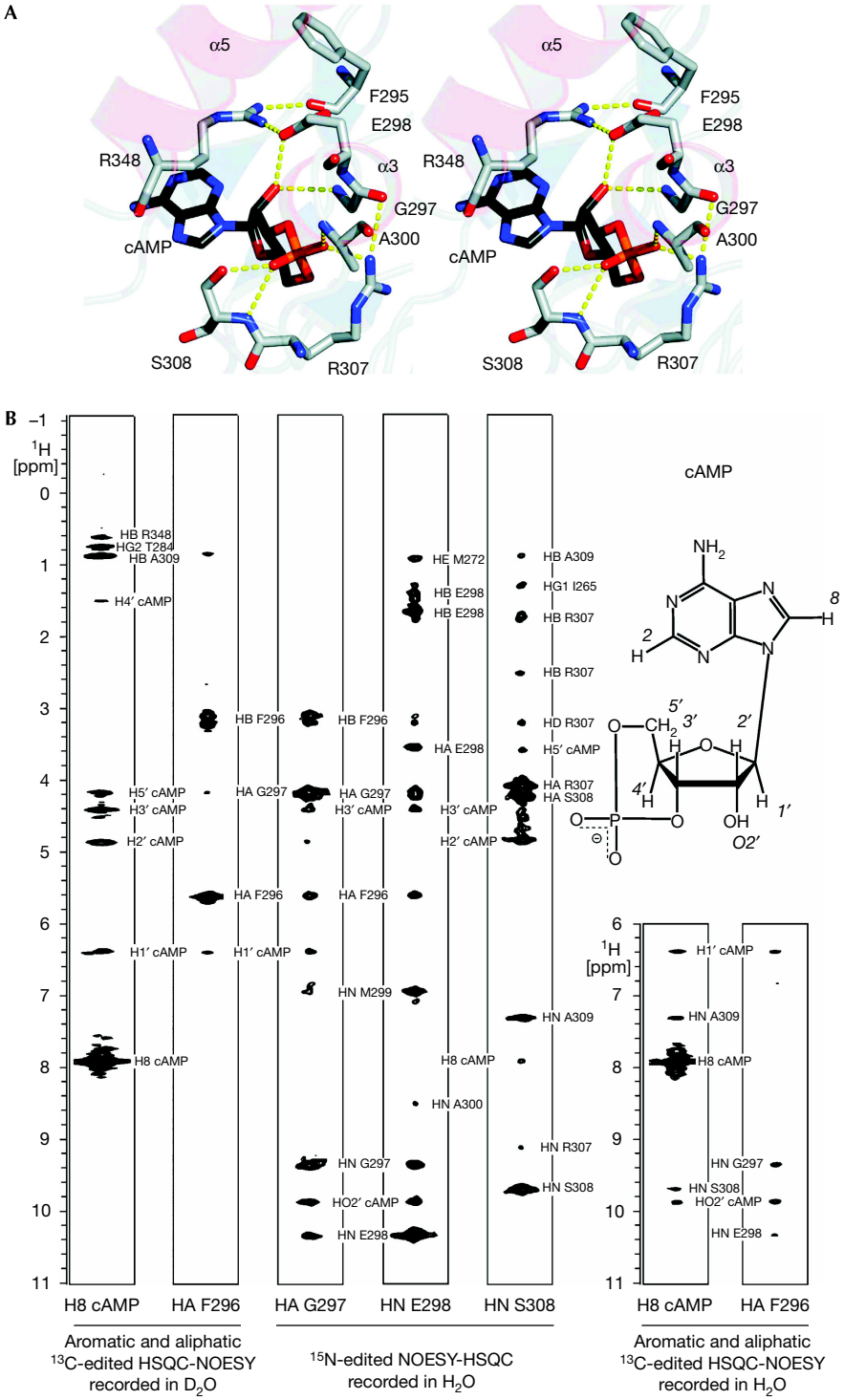

Fig 2 | Interactions between cyclic AMP and the cyclic nucleotide-binding domain. (**A**) Stereo view of the binding pocket. The binding pocket consists of highly conserved residues known as the phosphate-binding cassette (PBC). The PBC includes G297, E298, A300, R307 and S308, which form polar contacts (shown as yellow dotted lines) with the cyclic nucleotide. The purine of cAMP is positioned towards the exit of the binding pocket. (**B**) Strips of various ^{13}C-edited HSQC-NOESY and ^{15}N-edited NOESY-HSQC spectra containing intermolecular NOEs between CNBD and cAMP. The respective NOE is characterized by the cAMP proton labelled at the bottom of each strip (schematic shown in the upper right corner) and the CNBD proton labelled to the right of each cross-resonance within the respective strip. CNBD, cyclic nucleotide-binding domain; HSQC, heteronuclear single quantum coherence; NOE, nuclear Overhauser effect; NOESY, nuclear Overhauser enhancement spectroscopy.

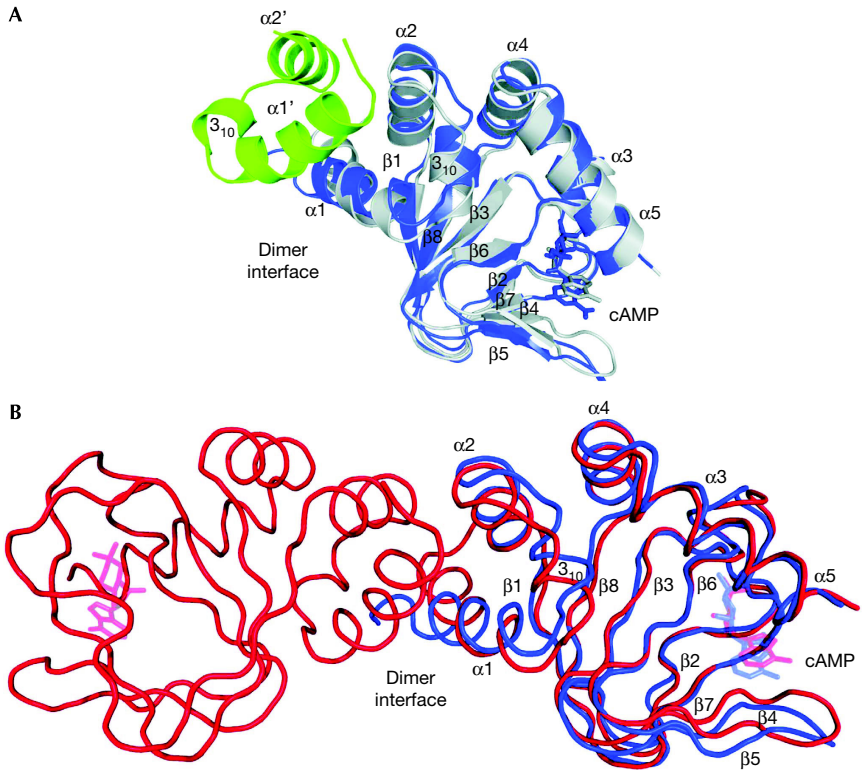

Fig 3 | Comparison of nuclear magnetic resonance and crystal structure. (**A**) Comparison of the solution structure (blue) and the crystal structure of the cyclic nucleotide-binding domain (CNBD; white). A part of the second domain in the dimer crystal structure that is involved in the dimer interface is shown in green. Alignment of the solution and crystal structure backbones (residues V218–G350) yielded an r.m.s. displacement of 0.21 nm. A comparison of the solution and crystal structures, excluding the amino-terminal residues (V218–P241), results in an r.m.s. displacement value of 0.12 nm. (**B**) CNBD backbone comparison of the monomeric solution structure (shown in blue) and the backbone of the crystal structure dimer (shown in red).

METHODS

Protein expression and purification. The isolated CNBD was expressed as a fusion protein with glutathione *S*-transferase. Thrombin cleavage yielded the isolated CNBD (Q216–A355) with additional glycine and serine residues at the N-terminus. Details of cloning, expression and purification of isotopically [*U*-^{15}N, ^{13}C]-labelled recombinant protein have been described previously (Schünke *et al*, 2007).

NMR spectroscopy. NMR samples contained 0.5 mM uniformly [*U*-^{15}N, ^{13}C]-labelled protein with an equivalent amount of cAMP in aqueous solution (10 mM potassium phosphate, pH 7, 100 mM potassium chloride, 100 μM EDTA, 5% (v/v) $^{2}H_2O$ and 0.02% (w/v) sodium azide). All NMR experiments were carried out at 298 K on a Varian ^{Unity}INOVA spectrometer equipped with a 5 mm cryogenic Z-axis PFG-^{1}H[^{13}C, ^{15}N] triple resonance probe at a proton frequency of 800 MHz.

Backbone and side chain assignments of CNBD were carried out as reported previously (Schünke *et al*, 2007). The resonances of cAMP were identified and assigned using a combination of the following experiments: aliphatic and aromatic 2D (^{1}H–^{13}C)-HSQC (Kay *et al*, 1992), 2D ct-(^{1}H–^{13}C)-HSQC (Santoro & King, 1992; Vuister & Bax, 1992), 3D aliphatic ^{13}C-edited HSQC-NOESY (100 ms mixing time), 3D aromatic ^{13}C-edited HSQC-NOESY (140 ms mixing time; Norwood *et al*, 1990) and ^{15}N-edited NOESY-HSQC (120 ms mixing time; Zuiderweg & Fesik, 1989). Adenine H2 resonance was distinguished from other aromatic resonances and assigned by the unique chemical shift of the attached C2 carbon, and the H8 resonance was respectively assigned. Proton resonances of the ribose were successively identified by using the unique H1′ resonance as a starting point for interpretation of the NOE experiments. Structural constraints were derived from 3D ^{15}N-edited NOESY-HSQC (120 ms mixing time), aliphatic ^{13}C-edited HSQC-NOESY (100 ms mixing time) and aromatic ^{13}C-edited HSQC-NOESY (140 ms mixing time) experiments. Aliphatic ^{13}C-edited HSQC-NOESY (100 ms mixing time) and aromatic ^{13}C-edited HSQC-NOESY (140 ms mixing time) experiments were also used for structural constraints with protein in buffer after replacement of H_2O by D_2O.

Data evaluation and structure calculation. On the basis of the almost complete assignment of ^{1}H, ^{13}C and ^{15}N resonances of CNBD, NOE cross-peak assignments were obtained by an iterative procedure using a combination of manual and automatic steps. As an initial step, the program CARA (Keller, 2004) was used to evaluate NOE spectra and to manually assign nearly all of the apparently unambiguous NOEs. NOE cross-peak intensities were classified as strong, medium or weak, corresponding to upper limit distance constraints of 2.7, 3.8 and 5.5 Å, respectively. The cross-peak intensities of NOEs between protons of known distances

were used for calibration. For NOEs involving methyl groups, upper limit distance constraints of 2.9, 4.0 and 5.7 Å for strong, medium or weak interactions, respectively, were used. To perform the structural calculation with simulated annealing in torsion angle space, the program CYANA version 1.1 (Guntert *et al*, 1997) was used. All of the 25 intermolecular NOEs between the protein and cAMP were manually assigned. According to the manually assigned NOEs, an initial fold of the protein was calculated. CYANA runs were performed according to the protocol for simulated annealing with 100 randomly generated starting conformations, 25,000-steps torsion angle dynamics and 2,000 conjugate gradients minimization steps. With subsequent use of the ATNOS/CANDID version 1.1 software package in combination with CYANA, additional NOEs were automatically assigned in an iterative approach. The package incorporates the functionalities of the following two algorithms: ATNOS (Herrmann *et al*, 2002a) for automated NOE peak picking, and NOE signal identification in 2D homonuclear- and 3D heteronuclear-resolved [^{1}H,^{1}H]-NOE spectra, and CANDID (Herrmann *et al*, 2002b) for automated NOE assignment. The input consisted of nearly complete assignments of ^{1}H, ^{13}C and ^{15}N resonances, the previously assigned NOEs and the three mentioned NOE spectra. The standard protocol with seven cycles of peak picking, NOE assignment and subsequent structural calculation with CYANA was applied (Guntert *et al*, 1997; Herrmann *et al*, 2002a,b). In the final step, dihedral angle restraints for the backbone φ and ψ angles were derived from H^{α}, C^{α}, C^{β}, C′ and N chemical shifts using the program TALOS (Cornilescu *et al*, 1999). Restraints were applied for the 111 high-confidence predictions found by the program using the calculated range ± 10 °. For further refinement, CYANA runs were performed according to the protocol for simulated annealing with 100 randomly generated starting conformations, 35,000-steps torsion angle dynamics and 2,000 conjugate gradients minimization steps. A final bundle of 15 NMR structures with the lowest target function that did not show any distance constraint violations of more than 0.019 nm were used for further analysis. Geometry of the structures, structural parameters and secondary structural elements were analysed and visualized using the following programs: MOLMOL (Koradi *et al*, 1996), PyMOL (DeLano, 2002), WHATIF (Vriend, 1990) and PROCHECK (Laskowski *et al*, 1993).

For the characterization of overall and internal motions, ^{15}N longitudinal (R_1) and transverse (R_2) relaxation rates, together with the steady-state [^{1}H]^{15}N NOE, were recorded at 298 K on a uniformly [*U*-^{15}N]-labelled protein sample using standard methods at 800 MHz proton frequency. Peak integral values were obtained by fitting signals to an adjustable 'peak model' shape using the program CARA. A superposition of the Gauss and Lorentz functions was used, and adjusted manually and independently for both spectral dimensions. For ^{15}N R_1 measurement, relaxation delay values of 11, 60, 140, 240, 360, 530, 750 and 1,150 ms were applied. For R_2, delays of 10, 30, 50, 70, 90 and 110 ms were used. Data of R_1 and R_2 relaxation experiments were fitted to a mono-exponential decay using the program CURVEFIT (A.G. Palmer, Columbia University, USA). The correlation time was determined for an isotropic tumbling model using the TENSOR2 package (Dosset *et al*, 2000). [^{1}H]–^{15}N NOE-TROSY spectra (Farrow *et al*, 1994; Pervushin *et al*, 1997; Zhu *et al*, 2000) were acquired with a 2.5 s proton saturation.

Database depositions. Resonance assignments and the atomic coordinates for the resulting 15 NMR structures with the lowest target function are available at the BioMagResBank and at the Research Collaboratory for Structural Bioinformatics (RCSB) Protein Data Bank (codes 15249 and 2K0G), respectively.
Supplementary information is available at *EMBO reports* online (http://www.emboreports.org).

ACKNOWLEDGEMENTS
This study was supported by a research grant from the Helmholtzgemeinschaft ('Virtual Institute of Structural Biology') to D.W. and a fellowship from the International Research School 'BioStruct' to S.S.

CONFLICT OF INTEREST
The authors declare that they have no conflict of interest.

REFERENCES
Chiu PL, Pagel MD, Evans J, Chou HT, Zeng X, Gipson B, Stahlberg H, Nimigean CM (2007) The structure of the prokaryotic cyclic nucleotide-modulated potassium channel MloK1 at 16 A resolution. *Structure* **15:** 1053–1064

Clayton GM, Silverman WR, Heginbotham L, Morais-Cabral JH (2004) Structural basis of ligand activation in a cyclic nucleotide regulated potassium channel. *Cell* **119:** 615–627

Clayton GM, Altieri S, Heginbotham L, Unger VM, Morais-Cabral JH (2008) Structure of the transmembrane regions of a bacterial cyclic nucleotide-regulated channel. *Proc Natl Acad Sci USA* **105:** 1511–1515

Cornilescu G, Delaglio F, Bax A (1999) Protein backbone angle restraints from searching a database for chemical shift and sequence homology. *J Biomol NMR* **13:** 289–302

Craven KB, Zagotta WN (2006) CNG and HCN channels: two peas, one pod. *Annu Rev Physiol* **68:** 375–401

Cukkemane A, Gruter B, Novak K, Gensch T, Bonigk W, Gerharz T, Kaupp UB, Seifert R (2007) Subunits act independently in a cyclic nucleotide-activated K(+) channel. *EMBO Rep* **8:** 749–755

DeLano W (2002) *The PyMOL Molecular Graphics System*. San Carlos, CA, USA: DeLano Scientific LLC

Diller TC, Madhusudan M, Xuong NH, Taylor SS (2001) Molecular basis for regulatory subunit diversity in cAMP-dependent protein kinase: crystal structure of the type II beta regulatory subunit. *Structure* **9:** 73–82

Dosset P, Hus JC, Blackledge M, Marion D (2000) Efficient analysis of macromolecular rotational diffusion from heteronuclear relaxation data. *J Biomol NMR* **16:** 23–28

Farrow NA, Muhandiram R, Singer AU, Pascal SM, Kay CM, Gish G, Shoelson SE, Pawson T, Forman-Kay JD, Kay LE (1994) Backbone dynamics of a free and phosphopeptide-complexed Src homology 2 domain studied by 15N NMR relaxation. *Biochemistry* **33:** 5984–6003

Flynn GE, Black KD, Islas LD, Sankaran B, Zagotta WN (2007) Structure and rearrangements in the carboxy-terminal region of SpIH channels. *Structure* **15:** 671–682

Gordon SE, Zagotta WN (1995) Localization of regions affecting an allosteric transition in cyclic nucleotide-activated channels. *Neuron* **14:** 857–864

Guntert P, Mumenthaler C, Wuthrich K (1997) Torsion angle dynamics for NMR structure calculation with the new program DYANA. *J Mol Biol* **273:** 283–298

Heginbotham L, Lu Z, Abramson T, MacKinnon R (1994) Mutations in the K+ channel signature sequence. *Biophys J* **66:** 1061–1067

Herrmann T, Guntert P, Wuthrich K (2002a) Protein NMR structure determination with automated NOE-identification in the NOESY spectra using the new software ATNOS. *J Biomol NMR* **24:** 171–189

Herrmann T, Guntert P, Wuthrich K (2002b) Protein NMR structure determination with automated NOE assignment using the new software CANDID and the torsion angle dynamics algorithm DYANA. *J Mol Biol* **319:** 209–227

Johnson JP Jr, Zagotta WN (2001) Rotational movement during cyclic nucleotide-gated channel opening. *Nature* **412:** 917–921

Kaupp UB, Seifert R (2001) Molecular diversity of pacemaker ion channels. *Annu Rev Physiol* **63:** 235–257

Kaupp UB, Seifert R (2002) Cyclic nucleotide-gated ion channels. *Physiol Rev* **82:** 769–824

Kay L, Keifer P, Saarinen T (1992) Pure absorption gradient enhanced heteronuclear single quantum correlation spectroscopy with improved sensitivity. *J Am Chem Soc* **114:** 10663–10665

Kay LE, Torchia DA, Bax A (1989) Backbone dynamics of proteins as studied by 15N inverse detected heteronuclear NMR spectroscopy: application to staphylococcal nuclease. *Biochemistry* **28:** 8972–8979

Keller R (2004) *The Computer Aided Resonance Assignment Tutorial*. Zurich, Switzerland: Cantina

Koradi R, Billeter M, Wuthrich K (1996) MOLMOL: a program for display and analysis of macromolecular structures. *J Mol Graph* **14:** 51–55, 29–32

Laskowski RA, MacArthur MW, Moss DS, Thornton JM (1993) PROCHECK: a program to check the stereochemical quality of protein structures. *J Appl Crystallogr* **26:** 283–291

Nimigean CM, Pagel MD (2007) Ligand binding and activation in a prokaryotic cyclic nucleotide-modulated channel. *J Mol Biol* **371:** 1325–1337

Nimigean CM, Shane T, Miller C (2004) A cyclic nucleotide modulated prokaryotic K+ channel. *J Gen Physiol* **124:** 203–210

Norwood TJ, Boyd J, Heritage JE, Soffe N, Campbell ID (1990) Comparison of techniques for ^{1}H-detected heteronuclear ^{1}H-^{15}N spectroscopy. *J Magn Reson* **87:** 488–501

Paoletti P, Young EC, Siegelbaum SA (1999) C-Linker of cyclic nucleotide-gated channels controls coupling of ligand binding to channel gating. *J Gen Physiol* **113:** 17–34

Pervushin K, Riek R, Wider G, Wuthrich K (1997) Attenuated T2 relaxation by mutual cancellation of dipole-dipole coupling and chemical shift anisotropy indicates an avenue to NMR structures of very large biological macromolecules in solution. *Proc Natl Acad Sci USA* **94:** 12366–12371

Rehmann H, Prakash B, Wolf E, Rueppel A, de Rooij J, Bos JL, Wittinghofer A (2003) Structure and regulation of the cAMP-binding domains of Epac2. *Nat Struct Biol* **10:** 26–32

Robinson RB, Siegelbaum SA (2003) Hyperpolarization-activated cation currents: from molecules to physiological function. *Annu Rev Physiol* **65:** 453–480

Santoro J, King GC (1992) A constant-time 2D overbodenhausen experiment for inverse correlation of isotopically enriched species. *J Magn Reson* **97:** 202–207

Schünke S, Novak K, Stoldt M, Kaupp UB, Willbold D (2007) Resonance assignment of the cyclic nucleotide binding domain from a cyclic nucleotide-gated K^{+} channel in complex with cAMP. *Biomol NMR Assign* **1:** 179–181

Su Y, Dostmann WR, Herberg FW, Durick K, Xuong NH, Ten Eyck L, Taylor SS, Varughese KI (1995) Regulatory subunit of protein kinase A: structure of deletion mutant with cAMP binding domains. *Science* **269:** 807–813

Taraska JW, Zagotta WN (2007) Cyclic nucleotide-regulated ion channels: spotlight on symmetry. *Structure* **15:** 1023–1024

Vriend G (1990) WHAT IF: a molecular modeling and drug design program. *J Mol Graph* **8:** 52–56, 29

Vuister GW, Bax A (1992) Resolution enhancement and spectral editing of uniformly ^{13}C-enriched proteins by homonuclear ^{13}C broadband decoupling. *J Magn Reson* **98:** 428–435

Wang J, Chen S, Siegelbaum SA (2001) Regulation of hyperpolarization-activated HCN channel gating and cAMP modulation due to interactions of COOH terminus and core transmembrane regions. *J Gen Physiol* **118:** 237–250

Weber IT, Steitz TA (1987) Structure of a complex of catabolite gene activator protein and cyclic AMP refined at 2.5 A resolution. *J Mol Biol* **198:** 311–326

Yao J, Chung J, Eliezer D, Wright PE, Dyson HJ (2001) NMR structural and dynamic characterization of the acid-unfolded state of apomyoglobin provides insights into the early events in protein folding. *Biochemistry* **40:** 3561–3571

Zagotta WN, Olivier NB, Black KD, Young EC, Olson R, Gouaux E (2003) Structural basis for modulation and agonist specificity of HCN pacemaker channels. *Nature* **425:** 200–205

Zhou L, Siegelbaum SA (2007) Gating of HCN channels by cyclic nucleotides: residue contacts that underlie ligand binding, selectivity, and efficacy. *Structure* **15:** 655–670

Zhu G, Xia Y, Nicholson LK, Sze KH (2000) Protein dynamics measurements by TROSY-based NMR experiments. *J Magn Reson* **143:** 423–426

Zong X, Zucker H, Hofmann F, Biel M (1998) Three amino acids in the C-linker are major determinants of gating in cyclic nucleotide-gated channels. *EMBO J* **17:** 353–362

Zuiderweg ER, Fesik SW (1989) Heteronuclear three-dimensional NMR spectroscopy of the inflammatory protein C5a. *Biochemistry* **28:** 2387–2391

Supplementary Information to

Solution structure of the *Mesorhizobium loti* K1 channel cyclic nucleotide-binding domain in complex with cAMP

Sven Schünke[1,2], Matthias Stoldt[1,2], Kerstin Novak[3], U. Benjamin Kaupp[4] and Dieter Willbold[1,2]

[1]Institut für Strukturbiologie und Biophysik, Strukturbiochemie (ISB-3), Forschungszentrum Jülich, 52425 Jülich, [2]Institut für Physikalische Biologie, Heinrich-Heine-Universität, 40225 Düsseldorf, [3]Institut für Strukturbiologie und Biophysik, Zelluläre Biophysik (ISB-1), Forschungszentrum Jülich, 52425 Jülich, [4]Center for Advanced European Studies and Research (caesar), Abteilung Molekulare Neurosensorik, 53175 Bonn, Germany.

Correspondence should be addressed to D.W. (dieter.willbold@uni-duesseldorf.de).

Supplementary table, text and figures:

Supplementary Table S1	Constraints and structural statistics for the resulting 15 NMR structures of MloK1-CNBD
Supplementary Figure S1	Experimental values of ^{15}N longitudinal (R_1) and transverse (R_2) relaxation rates for CNBD with respect to protein sequence
Supplementary Figure S2	Precision of local conformation and number of distance constraints per residue for the resulting 15 NMR structures of the CNBD with the lowest CYANA target function

SUPPLEMENTARY TABLE

Table S1: Constraints and structural statistics for the resulting 15 NMR structures of MloK1-CNBD.

Number of experimental restraints:	
total number of assigned NOEs	2,388
intraresidue (|i-j| = 0)	442
interresidue sequential (|i-j| = 1)	624
interresidue medium range (1 < |i-j| ≤ 5)	477
long range (|i-j| > 5)	820
protein – cAMP NOEs	25
average number of NOE constraints per residue	17
dihedral φ and ψ angle constraints from TALOS[$]	215
CYANA structural statistics[§]:	
RMS deviations (nm) to the mean structure[*]:	
backbone heavy atoms	0.025 ± 0.004
all heavy atoms	0.068 ± 0.007
CYANA target function (nm^2)	0.0111 ± 0.0006
NOE distance constraints, sum (nm)	0.68 ± 0.050
NOE distance constraints, max (nm)	0.015 ± 0.001
dihedral angle constraints, max (degrees)	3.17 ± 0.52
Φ, Ψ angles consistent with Ramachandran plot[#] (%):	
most favored regions	86.8 %
allowed regions	98.3 %
generously allowed regions	99.4 %
disallowed regions	0.6 %

[#]Ramachandran analysis was determined using PROCHECK-NMR.
[$]Derived from C^{α}, C^{β}, C, N and H^{α} chemical shifts for 111 high confidence predictions found by TALOS using the calculated range of ±10°.
[§]Average value ± standard deviation.
[*]Superposition made for all heavy atoms including ligand (except N- and C-terminal residues 216-219 and 351-355).

SUPPLEMENTARY FIGURES

Figure S1: Experimental values of ^{15}N longitudinal (R_1) and transverse (R_2) relaxation rates for CNBD with respect to protein sequence: top, R_1 (s^{-1}); middle, R_2 (s^{-1}); and bottom steady-state heteronuclear $\{^1H\}$-^{15}N-NOE values of amide resonances at 18.8 T and 298 K. Residues for which no results are shown correspond to prolines and residue D270. Secondary structure elements are shown at the bottom of the figure (arrows indicate β-strand and cylinders indicate helical conformation).

Figure S2: Precision of local conformation and number of distance constraints per residue for the resulting 15 NMR structures of the CNBD with the lowest CYANA target function. **A**: Local displacement values among the 15 calculated NMR structures. The global displacement for backbone (dashed gray line) and all heavy atoms (dashed black line) is plotted against the corresponding residue number. For each three-residue segment the calculated local root mean squared (r.m.s.) deviation of the backbone atoms is plotted against the residue number of the central residue (black line). **B**: Number of intraresidual (black), sequential (light gray), medium-range (dark gray) and long-range (white) NOE distance constraints per residue.

Figure S1

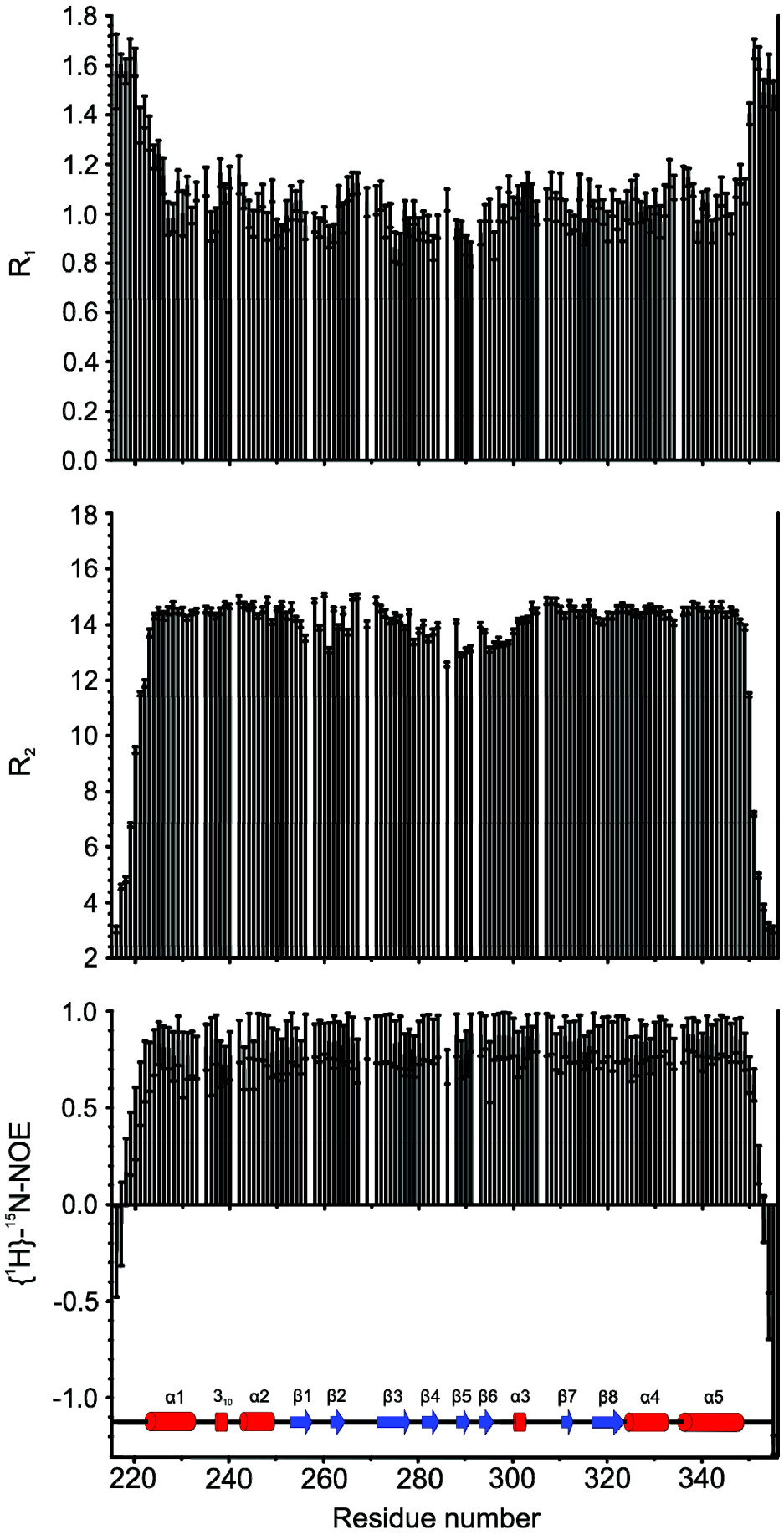
R1
R2
{1H}-15N-NOE
α1
310
α2
β1
β2
β3
β4
β5
β6
α3
β7
β8
α4
α5
Residue number

Figure S2

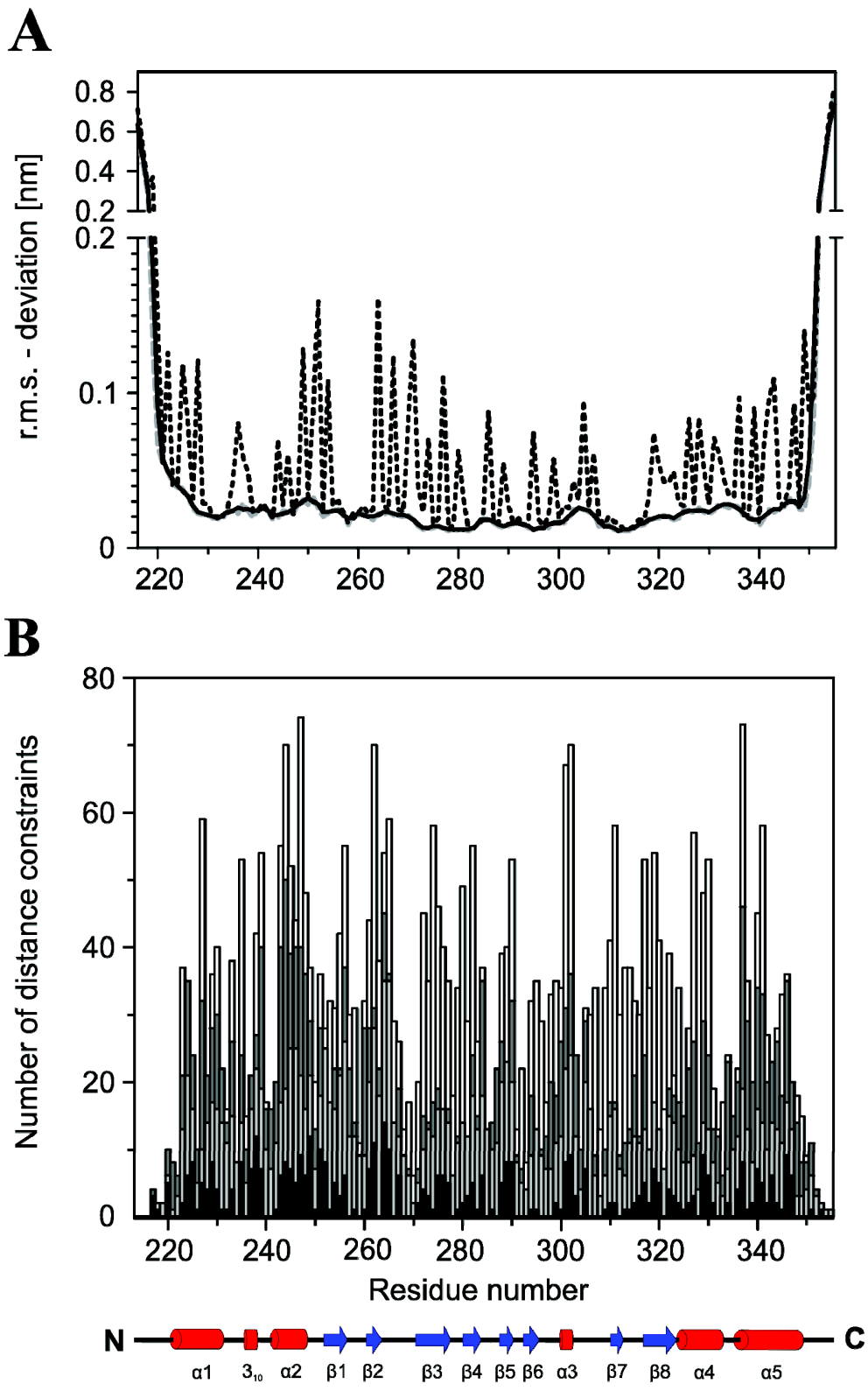
A
r.m.s. - deviation [nm]
0.8
0.6
0.4
0.2
0.2
0.1
0
220
240
260
280
300
320
340
B
Number of distance constraints
80
60
40
20
0
220
240
260
280
300
320
340
Residue number
N
C
α1
3₁₀
α2
β1
β2
β3
β4
β5
β6
α3
β7
β8
α4
α5

3.3 Resonance assignments of the nucleotide-free wild-type MloK1 cyclic nucleotide-binding domain

published in: ***Biomolecular NMR Assignments***
Vol. 4, Issue 2, May 2010, Pages: 147-150

Sven Schünke[1,2], Justin Lecher[1,2], Matthias Stoldt[1,2],
U. Benjamin Kaupp[3] and Dieter Willbold[1,2]

[1]Institut für Strukturbiologie und Biophysik,
Strukturbiochemie (ISB-3),
Forschungszentrum Jülich,
52425 Jülich,
Germany

[2]Institut für Physikalische Biologie,
Heinrich-Heine-Universität,
40225 Düsseldorf,
Germany

[3]Center of Advanced European Studies and Research (caesar),
Molekulare Neurosensorik,
53175 Bonn,
Germany

Biomol NMR Assign (2010) 4:147–150
DOI 10.1007/s12104-010-9231-z

ARTICLE

Resonance assignments of the nucleotide-free wildtype MloK1 cyclic nucleotide-binding domain

Sven Schünke · Justin Lecher · Matthias Stoldt · U. Benjamin Kaupp · Dieter Willbold

Received: 18 February 2010 / Accepted: 22 April 2010 / Published online: 7 May 2010

Abstract Cyclic nucleotide-sensitive ion channels, known as HCN and CNG channels play crucial roles in neuronal excitability and signal transduction of sensory cells. These channels are activated by binding of cyclic nucleotides to their intracellular cyclic nucleotide-binding domain (CNBD). A comparison of the structures of wildtype ligand-free and ligand-bound CNBD is essential to elucidate the mechanism underlying nucleotide-dependent activation of CNBDs. We recently reported the solution structure of the *Mesorhizobium loti* K1 (MloK1) channel CNBD in complex with cAMP. We have now extended these studies and achieved nearly complete assignments of ^{1}H, ^{13}C and ^{15}N resonances of the nucleotide-free CNBD. A completely new assignment of the nucleotide-free wildtype CNBD was necessary due to the sizable chemical shift differences as compared to the cAMP bound CNBD and the slow exchange behaviour between both forms. Scattering of these chemical shift differences over the complete CNBD suggests that nucleotide binding induces significant overall conformational changes.

S. Schünke · J. Lecher · M. Stoldt · D. Willbold (✉)
Institut für Strukturbiologie und Biophysik, Strukturbiochemie (ISB-3), Forschungszentrum Jülich, 52425 Jülich, Germany
e-mail: dieter.willbold@uni-duesseldorf.de

S. Schünke · J. Lecher · M. Stoldt · D. Willbold
Institut für Physikalische Biologie, Heinrich-Heine-Universität, 40225 Düsseldorf, Germany

U. Benjamin Kaupp
Molekulare Neurosensorik, Center of Advanced European Studies and Research (caesar), 53175 Bonn, Germany

Keywords Ion channels · Cyclic nucleotide binding domain · CNBD · HCN · CNG · Heteronuclear NMR

Biological context

Ion channels activated by cyclic nucleotides play key roles in neuronal excitability and signaling of visual and olfactory neurons. They belong to two subfamilies: Cyclic nucleotide-gated (CNG) channels, and hyperpolarization-activated and cyclic nucleotide-gated (HCN) channels (Kaupp and Seifert 2001, 2002; Robinson and Siegelbaum 2003). CNG channels are virtually voltage independent and require cyclic nucleotides to open. In contrast, HCN channels are activated by hyperpolarization and their activity is modulated by cyclic nucleotides. In both cases, ligand binding to an intracellular cyclic nucleotide-binding domain (CNBD) promotes the opening of the channel—probably a conformational change in the CNBD is propagated to the pore. The mechanisms that underlie nucleotide activation are not well understood.

A prokaryotic cyclic nucleotide-sensitive K^+-channel, designated MloK1, has been identified in *Mesorhizobium loti* (Nimigean et al. 2004; Nimigean and Pagel 2007). The channel consists of four identical subunits and each subunit encompasses six transmembrane domains, a 'GYG' signature sequence for K^+ selectivity and a conserved CNBD. The CNBD is connected by a short C-linker to the last transmembrane domain of the channel. The MloK1 CNBD is a 15 kDa (142 aa) monomeric single-chain protein. Moreover, this CNBD is reported to have extremely high affinity ($K_D = 107$ nM) for cAMP (Cukkemane et al. 2007). The crystal structures of the cAMP bound form of MloK1 and a mutated form of

MloK1 unable to bind cAMP have been reported previously together with the conclusion that the observed dimeric arrangement was important for its function in vivo (Clayton et al. 2004). However, the electron microscopy structure of the full-length MloK1 channel in the presence of cAMP revealed the CNBDs as independent domains separated by discrete gaps, suggesting that CNBDs are not interacting with each other (Chiu et al. 2007). Therefore, we set out to investigate the structures of cAMP-free and cAMP-complexed wildtype CNBD by NMR spectroscopy. In addition to our recently reported assignments of the CNBD in complex with cAMP (Schünke et al. 2007) and its solution structure (Schünke et al. 2009), we now report the ^{1}H, ^{13}C, ^{15}N sequence-specific backbone and side-chain resonance assignment of the nucleotide-free CNBD.

Structural data of nucleotide-free and nucleotide-bound wildtype CNBDs are essential prerequisites to elucidate the mechanism of cyclic nucleotide-gated channel opening. Therefore, we add the ^{1}H, ^{13}C, ^{15}N sequence-specific backbone and side-chain resonance assignments of the nucleotide-free CNBD to our recently reported assignments and the solution structure of the CNBD in complex with cAMP.

Methods and experiments

Recombinant *M. loti* CNBD was expressed as a GST-fusion protein. DNA encoding the full-length MloK1 channel was amplified from genomic DNA. The coding region for residues Q216 to A355 of MloK1 protein was cloned into pGEX-2T (Amersham Biosciences) and verified by DNA sequencing. Details of protein expression and purification were described previously (Schünke et al. 2007). Thrombin cleavage yielded an additional glycine and serine residue at the N-terminus. The procedure yields exclusively nucleotide-bound MloK1 CNBD. We expanded the procedure and introduced an additional washing step to remove tightly bound cAMP from MloK1 CNBD during the affinity chromatography. A subsequent ion exchange chromatography step using a Mono S HR 5/5 column (GE Healthcare, München, Germany) was finally used to separate cAMP-free and remaining cAMP-bound MloK1 CNBD protein of each other.

NMR samples contained 0.5 mM [*U*-^{15}N] or [*U*-^{15}N, ^{13}C] labelled CNBD in aqueous solution (10 mM deuterated Tris (D11, 98%, Cambridge Isotopes)/HCl (pH 7), 100 mM sodium chloride, 200 µM EDTA, 5% (v/v) $^{2}H_2O$ and 0,02% (w/v) sodium azide).

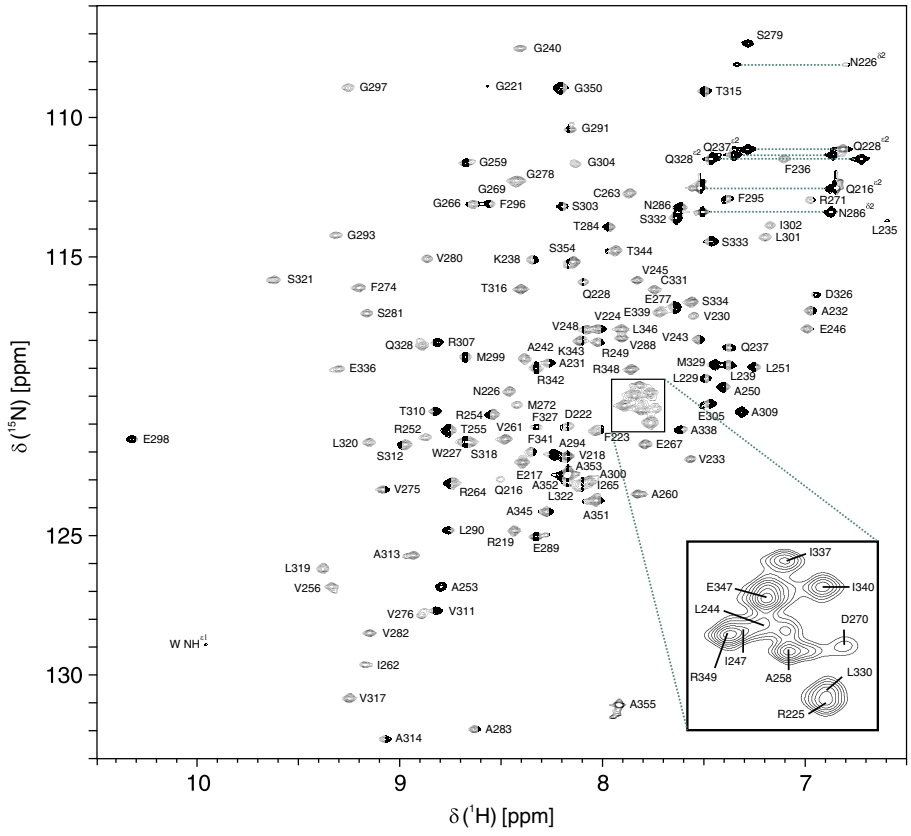

Fig. 1 2D (^{1}H–^{15}N)-HSQC spectrum of the nucleotide-free [*U*-^{15}N]-labeled cyclic nucleotide binding domain from *M. loti* (protein concentration = 0.5 mM, T = 298 K, pH 7, 95% H_2O/5% $^{2}H_2O$) recorded at 800 MHz. Backbone resonance assignments are indicated by one-letter amino acid code and the sequence number. The side-chain amide groups of asparagine and glutamine residues are connected by horizontal lines. Amide resonances of residues S215, R220, S308, H323, S324 and A325 could not be found in the 2D (^{1}H–^{15}N)-HSQC spectrum

NMR experiments were performed at 25°C on Varian ^{Unity}INOVA and VNMRS instruments, equipped with a cryogenic *Z*-axis PFG triple resonance probe at proton frequencies of 800 and 600 MHz. Resonance assignment was accomplished using the following experiments: 2D (^{1}H–^{15}N)-HSQC, 2D ct-(^{1}H–^{13}C)-HSQC, 3D HNCACB, HNCO, HNHA, H(C)CH-COSY, H(C)CH-TOCSY (14 ms mixing time), (^{1}H–^{13}C–^{1}H)-HSQC-NOESY (100 ms mixing time) and (^{1}H–^{1}H–^{15}N)-NOESY-HSQC (120 ms mixing time). Aromatic side chain resonances were assigned using aromatic 2D (^{1}H–^{13}C)-HSQC, 2D ct-(^{1}H–^{13}C)-HSQC, 2D (^{1}H–^{13}C–^{1}H)-HSQC-NOESY (100 ms mixing time) and 3D (^{1}H–^{13}C–^{1}H)-HSQC-NOESY (140 ms mixing time) experiments. Decoupling of ^{15}N and ^{13}C nuclei during proton aquisition has been performed by application of GARP or WURST sequences. DIPSI-2 isotropic mixing scheme was used during TOCSY-^{13}C spin lock periods. ^{1}H chemical shifts were referenced internal to DSS at 0 ppm and ^{13}C and ^{15}N shifts were referenced indirectly to DSS, using the absolute frequency ratios. All NMR data were processed using NMRPipe and evaluated with CARA software.

Assignments and data deposition

Due to significant chemical-shift differences and the slow exchange behaviour between nucleotide-free and nucleotide-bound CNBD, a complete reassignment of the nucleotide-free CNBD was required. Interpretation of the triple resonance spectra lead to sequence-specific assignments of 97% of the backbone (excluding ^{15}N resonances and ^{13}C′ resonances of the predecessor residues correlated with the nine proline residues) and 90% of the aliphatic and aromatic side chain amide, carbon and proton resonances (excluding ^{1}H–^{15}N and ^{15}N of Lysine and Arginine, OH, side chain ^{13}C′, C^{ζ} and aromatic quaternary ^{13}C). In particular, amide resonances of residues S215, R220, S308, H323, S324 and A325 were not found in the 2D (^{1}H–^{15}N)-HSQC (Fig. 1). The amide proton of E298 shows a somewhat unusual chemical shift (10.3 ppm). However, there is not much difference between its chemical shifts in the nucleotide-free and nucleotide-bound states. The structure of the nucleotide-bound CNBD revealed close proximity of the phenylalanine residue 295 to cause this downfield shift. Thus, this situation might be similar in the nucleotide-free CNBD. Resonance assignments of ^{1}H, ^{13}C, ^{15}N backbone and side chain chemical shifts have been deposited at BioMagResBank (www.bmrb.wisc.edu) under accession number 16628.

Differences of amide backbone chemical shifts between nucleotide-free and nucleotide-bound CNBD clearly show that cAMP binding affects virtually all residues of the CNBD (Fig. 2a, b, c). Even the amide resonance of L235, which is far away from the ligand binding-site, showed a large shift. Together with the observation of slow exchange

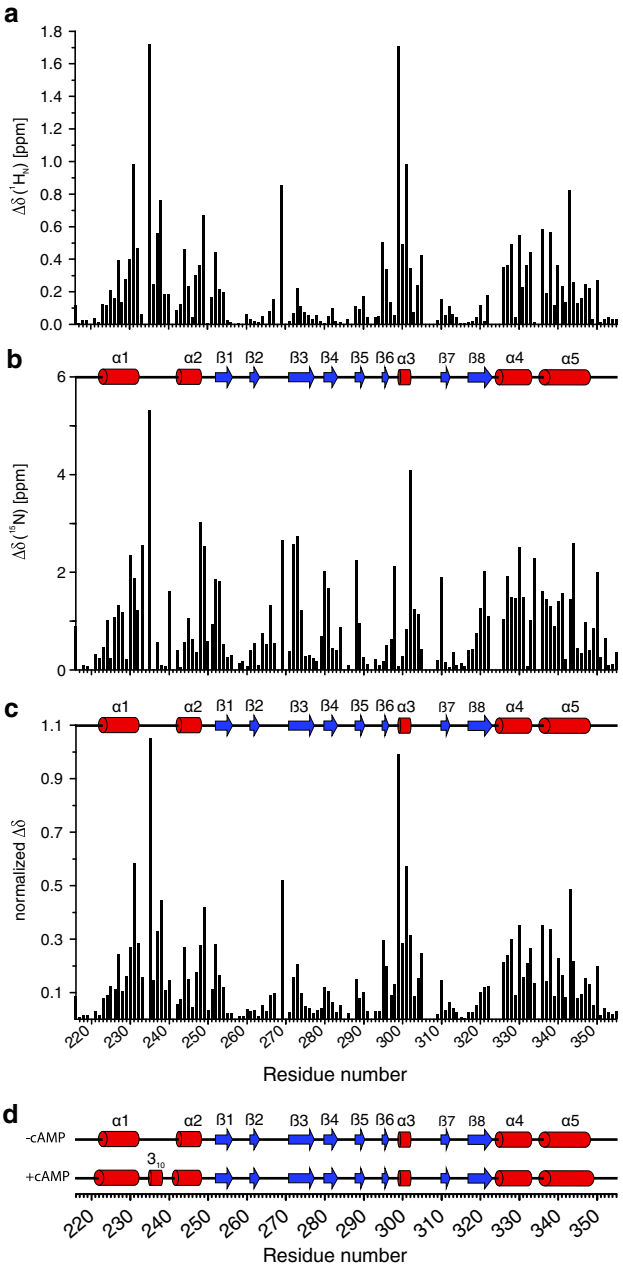

Fig. 2 NMR chemical shift differences between the nucleotide-free and cAMP-bound state (Schünke et al. 2007) of MloK1 CNBD. Change of the amide proton (**a**) and nitrogen (**b**) chemical shifts. The normalized chemical shift differences (**c**) were calculated according to the following equation: $\Delta\delta_{norm.} = [(\Delta\delta H_N/\Delta\delta_{max}H_N)^2 + (\Delta\delta N/10\ \Delta\delta_{max}N)^2]^{1/2}$. **d** Secondary structure elements of the cAMP-bound (*lower line*) and secondary structure prediction for the nucleotide-free MloK1 CNBD based on obtained C^{α}, C^{β}, C' and H^{α} chemical shifts by chemical shift index (*upper line*). Arrows indicate *β*-strand (*blue*) and cylinders helical conformation (*red*). Compared to the cAMP-bound CNBD, only the helical secondary structure content of the unliganded CNBD, especially in the N-terminal region, is slightly decreased

behaviour, between the liganded and unliganded state of the CNBD, this supports the idea that major conformational changes occur on cAMP binding.

Secondary structure prediction based on the C^{α}, C^{β}, C′, and H^{α} chemical shifts lead to the prediction of five α-helical (α1: D222-A232; α2: A242-V248; α3: M299-I302; α4: S324-S333; α5: P335-R348) and eight β-strand (β1: R252-V256; β2: V261-C263; β3: R271-E277; β4: V280-A283; β5: V288-L290; β6: F295-F296; β7: T310-S312; β8: V317-H323) segments (Fig. 2d). Compared to the cAMP-bound CNBD, the secondary chemical shift data suggest a loss of the short 3_{10}-helix between α1 and α2 as well as slightly shortenend N- and C-terminal helices in the unliganded CNBD. This is the first report on structural data of the wildtype MloK1 CNBD.

Acknowledgments This work was supported by a fellowship from the International Research School "BioStruct" to S. Schünke and a research grant from the Helmholtz-Gemeinschaft ("Virtual Institute of Structural Biology") to D. Willbold.

References

Chiu PL, Pagel MD, Evans J, Chou HT, Zeng X, Gipson B, Stahlberg H, Nimigean CM (2007) The structure of the prokaryotic cyclic nucleotide-modulated potassium channel MloK1 at 16 A resolution. Structure 15:1053–1064. doi:10.1016/j.str.2007.06.020

Clayton GM, Silverman WR, Heginbotham L, Morais-Cabral JH (2004) Structural basis of ligand activation in a cyclic nucleotide regulated potassium channel. Cell 119:615–627. doi:10.1016/j.cell.2004.10.030

Cukkemane A, Gruter B, Novak K, Gensch T, Bonigk W, Gerharz T, Kaupp UB, Seifert R (2007) Subunits act independently in a cyclic nucleotide-activated K(+) channel. EMBO Rep 8:749–755. doi:10.1038/sj.embor.7401025

Kaupp UB, Seifert R (2001) Molecular diversity of pacemaker ion channels. Annu Rev Physiol 63:235–257. doi:10.1146/annurev.physiol.63.1.235

Kaupp UB, Seifert R (2002) Cyclic nucleotide-gated ion channels. Physiol Rev 82:769–824. doi:10.1152/physrev.00008.2002

Nimigean CM, Pagel MD (2007) Ligand binding and activation in a prokaryotic cyclic nucleotide-modulated channel. J Mol Biol 371:1325–1337. doi:10.1016/j.jmb.2007.06.030

Nimigean CM, Shane T, Miller C (2004) A cyclic nucleotide modulated prokaryotic K+ channel. J Gen Physiol 124:203–210. doi:10.1085/jgp.200409133

Robinson RB, Siegelbaum SA (2003) Hyperpolarization-activated cation currents: from molecules to physiological function. Annu Rev Physiol 65:453–480. doi:10.1146/annurev.physiol.65.092101.142734

Schünke S, Novak K, Stoldt M, Kaupp UB, Willbold D (2007) Resonance assignment of the cyclic nucleotide binding domain from a cyclic nucleotide-gated K^{+} channel in complex with cAMP. Biomol NMR Assign 1:179–181. doi:10.1007/s12104-007-9049-5

Schünke S, Stoldt M, Novak K, Kaupp UB, Willbold D (2009) Solution structure of the *Mesorhizobium loti* K1 channel cyclic nucleotide-binding domain in complex with cAMP. EMBO Rep 10:729–735. doi:10.1038/embor.2009.68

3.4 Structural insights into conformational changes of a cyclic nucleotide-binding domain in solution from *Mesorhizobium loti* K1 channel

published in: ***Proceedings of the National Academy of Sciences of the United States of America***
Vol. 108, Issue 15, April 2011, Pages: 6121-6126

Sven Schünke[1,2], Matthias Stoldt[1,2], Justin Lecher[1,2],
U. Benjamin Kaupp[3] and Dieter Willbold[1,2]

[1]Institute of Complex Systems,
Structural Biochemistry (ICS-6),
Research Center Jülich,
52425 Jülich,
Germany

[2]Institut für Physikalische Biologie,
Heinrich-Heine-Universität,
40225 Düsseldorf,
Germany

[3]Center of Advanced European Studies and Research (caesar),
Molekulare Neurosensorik,
53175 Bonn,
Germany

Structural insights into conformational changes of a cyclic nucleotide-binding domain in solution from *Mesorhizobium loti* K1 channel

Sven Schünke[a,b], Matthias Stoldt[a,b], Justin Lecher[a,b], U. Benjamin Kaupp[c,1], and Dieter Willbold[a,b,1]

[a]Institute of Complex Systems, Structural Biochemistry (ICS-6), Research Center Jülich, 52425 Jülich, Germany; [b]Institut für Physikalische Biologie, Heinrich-Heine-Universität Düsseldorf, 40225 Düsseldorf, Germany; and [c]Center of Advanced European Studies and Research, Molecular Sensory Systems, 53175 Bonn, Germany

Edited* by Francisco Bezanilla, University of Chicago, Chicago, IL, and approved February 18, 2011 (received for review November 10, 2010)

Cyclic nucleotide-sensitive ion channels, known as HCN and CNG channels, are activated by binding of ligands to a domain (CNBD) located on the cytoplasmic side of the channel. The underlying mechanisms are not well understood. To elucidate the gating mechanism, structures of both the ligand-free and -bound CNBD are required. Several crystal structures of the CNBD from HCN2 and a bacterial CNG channel (MloK1) have been solved. However, for HCN2, the cAMP-free and -bound state did not reveal substantial structural rearrangements. For MloK1, structural information for the cAMP-free state has only been gained from mutant CNBDs. Moreover, in the crystal, the CNBD molecules form an interface between dimers, proposed to be important for allosteric channel gating. Here, we have determined the solution structure by NMR spectroscopy of the cAMP-free wild-type CNBD of MloK1. A comparison of the solution structure of cAMP-free and -bound states reveals large conformational rearrangement on ligand binding. The two structures provide insights on a unique set of conformational events that accompany gating within the ligand-binding site.

NMR solution structure | apo state | ligand removal method | potassium channel

Ion channels activated by cyclic nucleotides play key roles in neuronal excitability and sensory signaling. They belong to two subfamilies: cyclic nucleotide-gated (CNG) channels, and hyperpolarization-activated and cyclic nucleotide-gated (HCN) channels (1–4). CNG channels are voltage independent and require cyclic nucleotides to open, whereas HCN channels are activated by hyperpolarization, and their activity is modulated by cyclic nucleotides. In both channels, ligand binding to an intracellular cyclic nucleotide-binding domain (CNBD) promotes the opening of the channel by conformational changes in the CNBD that propagate via a connecting linker (C linker) to transmembrane segment S6. However, the activation mechanisms are poorly understood in part because the nature of the pore gate is not known precisely (4).

Understanding of the structural rearrangements underlying gating has been greatly advanced by several crystal structures of isolated CNBDs from HCN channels (5–8) and a prokaryotic K^+-selective CNG channel, designated MloK1 (9–11). The MloK1 channel consists of four identical subunits, each encompassing six transmembrane domains (S1–S6), a "GYG" signature sequence for K^+ selectivity, and a conserved CNBD. However, the C linker (approximately 20 residues) is much shorter than the C linker of mammalian CNG and HCN channels (approximately 80 residues) that is important for relaying the binding signal from the CNBD to the channel gate (12–17). In the crystal, the CNBDs from HCN channels are arranged in tetramers, where neighboring C linkers contribute most contacts between subunits (6, 8), whereas the MloK1 CNBD forms a dimer; the dimer interface between the short C linker has been proposed to be involved in channel gating (9, 11). The solution structure solved by nuclear magnetic resonance (NMR) spectroscopy of the monomeric MloK1 CNBD in complex with cAMP (18) is similar to that of the monomers in the dimer crystal (11), except for the C linker, which forms the dimer interface in the crystal structure. Therefore, the C-linker contact in the crystal might have been enforced by packing of dimers. Moreover, in a cryoelectron microscopy structure of the full-length MloK1 channel, the CNBDs appear as independent domains separated by discrete gaps, suggesting that CNBDs are not interacting with each other (19). Furthermore, ligand binding to both the tetrameric MloK1 channel and the monomeric CNBD occurs noncooperatively with similar affinity (20), suggesting that the MloK1 CNBDs are functionally and structurally independent of each other.

To elucidate the mechanism of channel gating in MloK1, knowledge of the CNBD structure in the ligand-free and -bound state is required. Because of the high affinity, cAMP copurifies with the protein and even extensive dialysis fails to remove bound ligand quantitatively (9, 11, 18, 20). For this reason, crystal structures of ligand-free CNBD were obtained from R348A and R307W mutants (9, 11). Both arginine residues are directly involved in cAMP binding and mutation of either one drastically lowers cAMP binding, and thereby allows to prepare ligand-free protein. However, considering the crucial importance of these residues for ligand binding, the mutant structure might not reflect the true wild-type structure and the conformational changes on ligand binding might be altered. We have, therefore, developed a procedure to prepare cAMP-free wild-type protein in quantities sufficient for structure determination. Here, we report the solution structure of the ligand-free CNBD and compare it with the solution structure of the cAMP-bound CNBD and with crystal structures.

Results

Solution Structure of the Wild-Type cAMP-Free CNBD. In this study, we have determined the solution structure of the native unliganded CNBD of the MloK1 channel using NMR spectroscopy. The isolated CNBD shows high affinity for cAMP (K_D = 107 nM) (20) and copurifies with the ligand, which cannot be removed by size-exclusion chromatography or extensive dialysis

Author contributions: S.S., M.S., U.B.K., and D.W. designed research; S.S. and J.L. performed research; S.S. and M.S. analyzed data; and S.S., U.B.K., M.S., and D.W. wrote the paper.

The authors declare no conflict of interest.

*This Direct Submission article had a prearranged editor.

Freely available online through the PNAS open access option.

Data deposition: Resonance assignments and the atomic coordinates for the resulting 15 NMR structures with the lowest target function have been deposited in the BioMagResBank (accession code 16628) and the Protein Data Bank, www.pdb.org (PDB ID code 2KXL), respectively.

[1]To whom correspondence may be addressed. E-mail: dieter.willbold@uni-duesseldorf.de or u.b.kaupp@caesar.de.

This article contains supporting information online at www.pnas.org/lookup/suppl/doi:10.1073/pnas.1015890108/-/DCSupplemental.

(9, 11, 18, 20). For this reason, tightly bound cAMP was either removed by protein denaturation and refolding (20) or by a competition assay (9, 20). The resulting protein sample was free of cAMP, but the final yield was low. For structure determination by NMR spectroscopy or X-ray crystallography, however, large amounts of pure protein are required, preferentially prepared under nondenaturing conditions. We have therefore developed a procedure to prepare wild-type cAMP-free and -bound MloK1 CNBD in quantities sufficient for structure determination. The procedure is based on extensive washing of matrix-bound CNBD–GST fusion protein followed by ion-exchange chromatography that separated cAMP-free from cAMP-bound protein (Fig. S1). The CNBD eluted as two peaks, representing the pure monomeric forms of the cAMP-free and -bound CNBD (Fig. 1).

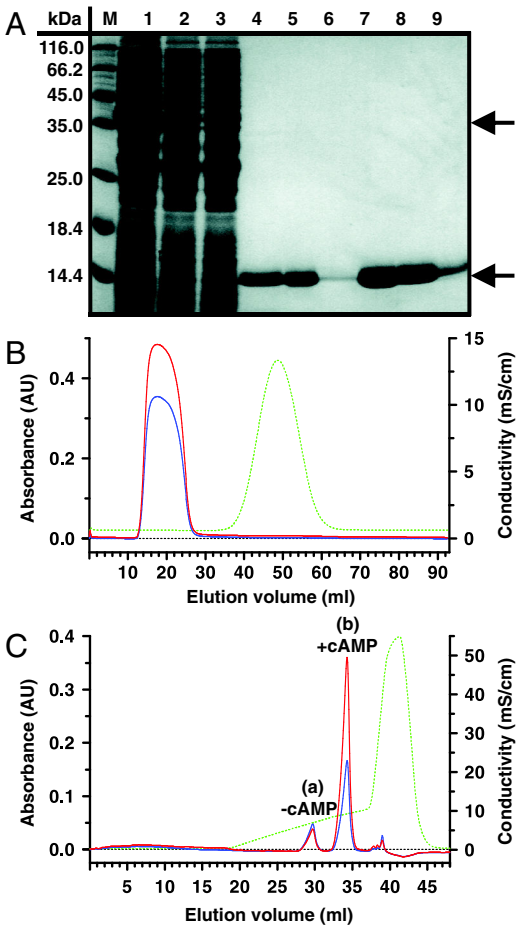

Fig. 1. Purification and characterization of the MloK1 CNBD protein. (*A*) Recombinant MloK1 CNBD-GST fusion protein was expressed in *Escherichia coli* and purified by affinity chromatography (M: marker; lane 1: column input; lane 2–3: nonbound; lane 4–6: elution after major wash and thrombin cleavage; lane 7–9: double amount of protein as in lane 4–6). Upper and lower arrows indicate CNBD-GST fusion and cleaved CNBD protein, respectively. The sizes of the molecular weight markers (M) are indicated. The SDS-polyacrylamide gel was stained with Coomassie blue. (*B*) Size-exclusion chromatogram of CNBD protein desalting step (10 ml sample volume) after affinity chromatography. The CNBD protein was loaded on a HiPrep 26/10 desalting column and the desalting step was monitored at 280 nm (blue line) and 260 nm (red line). The desalting step was followed by measuring the conductivity (green dashed line). (*C*) Final purification of cAMP-free and -bound CNBD protein by cation-exchange chromatography. A Mono S HR 5/5 cation-exchange column was used. The absorption was monitored at 280 nm (blue line) and 260 nm (red line); the conductivity is shown in green (dashed line). cAMP-free and cAMP-bound CNBD protein were separately eluted at 6.92 mS/cm and 9.22 mS/cm, respectively.

The final yield was roughly 7 mg/l cell culture of [U-^{15}N, ^{13}C], or [U-^{15}N] isotopically enriched protein. The absence of the ligand was verified by the 260/280 nm absorbance ratio (values of approximately 0.9 for cAMP-free and approximately 2 for cAMP-bound CNBD), and by NMR spectra. ^{1}H, ^{15}N, and ^{13}C chemical-shift assignment of the unliganded CNBD was almost complete (97% of the backbone and 90% of the side chain CH) using multidimensional heteronuclear NMR spectroscopy with [U-^{15}N]- or [U-^{15}N, ^{13}C] labeled CNBD (21). Assignments have been deposited in the BioMagResBank (accession number 16628). All spectra of the cAMP-free CNBD showed a single set of resonance signals, indicating that the protein is pure and adopts a single conformation. Moreover, the linewidths of the NMR spectra also reflect a monomeric form.

We carried out ^{15}N relaxation experiments to characterize the dynamics and the oligomeric state of the cAMP-free CNBD (Fig. S2). From ^{15}N average longitudinal and transverse relaxation rates of 1.01 ± 0.05 s^{-1} and 13.76 ± 0.10 s^{-1}, respectively, an isotropic rotational correlation time of 8.4 ns was derived. This value is consistent with a CNBD monomer. Nuclear Overhauser enhancement (NOE) cross-peak assignments were obtained by an iterative procedure using a combination of manual and automatic approaches. For the structure calculations, a total of 2,380 intramolecular NOE distance constraints, including 632 long-range NOEs, have been evaluated. In addition, 254 dihedral constraints were derived from chemical-shift data and used for structure calculations. A final ensemble of 15 NMR structures with the lowest CYANA target functions were used to determine the cAMP-free CNBD structure. None of the 15 structures violated NOE distances more than 0.019 nm. No dihedral-angle constraint was violated more than 4°. The vast majority of residues (89.9%) was found in the most favored regions of the Ramachandran plot. The root-mean-squared (rms) displacement of the structure ensemble compared to the average structure was 0.037 nm for backbone and 0.070 nm for all heavy atoms. These data demonstrate that the structure is well defined (Fig. 2*A*). Only the very N- and C-terminal residues (Q216 to R220 and A351 to A355) show higher values of rms displacement and a lower number of NOE-derived distance constraints (Fig. S3). A summary of the distance constraints and structural statistics is given in (Table S1).

The cAMP-free CNBD structure (Fig. 2*B*) features an antiparallel β roll with a short internal α helix, known as phosphate-binding cassette (PBC) similar to other CNBDs from HCN channels (6–8), the cAMP-dependent protein kinase A (PKA) (22, 23), the exchange protein activated by cAMP (Epac) (24), and the catabolite activator protein (CAP) (25), which lacks, however, the

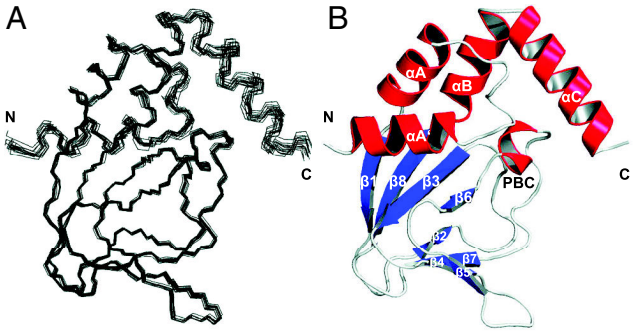

Fig. 2. Solution structure of the wild-type cAMP-free CNBD. (*A*) Superposition of backbone traces of a family of 15 NMR structures with the lowest CYANA target function. Backbone atoms of the amino- and carboxy-terminal ends (residues Q216-R220 and A351-A355, respectively) are not shown and were not used for least-square superposition of the structures. (*B*) Ribbon representation of wild-type cAMP-free CNBD. Secondary structure elements are labeled.

internal α helix. This core element consists of eight antiparallel β strands (β1: R252–V256, β2: V261–C263, β3: R271–E277, β4: V280–V282, β5: V288–L290, β6: F295–F296, β7: V311–A313, β8: V317–H323) and one α helix (PBC helix: E298–I302). The core element is topped by a region of four α helices (αA': F223–A231, αA: P241–A250, αB: S324–S333, αC: P335–R349).

In the cAMP-bound CNBD structure, the binding site is formed by the β roll and the PBC helix that provide interactions with the phosphate and ribose moieties of cAMP. The C-terminal helix αC is placed like a "lid" above the binding pocket and thereby stabilizes the complex. In the cAMP-bound CNBD structure, 25 intermolecular NOE distance constraints between the CNBD and cAMP have been derived. In the cAMP-free form, significant changes in chemical shifts and NOE pattern for atoms located in the binding site and in contact with cAMP have been observed (Fig. S4).

Titration of the Ligand-Free CNBD with cAMP. To verify that the cAMP-free CNBD is functional, cAMP was stepwise added to cAMP-free CNBD and (^{15}N-^{1}H)-HSQC spectra were recorded (Fig. 3*A*). During the initial steps of titration, a second set of NMR signals appeared originating from cAMP-bound CNBD (Fig. 3*B*). At an equimolar ratio of CNBD and cAMP, NMR signals from the cAMP-free protein disappeared, demonstrating that the protein is homogenous with respect to binding of cAMP. Moreover, the HSQC spectrum recorded after cAMP titration is indistinguishable from HSQC spectra of CNBD samples that copurified with cAMP (Fig. 3*C*) (18).

Comparison of the (^{15}N-^{1}H)-HSQC spectra of cAMP-free and -bound CNBD shows that chemical shifts of more than half of the resonances changed on binding (Fig. 3*D*). The chemical-shift differences were mapped on ribbon diagrams of the cAMP-free and -bound structures (Fig. 3 *E* and *F*). Although differences are not localized to a particular region, changes are most prominent in the helical parts rather than the β roll. In particular, a cluster of residues in the cAMP-binding site making contact with cAMP and regions nearby display pronounced differences of their chemical shifts. These differences primarily reflect changes in the chemical environment induced by cAMP. Furthermore, a multitude of resonances from residues located further away from the cAMP-binding site undergo significant changes in their chemical shifts (Fig. 3*D*; e.g., R249, A231, L235, L301, L330, and E336).

Superposition of cAMP-bound and -free CNBD shows that the β roll core is almost identical with an rms displacement of only 0.084 nm (Fig. 4). In contrast, the helical parts show substantial rearrangements between the two forms (rms displacement of

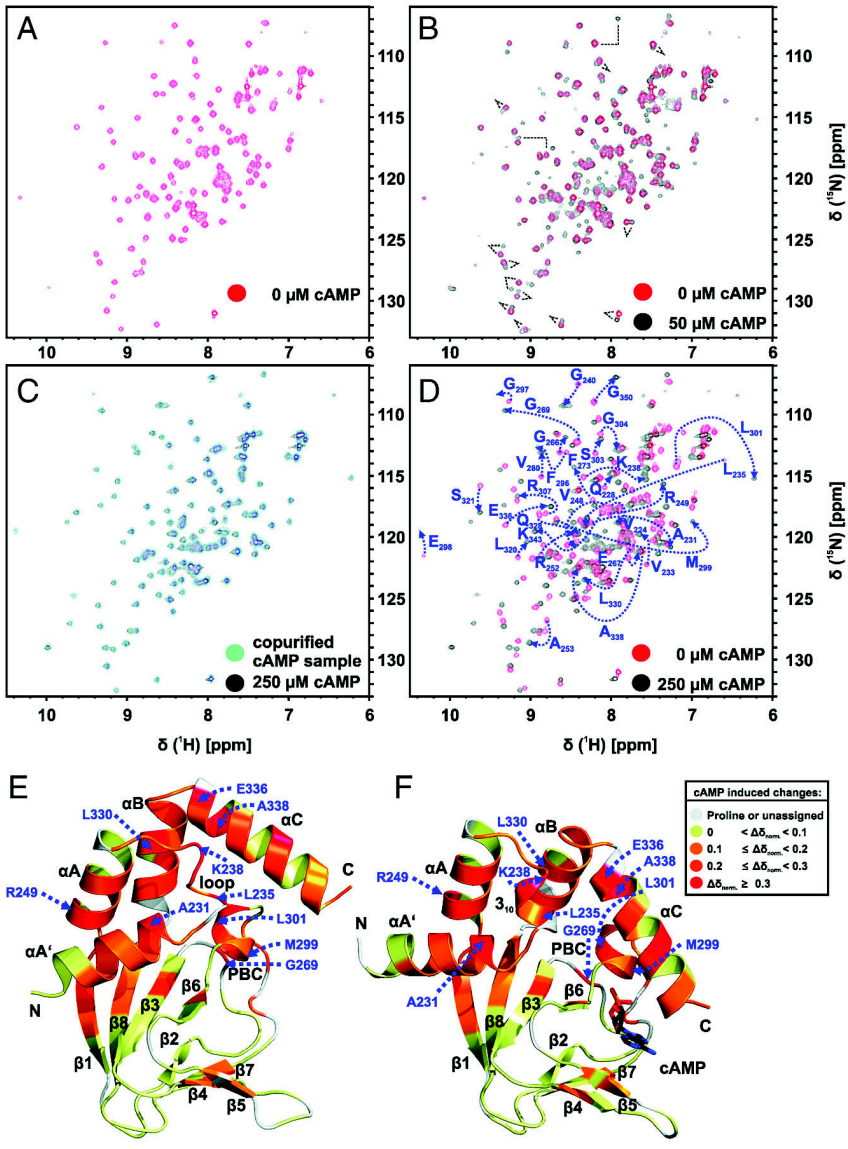

Fig. 3. Titration of cAMP-free CNBD with cAMP. (*A*) 2D (^{15}N–^{1}H)-HSQC spectrum of 0.2 mM cAMP-free [*U*–^{15}N]-labeled CNBD ($T = 25$ °C, 10 mM Tris/HCl, pH 7, 100 mM sodium chloride, 0.2 mM EDTA, 0.02% (w/v) sodium azide, 5% (v/v) $^{2}H_2O$). (*B*) 2D (^{15}N–^{1}H)-HSQC spectrum recorded in the presence of 50 μM cAMP. A second set of NMR signals emerged that originate from CNBD that has bound to cAMP. Two resonance signals characteristic for some amides are highlighted by brackets. Resonance signals of the cAMP-free CNBD spectrum are shown in red. (*C*) 2D (^{15}N–^{1}H)-HSQC spectrum recorded in the presence of 250 μM cAMP. NMR signals originating from cAMP-free CNBD disappeared, proving that all CNBD protein has bound to cAMP. The spectrum is indistinguishable from spectra that were recorded using samples where cAMP copurified with CNBD (shown in blue) and that were reported previously (18). (*D*) Chemical-shift differences of resonance signals between cAMP-free and -bound CNBD; the most pronounced perturbations are highlighted by blue arrows. The chemical-shift differences were mapped on ribbon diagrams of the cAMP-free (*E*) and cAMP-bound (*F*) solution structures. cAMP-induced changes in both spectrum dimensions ($^{1}H_N$ and ^{15}N) were classified according to the following equation: $\Delta\delta_{norm.} = [(\Delta\delta^{1}H_N/\Delta\delta_{max}{}^{1}H_N)^2 + (\Delta\delta^{15}N/10\cdot\Delta\delta_{max}{}^{15}N)^2]^{1/2}$. The cAMP molecule is shown in stick representation.

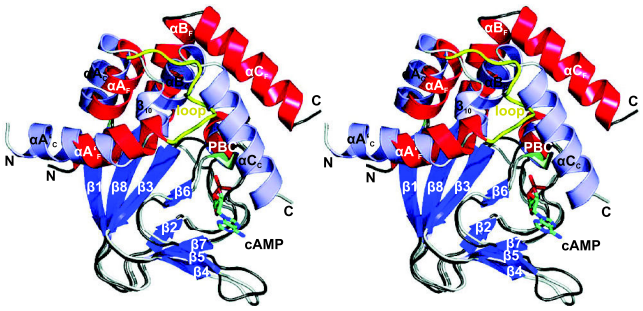

Fig. 4. Structure comparison of cAMP-free and -bound CNBD. Stereoview of the cAMP-free and -bound CNBD structure overlay. The helical portion of the cAMP-bound and cAMP-free CNBD is shown in white and red, respectively. β strands in both structures are shown in blue, and the N-terminal loop region in the cAMP-free structure is highlighted in yellow. Secondary structure elements are labeled (label "$_C$" stands for "cAMP-bound state"; label "$_F$" stands for "cAMP-free state").

0.271 nm). The orientation of all helices, in particular αA', αB, and αC, with respect to the β roll differs remarkably in the two structures, whereas the position of αB and αC relative to each other is similar: The angle between the two helices in the cAMP-free and -bound state is 65.5° and 60.5°, respectively (rms displacement of 0.053 nm for αB-turn-αC). This almost static behavior is likely mediated by hydrophobic interactions between residues F327 and F341 in αB and αC, respectively (Fig. S5). In the cAMP-free state, a network of mainly hydrophobic interactions is observed within the helical region and those parts of the β roll that form the interface with the helical region [including residues in αA' (W227, L229, V230, A231), loop region between αA' and αA (L235, F236, L239), αA (V243, L244, I247, V248), PBC helix (L301), αB (F327, L330), αC (F341, I340, I337), β3 (M272, F274, V276), and β8 (L322)]. These interactions are also present in the cAMP-bound state, in addition to the hydrophobic interactions of residues in the 3_{10}-helix (V233), αA (L251), PBC helix (I302), αB (M329), αC (A345), β1 (A253), β6 (F295), and β8 (L320).

The movement of αC is accompanied by a substantial displacement of other helical parts right up to the N-terminal helix αA', and residues in the helical parts undergo a significant change in their chemical shift (e.g., A231, L235, K238, R249, G269, M299, L301, L330, E336, and A338; Fig. 3 *D–F*). For example, the position of two residues D222 and P234 located in the αA' and loop region, respectively, shifted by 0.8 nm relative to their position in the cAMP-bound structure. In the cAMP-bound state, a short 3_{10}-helix formed by residues P234 to K238 is located between αA' and αA. This 3_{10}-helix is adjacent to αC. In particular, L235 and K238 of the 3_{10}-helix undergo hydrophobic interactions with I337, I340, and F341 in αC. This short 3_{10}-helix is absent in the cAMP-free state. However, residues in this loop region show heteronuclear NOE values close to 0.8, indicating a rather rigid region. Furthermore, residues L235, F236, K238, and L239 in this loop region show hydrophobic interactions similar to residues I337, I340, and F341 located in αC. These interactions might be responsible for the fixed orientation of αC.

The cAMP-Free CNBD Is Rigid. Hydrogen exchange of protons can provide valuable information on a protein's local flexibility, structure, and function (26–28). The proton-deuterium exchange rates provide information on slow internal motions (slower than minutes) that permit breaking of hydrogen bonds whereby labile protons can exchange with the solvent (29). The exchange rates of the cAMP-free and -bound state have been determined by a set of sequentially recorded (^{15}N-^{1}H)-HSQC spectra (Fig. S6).

In both states, residues in the β roll showed slow exchange rates, indicating that the β roll is structurally rigid (Fig. S6). Calculated protection factors indicate that parts of β1, β3, and β8 are even more protected in the cAMP-free compared to the cAMP-bound state (Fig. S6 *E* and *G*). This might be due to the spatial rearrangement of αA', which covers more of the β sheet in the cAMP-free state. However, exchange rates of the helical parts revealed major differences. In the cAMP-free state, only residues in the αA helix exhibited slow exchange rates (Fig. S6 *A*, *C*, and *G*), perhaps reflecting a specific interaction between αA' and αA, whereby αA becomes shielded from the solvent. Furthermore, αA and the β roll present the structurally most invariant parts of the CNBD. Amide protons of all other helices were already exchanged before recording of the first HSQC spectrum (600 s after dissolving protein in D_2O). In contrast, in the cAMP-bound state, residues forming the cAMP-binding pocket displayed slower exchange rates (e.g., E298, A301, R307, V282, V288, L290, and V311; Fig. S6 *B*, *D*, and *F*). Additionally, amide protons of a cluster of residues in the hinge region (αB), in αC, and in the PBC helix exhibited slow exchange rates (e.g., F327, M329 to C331 and A338 to R342). However, helical propensities calculated from secondary ^{13}C chemical shifts do not differ substantially for both states (Fig. S5*C*).

Furthermore, we carried out heteronuclear steady-state {^{1}H}-^{15}N-NOE experiments to characterize the dynamic behavior of the cAMP-free CNBD on a subnanosecond time scale (30, 31). Heteronuclear NOE values are sensitive to dynamics of the local environment. Positive values close to 0.8 are expected in the absence of rapid internal motions of protein backbone N-H bond vectors, whereas values <0.8 reveal fast internal motions; for highly mobile residues, NOE values even might become negative.

Most residues of the cAMP-free CNBD show heteronuclear NOE values close to 0.8 (with an average value of 0.75 for residues G221 to G350), indicating a rigid fold (Fig. S2). However, residues of the very N- and C-terminal regions (Q216 to R219 and G350 to A355) exhibit higher values of average local displacement and a lower number of NOE-derived distance constraints (Fig. S3). The small heteronuclear NOE values for these residues support the idea that the N- and C-terminal ends (five residues each) are more flexible.

Discussion

Previously, crystal structures were reported from two CNBD mutants R307W and R348A. These two Arg residues undergo key interactions with the ligand and their replacement lowers the cAMP affinity by >100-fold (9, 11, 20). Arg 307 makes Coulomb contact with the charged phosphoryl group of cAMP, which perhaps represents the first step of binding. During or after seating of the ligand in the β roll, the αC helix repositions and stacks on top of the cAMP purine ring to cap the mouth of the cavity, and the side chain of R348 undergoes an ion-pair interaction with E298 in the PBC. In a total of six crystal structures from these two mutants, the αC position varies considerably over large distances and is even disordered or unwound (9). The different structures might either reflect unique crystal environments or a conformational space that is explored by αC movements, or might represent functional intermediates during repositioning of αC. Moreover, all crystal structures of the CNBDs in the cAMP-free and -bound state (9, 11) reveal a dimer in the asymmetric unit. In solution, however, the CNBD exists as a monomer (18). The interactions within the dimer interface might also induce changes in the β roll or the αB and αC helices. Given the functional importance of the two Arg residues, the position of the αC helix, and the potential functional implications of the C-linker interface, it seems necessary to resolve the structure of the wild-type CNBD in either state by an independent technique.

The overall fold of the monomeric, cAMP-free state reported here is similar to the monomer structure in the dimer crystal (Fig. 5). The backbone coordinates for residues in the β roll are virtually identical (rms displacement value of approximately

0.07 nm). However, three major differences in αA' and αC helices and the $\beta4/\beta5$ loop come to light when comparing the solution and crystal coordinates. First, in the solution structure, the N-terminal αA' helix is straight rather than bent in the crystal structures. Consequently, the rms displacement values are largest for this segment of the superimposed solution and crystal structures (0.17 and 0.22 nm). A similar observation has been made for the cAMP-bound state (18). Second, the position of αC differs remarkably (rms displacement values for αC backbone coordinates of 0.24 to 0.57 nm between solution and all crystal structures). The ensemble of αC positions has been attributed to a looser conformation of the cAMP-free state and the enhanced flexibility might allow αC to sample a conformational space during binding. In contrast to the various crystal structures, the αC helix in the solution structure is rigid and adopts a single orientation. This conclusion is supported by various NMR spectroscopic parameters, including ^{15}N relaxation measurements (Fig. S2), a large number of long-range NOEs between αC and other parts of the molecule (Fig. S5*B*), and a high helical propensity as calculated from secondary ^{13}C chemical shifts (Fig. S5*C*).

In a similar vein, the $\beta4/\beta5$ hairpin in the crystal adopts a single conformation in the cAMP-bound state but adopts multiple orientations in the absence of the ligand (9). The $\beta4/\beta5$ hairpin is situated near the mouth of the binding pocket. On binding, the hairpin closes around the ligand. Thus, cAMP is sandwiched between R348 and three hydrophobic residues in the hairpin that can undergo van der Waals interaction with the purine ring of cAMP. However, in the solution structure of the cAMP-free state, the hairpin adopts a single conformation that is not significantly different from the conformation in the liganded state (Figs. 4 and 5).

We tentatively conclude that the conformations of some exposed regions are particularly sensitive to packing in the crystal and, therefore, might reflect different crystal environments rather than a functionally important conformational ensemble that becomes "frozen" in the crystal. A case in point is the HCN2 channel. The structures of the CNBD in the free and bound state of HCN2 (7, 8) are almost identical except for a coil-to-helix transition (αF'). This transition resembles the formation of the 3_{10}-helix in MloK1 CNBD, which occupies a similar position as αF'. However, rearrangements of the helical parts were not observed (Fig. S7). This surprising finding might result from crystal contacts in the αC helix region that lock the helix in a nonphysiological conformation (7). From experiments using transition metal ion FRET, it was argued that the αC helix is partially unstructured in the cAMP-free state and adopts a more α helical structure on ligand binding (7). In CAP, on cAMP binding, a coil-to-helix transition occurs that extends αC by three turns. (32). For the MloK1 channel, there is no evidence that the αC segment undergoes major changes either in secondary structure or length.

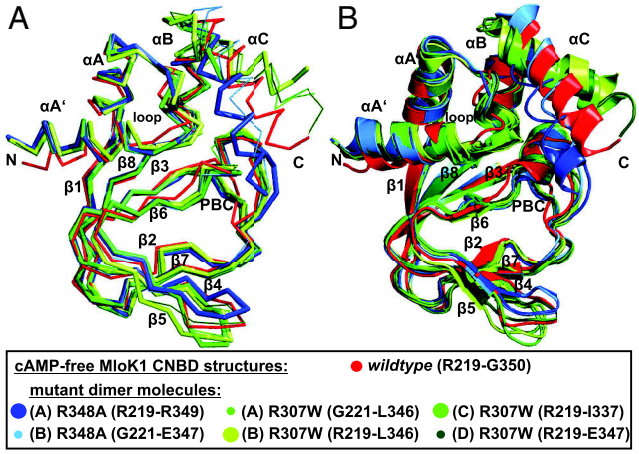

Fig. 5. Comparison of the monomeric cAMP-free wild-type solution structure with structures of mutant dimers in the crystal. (*A*) Superposition of backbone traces for all cAMP-free structures [wild-type PDB ID code 2KXL, R348A mutant dimer (11), molecules A and B, PDB ID code 1U12, R307W mutant dimer (9), molecules A–D, PDB ID code 3CO2]. (*B*) Superposition of ribbon representations for all cAMP-free structures. The least-square superposition of the structures was done using the backbone atoms of the β roll strands.

The solution structures of the cAMP-free and -bound CNBD, allow to reconstruct, unbiased by mutations or crystal contacts, the sequence of dynamical events that propagate through the binding fold on cAMP binding. There are commonalities and differences among different CNBDs. All CNBDs share a common fold consisting of a β roll and an α helical bundle. A common feature is also a lid region that caps the binding cavity of the β roll. In all CNBDs, except Epac, the αC helix forms the lid. Epac is lacking an αC helix; instead three β strands form the lid. Another commonality might be the structural rearrangements that move the hinge-lid region closer to the binding pocket. The PBC, αB, and αC put up a cavity that is filled with hydrophobic side chains that probably fix the relative position of these three helical elements (Fig. S5*A*). These hydrophobic residues (L301, F327, and F341) are highly conserved in almost all CNBDs. On ligand binding, the PBC is displaced, allowing the hydrophobic residues to enter the void, which gives rise to a tilting movement of the hinge-lid region. This mechanism has been first proposed for Epac (24, 33, 34). These structural rearrangements, however, are differently relayed to the effector domains that are located either N- or C-terminally of the CNBD. In ion channels, the signal is transferred via an N-terminal helix bundle to the transmembrane segment S6, involving the body movement of $\alpha B/\alpha C$ toward the β roll, the formation of a short 3_{10}-helix in the loop between αA' and αA, a sliding movement of αA' across the surface of the β roll, and displacement of αA relative to αA' (Movie S1). Although these structural rearrangements may serve as guideline, the "gating movements" in the CNBDs of other CNG or HCN channels might be different. Crucial amino acids like R348 in αC or the F327/F341 pair are absent in classic CNG channels. Moreover, classic CNG and HCN channels are cooperatively activated by ligand or voltage, respectively. The allosteric mechanisms involve intersubunit contacts between long C linkers (4); the C-linker interface seems to be less important in MloK1 or CNGK channels that are activated noncooperatively (4, 20, 35). In contrast, in CAP, Epac, and PKA the signal is relayed to the DNA-binding domain or catalytic sites, respectively, that are located in the C terminus.

To delineate the sequence of events, conformational movements need to be resolved with high spatio-temporal accuracy. One way to provide such structural information is the use of double electron-electron resonance (DEER) technique (36, 37). If combined with rapid-mixing techniques, DEER could provide a distance map of selected residues along the reaction pathway and, thereby, reveal the pattern of conformational movements. Thus CNG channels hold great promise to further our understanding of the interplay between ligand binding and gating.

Materials and Methods

Protein Preparation. Isotopically labeled MloK1 CNBD samples for NMR studies were prepared as detailed described in *SI Text*. NMR samples contained 0.5 mM [*U*-^{15}N] or [*U*-^{15}N, ^{13}C] labeled CNBD in aqueous solution.

NMR Spectroscopy, Data Evaluation, and Structure Calculation. A detailed description about NMR experiments, data evaluation and structure calculation is provided in *SI Materials and Methods*. In brief, the procedures were as follows. All NMR experiments were performed at 298 K on Varian ^{Unity}INOVA and VNMRS instruments, equipped with a cryogenic Z-axis pulse-field-gradient (PFG) triple resonance probe at proton frequencies of 800 and 600 MHz. Backbone and side chain assignments of cAMP-free and -bound CNBD were obtained using heteronuclear standard experiments as reported previously

(21, 38). All NMR spectra were processed using NMRPipe (39) and evaluated in CARA (40). Nuclear Overhauser Effect (NOE) distance constraints for structure calculations were derived from three- and two-dimensional NOESY experiments. NOE cross-peak assignments were obtained by an iterative procedure using a combination of manual and automatic steps. CARA was used to evaluate NOE spectra and to manually assign nearly all of the apparently unambiguous NOE distance constraints. NOE cross-peak intensities were classified as strong, medium, and weak, corresponding to upper limit distance constraints of 2.7, 3.8, and 5.5 Å, respectively. For NOE cross peaks involving methyl groups upper limit distance constraints of 2.9, 4.0, and 5.7 Å were used. Structure calculation was done with CYANA (41) using the standard protocol for simulated annealing. Using manually assigned NOEs an initial fold of the protein was calculated. Additional NOEs were automatically assigned in an iterative approach using ATNOS/CANDID (42, 43) algorithms in combination with CYANA. Dihedral-angle constraints and helical propensities were determined by TALOS (44, 45). Geometry of the resulting structures, structural parameters, and secondary structure elements were analyzed and visualized using the following programs: MOLMOL (46), PyMOL (47), MolProbity (48), and PROCHECK (49).

^{15}N longitudinal (R_1) and transverse (R_2) relaxation rates, together with the steady-state $\{^1H\}$-^{15}N-NOE, were recorded at 298 K on a [*U*-^{15}N] labeled protein sample using standard methods (30) at 600 MHz and 800 MHz proton frequency. The correlation time was determined for an isotropic tumbling model using the TENSOR2 (50) package. NMR titration experiments were carried out at 298 K using [*U*-^{15}N] labeled unliganded MloK1 CNBD sample. A set of (^{15}N-^{1}H)-HSQC spectra were recorded with increasing ligand concentrations. Proton-deuterium exchange experiments were performed at 298 K. Slowly exchanging amide protons were identified by sequently recording a set of two-dimensional SOFAST (^{15}N-^{1}H)-HMQC (51) spectra after dissolving the freeze-dried CNBD samples in D_2O. The last spectrum was recorded after 14 h for the cAMP-free and 24 h for the cAMP-bound CNBD.

ACKNOWLEDGMENTS. This study was supported by a fellowship from the International Research School BioStruct to S.S. and a research grant from the Helmholtz–Gemeinschaft (Virtual Institute of Structural Biology) to D.W.

1. Kaupp UB, Seifert R (2001) Molecular diversity of pacemaker ion channels. *Annu Rev Physiol* 63:235–257.
2. Kaupp UB, Seifert R (2002) Cyclic nucleotide-gated ion channels. *Physiol Rev* 82:769–824.
3. Robinson RB, Siegelbaum SA (2003) Hyperpolarization-activated cation currents: From molecules to physiological function. *Annu Rev Physiol* 65:453–480.
4. Cukkemane A, Seifert R, Kaupp UB (2011) Cooperative and uncooperative cyclic-nucleotide-gated ion channels. *Trends Biochem Sci* 36:55–64.
5. Craven KB, Zagotta WN (2006) CNG and HCN channels: Two peas, one pod. *Annu Rev Physiol* 68:375–401.
6. Flynn GE, Black KD, Islas LD, Sankaran B, Zagotta WN (2007) Structure and rearrangements in the carboxy-terminal region of SpIH channels. *Structure* 15:671–682.
7. Taraska JW, Puljung MC, Olivier NB, Flynn GE, Zagotta WN (2009) Mapping the structure and conformational movements of proteins with transition metal ion FRET. *Nat Methods* 6:532–537.
8. Zagotta WN, et al. (2003) Structural basis for modulation and agonist specificity of HCN pacemaker channels. *Nature* 425:200–205.
9. Altieri SL, et al. (2008) Structural and energetic analysis of activation by a cyclic nucleotide binding domain. *J Mol Biol* 381:655–669.
10. Clayton GM, Altieri S, Heginbotham L, Unger VM, Morais-Cabral JH (2008) Structure of the transmembrane regions of a bacterial cyclic nucleotide-regulated channel. *Proc Natl Acad Sci USA* 105:1511–1515.
11. Clayton GM, Silverman WR, Heginbotham L, Morais-Cabral JH (2004) Structural basis of ligand activation in a cyclic nucleotide regulated potassium channel. *Cell* 119:615–627.
12. Gordon SE, Zagotta WN (1995) Localization of regions affecting an allosteric transition in cyclic nucleotide-activated channels. *Neuron* 14:857–864.
13. Johnson JP, Jr, Zagotta WN (2001) Rotational movement during cyclic nucleotide-gated channel opening. *Nature* 412:917–921.
14. Paoletti P, Young EC, Siegelbaum SA (1999) C-Linker of cyclic nucleotide-gated channels controls coupling of ligand binding to channel gating. *J Gen Physiol* 113:17–34.
15. Wang J, Chen S, Siegelbaum SA (2001) Regulation of hyperpolarization-activated HCN channel gating and cAMP modulation due to interactions of COOH terminus and core transmembrane regions. *J Gen Physiol* 118:237–250.
16. Zhou L, Siegelbaum SA (2007) Gating of HCN channels by cyclic nucleotides: Residue contacts that underlie ligand binding, selectivity, and efficacy. *Structure* 15:655–670.
17. Zong X, Zucker H, Hofmann F, Biel M (1998) Three amino acids in the C-linker are major determinants of gating in cyclic nucleotide-gated channels. *EMBO J* 17:353–362.
18. Schünke S, Stoldt M, Novak K, Kaupp UB, Willbold D (2009) Solution structure of the *Mesorhizobium loti* K1 channel cyclic nucleotide-binding domain in complex with cAMP. *EMBO Rep* 10:729–735.
19. Chiu PL, et al. (2007) The structure of the prokaryotic cyclic nucleotide-modulated potassium channel MloK1 at 16 A resolution. *Structure* 15:1053–1064.
20. Cukkemane A, et al. (2007) Subunits act independently in a cyclic nucleotide-activated K(+) channel. *EMBO Rep* 8:749–755.
21. Schünke S, Lecher J, Stoldt M, Kaupp UB, Willbold D (2010) Resonance assignments of the nucleotide-free wildtype MloK1 cyclic nucleotide-binding domain. *Biomol NMR Assign* 4:147–150.
22. Diller TC, Madhusudan, Xuong NH, Taylor SS (2001) Molecular basis for regulatory subunit diversity in cAMP-dependent protein kinase: Crystal structure of the type II beta regulatory subunit. *Structure* 9:73–82.
23. Su Y, et al. (1995) Regulatory subunit of protein kinase A: Structure of deletion mutant with cAMP binding domains. *Science* 269:807–813.
24. Rehmann H, et al. (2003) Structure and regulation of the cAMP-binding domains of Epac2. *Nat Struct Biol* 10:26–32.
25. Weber IT, Steitz TA (1987) Structure of a complex of catabolite gene activator protein and cyclic AMP refined at 2.5 A resolution. *J Mol Biol* 198:311–326.
26. Hvidt A, Nielsen SO (1966) Hydrogen exchange in proteins. *Adv Protein Chem* 21:287–386.
27. Jeng MF, Dyson HJ (1995) Comparison of the hydrogen-exchange behavior of reduced and oxidized *Escherichia coli* thioredoxin. *Biochemistry* 34:611–619.
28. Taylor SS, et al. (2004) PKA: A portrait of protein kinase dynamics. *Biochim Biophys Acta* 1697:259–269.
29. Wagner G, Wüthrich K (1982) Amide protein exchange and surface conformation of the basic pancreatic trypsin inhibitor in solution. Studies with two-dimensional nuclear magnetic resonance. *J Mol Biol* 160:343–361.
30. Kay LE, Torchia DA, Bax A (1989) Backbone dynamics of proteins as studied by 15N inverse detected heteronuclear NMR spectroscopy: Application to staphylococcal nuclease. *Biochemistry* 28:8972–8979.
31. Yao J, Chung J, Eliezer D, Wright PE, Dyson HJ (2001) NMR structural and dynamic characterization of the acid-unfolded state of apomyoglobin provides insights into the early events in protein folding. *Biochemistry* 40:3561–3571.
32. Popovych N, Tzeng SR, Tonelli M, Ebright RH, Kalodimos CG (2009) Structural basis for cAMP-mediated allosteric control of the catabolite activator protein. *Proc Natl Acad Sci USA* 106:6927–6932.
33. Rehmann H, Wittinghofer A, Bos JL (2007) Capturing cyclic nucleotides in action: snapshots from crystallographic studies. *Nat Rev Mol Cell Biol* 8:63–73.
34. Rehmann H, et al. (2008) Structure of Epac2 in complex with a cyclic AMP analogue and RAP1B. *Nature* 455:124–127.
35. Bönigk W, et al. (2009) An atypical CNG channel activated by a single cGMP molecule controls sperm chemotaxis. *Sci Signal* 2:ra68.
36. Altenbach C, Kusnetzow AK, Ernst OP, Hofmann KP, Hubbell WL (2008) High-resolution distance mapping in rhodopsin reveals the pattern of helix movement due to activation. *Proc Natl Acad Sci USA* 105:7439–7444.
37. Fleissner MR, et al. (2009) Site-directed spin labeling of a genetically encoded unnatural amino acid. *Proc Natl Acad Sci USA* 106:21637–21642.
38. Schünke S, Novak K, Stoldt M, Kaupp UB, Willbold D (2007) Resonance assignment of the cyclic nucleotide binding domain from a cyclic nucleotide-gated K^+ channel in complex with cAMP. *Biomol NMR Assign* 1:179–181.
39. Delaglio F, et al. (1995) NMRPipe: A multidimensional spectral processing system based on UNIX pipes. *J Biomol NMR* 6:277–293.
40. Keller R (2004) *The Computer Aided Resonance Assignment Tutorial* (Cantina, Zurich).
41. Güntert P, Mumenthaler C, Wüthrich K (1997) Torsion angle dynamics for NMR structure calculation with the new program DYANA. *J Mol Biol* 273:283–298.
42. Herrmann T, Güntert P, Wüthrich K (2002) Protein NMR structure determination with automated NOE-identification in the NOESY spectra using the new software ATNOS. *J Biomol NMR* 24:171–189.
43. Herrmann T, Güntert P, Wüthrich K (2002) Protein NMR structure determination with automated NOE assignment using the new software CANDID and the torsion angle dynamics algorithm DYANA. *J Mol Biol* 319:209–227.
44. Cornilescu G, Delaglio F, Bax A (1999) Protein backbone angle restraints from searching a database for chemical shift and sequence homology. *J Biomol NMR* 13:289–302.
45. Shen Y, Delaglio F, Cornilescu G, Bax A (2009) TALOS+: A hybrid method for predicting protein backbone torsion angles from NMR chemical shifts. *J Biomol NMR* 44:213–223.
46. Koradi R, Billeter M, Wüthrich K (1996) MOLMOL: A program for display and analysis of macromolecular structures. *J Mol Graphics* 14:51–32.
47. DeLano W (2002) *The PyMOL Molecular Graphics System* (DeLano Scientific, San Carlos, CA).
48. Davis IW, et al. (2007) MolProbity: All-atom contacts and structure validation for proteins and nucleic acids. *Nucleic Acids Res* 35:W375–W383.
49. Laskowski RA, MacArthur MW, Moss DS, Thornton JM (1993) *PROCHECK*: A program to check the stereochemical quality of protein structures. *J Appl Crystallogr* 26:283–291.
50. Dosset P, Hus JC, Blackledge M, Marion D (2000) Efficient analysis of macromolecular rotational diffusion from heteronuclear relaxation data. *J Biomol NMR* 16:23–28.
51. Schanda P, Brutscher B (2005) Very fast two-dimensional NMR spectroscopy for real-time investigation of dynamic events in proteins on the time scale of seconds. *J Am Chem Soc* 127:8014–8015.

Supporting Information

Schünke et al. 10.1073/pnas.1015890108

SI Materials and Methods

NMR Sample Preparation. MloK1 CNBD was expressed as a fusion protein with glutathione S-transferase. Details of cloning, expression of [*U*-^{15}N, ^{13}C] or [*U*-^{15}N]-isotopically labeled recombinant CNBD protein, and cell lysis were described previously (1, 2). After cell lysis soluble and insoluble fractions were separated by centrifugation (50,000 × *g* for 30 min at 4 °C). The supernatant was passed over a glutathione-Sepharose 4B column (30 ml bed volume) equilibrated with cold 1 × PBS buffer (pH 7.4). After the supernatant has been applied, the column was washed with 10 column volumes of cold 1 × PBS binding buffer and about 8 liter washing buffer (50 mM MES, pH 6.5, 100 μM EDTA, 50 mM NaCl) overnight. Furthermore the column was washed with 1 × PBS buffer followed by incubation with thrombin for cleavage of the CNBD domain from the GST tag. Thrombin cleavage yielded the isolated cyclic nucleotide binding domain (Q216 to A355) with additional glycine and serine residues at the N terminus. Cleaved CNBD protein was eluted with two and a half column volumes of 1 × PBS buffer. Cleavage and final purity of CNBD protein after affinity chromatography were evaluated by SDS/PAGE analysis. The buffer was immediately exchanged to buffer A (10 mM MES, pH 6, 100 μM EDTA) on a HiPrep 26/10 desalting column mounted on an Äkta purifier system (GE Healthcare). The desalting step was monitored at 280 nm and 260 nm. Performance of the desalting step was observed by measuring the conductivity. Subsequently ion-exchange chromatography was used to separate both domains, cAMP-free and cAMP-bound CNBD. A cation-exchange chromatography column Mono S HR 5/5 (GE Healthcare) was used and the absorption was monitored at 260 and 280 nm. Buffer A was used as binding buffer and elution was directed with buffer A supplied with 1 M NaCl (buffer B). cAMP-free and -bound CNBD protein was separately eluted and the respective fractions were pooled. cAMP-free and -bound CNBD were dialyzed against buffer C (10 mM potassium phosphate, pH 7, 100 mM potassium chloride, 100 μM EDTA, 0.02% (w/v) sodium azide) and buffer D (10 mM Tris/HCl, pH 7, 100 mM sodium chloride, 200 μM EDTA, 0.02% (w/v) sodium azide), respectively. CNBD was concentrated with an Amicon stirred system (Ultracel PL-3, 3 kDa molecular weight cutoff, Millipore). During the final concentration steps the buffer was exchanged by four volumes of the respective NMR buffer including 5% (v/v) $^{2}H_2O$ and deuterated Tris (D11, 98%, Cambridge Isotope Laboratories)/HCl. The protein concentration was determined with Bradford assay (BioRad). NMR samples contained 0.5 mM [*U*-^{15}N] or [*U*-^{15}N, ^{13}C] labeled CNBD in aqueous solution.

NMR Spectroscopy. Nuclear Overhauser Effect (NOE) distance constraints for structure calculations were derived from three-dimensional (^{1}H-^{1}H-^{15}N)-NOESY-HSQC (3) (120 ms mixing time), aliphatic (^{1}H-^{13}C-^{1}H)-HSQC-NOESY (100 ms mixing time), aromatic (^{1}H-^{13}C-^{1}H)-HSQC-NOESY (4) (140 ms mixing time) and two-dimensional aromatic (^{1}H-^{13}C-^{1}H)-HSQC-NOESY (100 ms mixing time) experiments.

For the characterization of overall and internal motions, ^{15}N longitudinal (R_1) and transverse (R_2) relaxation rates, together with the steady-state {^{1}H}-^{15}N-NOE, were recorded at 298 K on a [*U*-^{15}N] labeled protein sample using standard methods at 600 MHz and 800 MHz proton frequency. Peak integral values were obtained by fitting signals to an adjustable "peak model" shape using the program CARA (5). A superposition of Lorentz and Gauss functions was employed and adjusted manually and independently for both spectral dimensions. For ^{15}N R_1 measurement relaxation delay values of 11, 65, 141, 249, 380, 542, 758, and 1192 ms were applied. For R_2 delays of 10, 30, 50, 70, 90, 110, and 150 ms were used. Data of R_1 and R_2 relaxation experiments were fitted to a mono-exponential decay using the program CurveFit (A.G. Palmer, Columbia University). The correlation time was determined for an isotropic tumbling model using the TENSOR2 (6) package. {^{1}H}-^{15}N-NOE-TROSY spectra (7–9) were acquired with 2.5 s proton saturation.

Proton-deuterium exchange experiments were performed at 298 K. Slowly exchanging amide protons were identified by sequentially recording a set of two-dimensional SOFAST (^{15}N-^{1}H)-HMQC (10) spectra using 0.5 mM [*U*-^{15}N] labeled MloK1 CNBD samples, either in the absence or presence of cAMP, which were lyophilized and resolved in deuterium oxide. The first (^{15}N-^{1}H)-HSQC data points were obtained after a delay of roughly 5 minutes, the last spectrum was recorded after 14 hours for the cAMP-free and 24 hours for the cAMP-bound CNBD. Total measuring time of each experiment was 10.83 and 6.67 minutes for the cAMP-free and -bound MloK1 CNBD, respectively. Relative cross-peak intensities were extracted and fitted using a mono-exponential decay to determine the exchange rate (k_{ex}).

Titration experiments were carried out to a 0.2 mM [*U*-^{15}N] labeled unliganded MloK1 CNBD sample by stepwise addition of small aliquots of concentrated cAMP stock solutions (Sigma-Aldrich). Eight (^{15}N-^{1}H)-HSQC spectra were recorded with increasing ligand concentrations of 5, 10, 25, 50, 75, 100, 250, and 500 μM cAMP.

Data Evaluation and Structure Calculation. Based on an almost complete assignment of ^{1}H, ^{15}N, and ^{13}C resonances of cAMP-free CNBD, NOE cross peak assignments were obtained by an iterative procedure using a combination of manual and automatic steps. CARA was used to evaluate NOE spectra and to manually assign nearly all of the apparently unambiguous NOE distance constraints. NOE cross-peak intensities were classified as strong, medium and weak, corresponding to upper limit distance constraints of 2.7, 3.8, and 5.5 Å, respectively. Intensities of NOE cross-peaks between protons of known distances were used for calibration. For NOE cross-peaks involving methyl groups upper limit distance constraints of 2.9, 4.0, and 5.7 Å for strong, medium or weak interactions were used. Structure calculations were performed using the program CYANA (11). CYANA runs were performed according to the protocol for simulated annealing with 100 randomly generated starting conformations, 25,000 steps torsion angle dynamics and subsequent 2,000 conjugate gradients minimization steps. Using only manually assigned NOE cross-peaks an initial fold of the protein was calculated. Additional NOE cross-peaks were automatically assigned in an iterative approach using ATNOS/CANDID (12, 13) algorithms in combination with CYANA, giving the resonance assignments, all manually assigned NOE cross-peaks and all three-dimensional NOESY spectra as input. The standard protocol with seven cycles of peak picking, cross-peak assignment, and subsequent structure calculation with CYANA was applied. In the final step dihedral angle restraints for backbone Φ and Ψ angles were included that were derived from H^{α}, C^{α}, C^{β}, C', and N chemical shifts using the pro-

gram TALOS (14). For further refinement CYANA runs were performed according to the protocol for simulated annealing with 100 randomly generated starting conformations, 35,000 steps torsion angle dynamics and subsequent 2,000 conjugate gradients minimization steps. A final bundle of 15 NMR structures with the lowest CYANA target function that did not show any distance constraint violations of more than 0.019 nm were used for further analysis.

1. Schünke S, Stoldt M, Novak K, Kaupp UB, Willbold D (2009) Solution structure of the *Mesorhizobium loti* K1 channel cyclic nucleotide-binding domain in complex with cAMP. *EMBO Rep* 10:729–735.
2. Schünke S, Novak K, Stoldt M, Kaupp UB, Willbold D (2007) Resonance assignment of the cyclic nucleotide binding domain from a cyclic nucleotide-gated K^+ channel in complex with cAMP. *Biomol NMR Assign* 1:179–181.
3. Zuiderweg ERP, Fesik SW (1989) Heteronuclear 3-dimensional NMR-spectroscopy of the inflammatory protein C5A. *Biochemistry* 28:2387–2391.
4. Norwood TJ, Boyd J, Heritage JE, Soffe N, Campbell ID (1990) Comparison of techniques for ^{1}H-detected heteronuclear ^{1}H-^{15}N spectroscopy. *J Magn Reson* 87:488–501.
5. Keller R (2004) *The Computer Aided Resonance Assignment Tutorial* (Cantina, Zurich).
6. Dosset P, Hus JC, Blackledge M, Marion D (2000) Efficient analysis of macromolecular rotational diffusion from heteronuclear relaxation data. *J Biomol NMR* 16:23–28.
7. Farrow NA, et al. (1994) Backbone dynamics of a free and a phosphopeptide-complexed Src homology 2 domain studied by ^{15}N NMR relaxation. *Biochemistry* 33:5984–6003.
8. Pervushin K, Riek R, Wider G, Wüthrich K (1997) Attenuated T2 relaxation by mutual cancellation of dipole-dipole coupling and chemical shift anisotropy indicates an avenue to NMR structures of very large biological macromolecules in solution. *Proc Natl Acad Sci USA* 94:12366–12371.
9. Zhu G, Xia Y, Nicholson LK, Sze KH (2000) Protein dynamics measurements by TROSY-based NMR experiments. *J Magn Reson* 143:423–426.
10. Schanda P, Brutscher B (2005) Very fast two-dimensional NMR spectroscopy for real-time investigation of dynamic events in proteins on the time scale of seconds. *J Am Chem Soc* 127:8014–8015.
11. Güntert P, Mumenthaler C, Wüthrich K (1997) Torsion angle dynamics for NMR structure calculation with the new program DYANA. *J Mol Biol* 273:283–298.
12. Herrmann T, Güntert P, Wüthrich K (2002) Protein NMR structure determination with automated NOE-identification in the NOESY spectra using the new software ATNOS. *J Biomol NMR* 24:171–189.
13. Herrmann T, Güntert P, Wüthrich K (2002) Protein NMR structure determination with automated NOE assignment using the new software CANDID and the torsion angle dynamics algorithm DYANA. *J Mol Biol* 319:209–227.
14. Cornilescu G, Delaglio F, Bax A (1999) Protein backbone angle restraints from searching a database for chemical shift and sequence homology. *J Biomol NMR* 13:289–302.
15. Shen Y, Delaglio F, Cornilescu G, Bax A (2009) TALOS+: A hybrid method for predicting protein backbone torsion angles from NMR chemical shifts. *J Biomol NMR* 44:213–223.

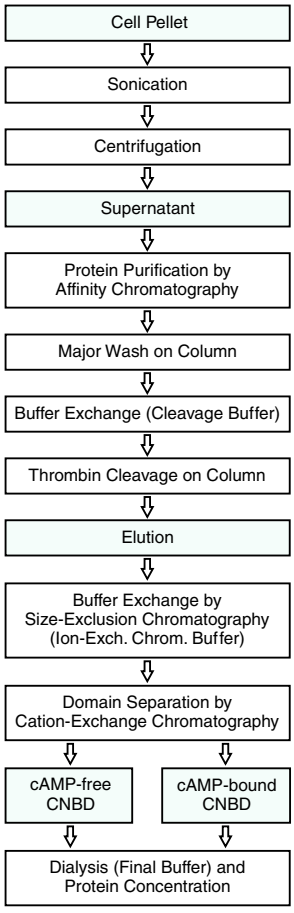

Fig. S1. Overview of the protein purification and separation protocol of cAMP-free and cAMP-bound MloK1 CNBD.

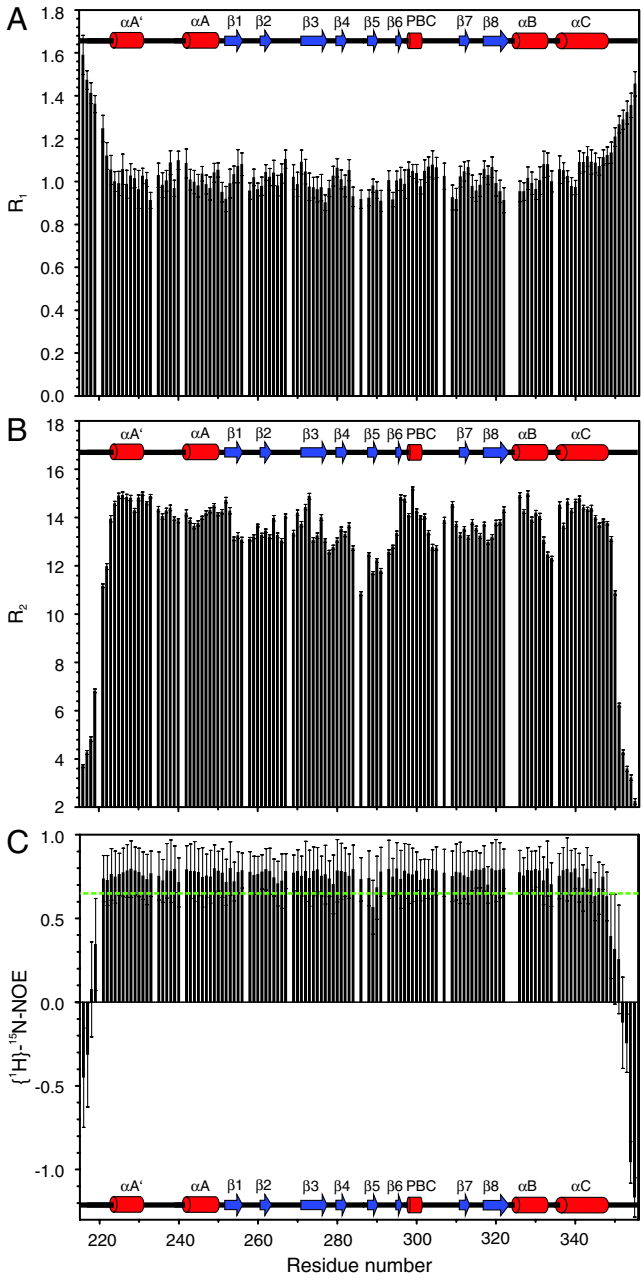

Fig. S2. Experimental values of ^{15}N longitudinal (R_1) and transverse (R_2) relaxation rates for cAMP-free CNBD with respect to the protein sequence: (*A*) R_1 (s^{-1}); (*B*) R_2 (s^{-1}); and (*C*) steady-state heteronuclear $\{^1H\}$-^{15}N-NOE values of amide resonances at 298 K, 14.1 T and 18.8 T. Residues for which no results are shown correspond to prolines and residues R220, S308, H323, S324, and A325. For residues with $\{^1H\}$-^{15}N-NOE values greater than 0.65 (green dashed line), an isotropic rotational correlation time of 8.4 ns at 298 K was derived. Secondary structure elements are shown in each panel (blue arrows indicate β strand and red cylinders indicate α helical conformation).

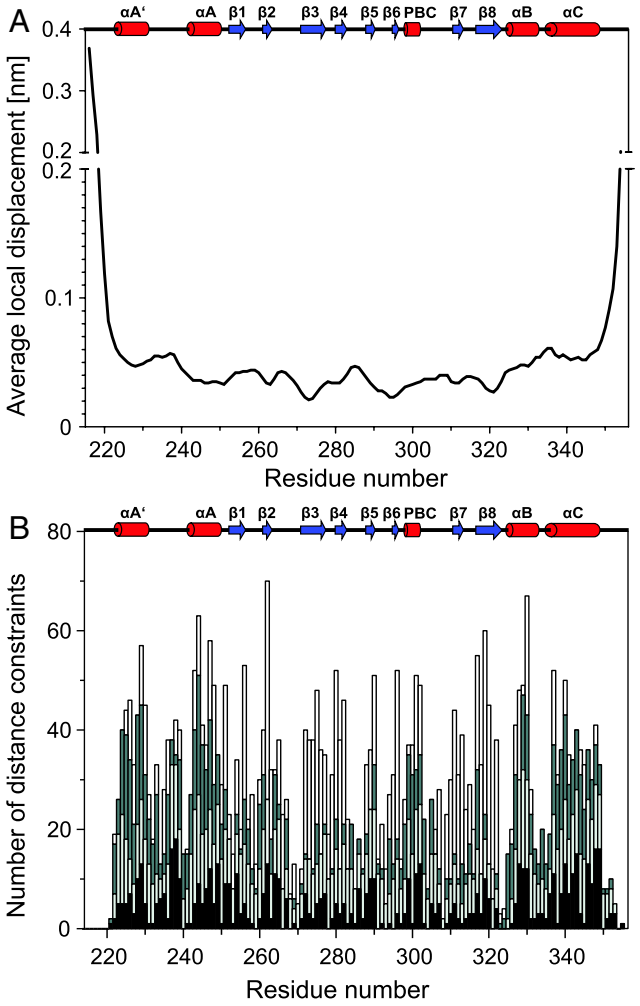

Fig. S3. Precision of local conformation and number of distance constraints per residue for the resulting 15 NMR structures of cAMP-free CNBD with the lowest CYANA target function. (*A*) Average local displacement values among the 15 calculated solution structures. For each three-residue segment the local root mean squared (rms) deviation of the backbone atoms was calculated and plotted against the residue number of the central residue. (*B*) Number of intraresidual (black), sequential (light gray), medium-range (dark gray), and long-range (white) NOE distance constraints per residue.

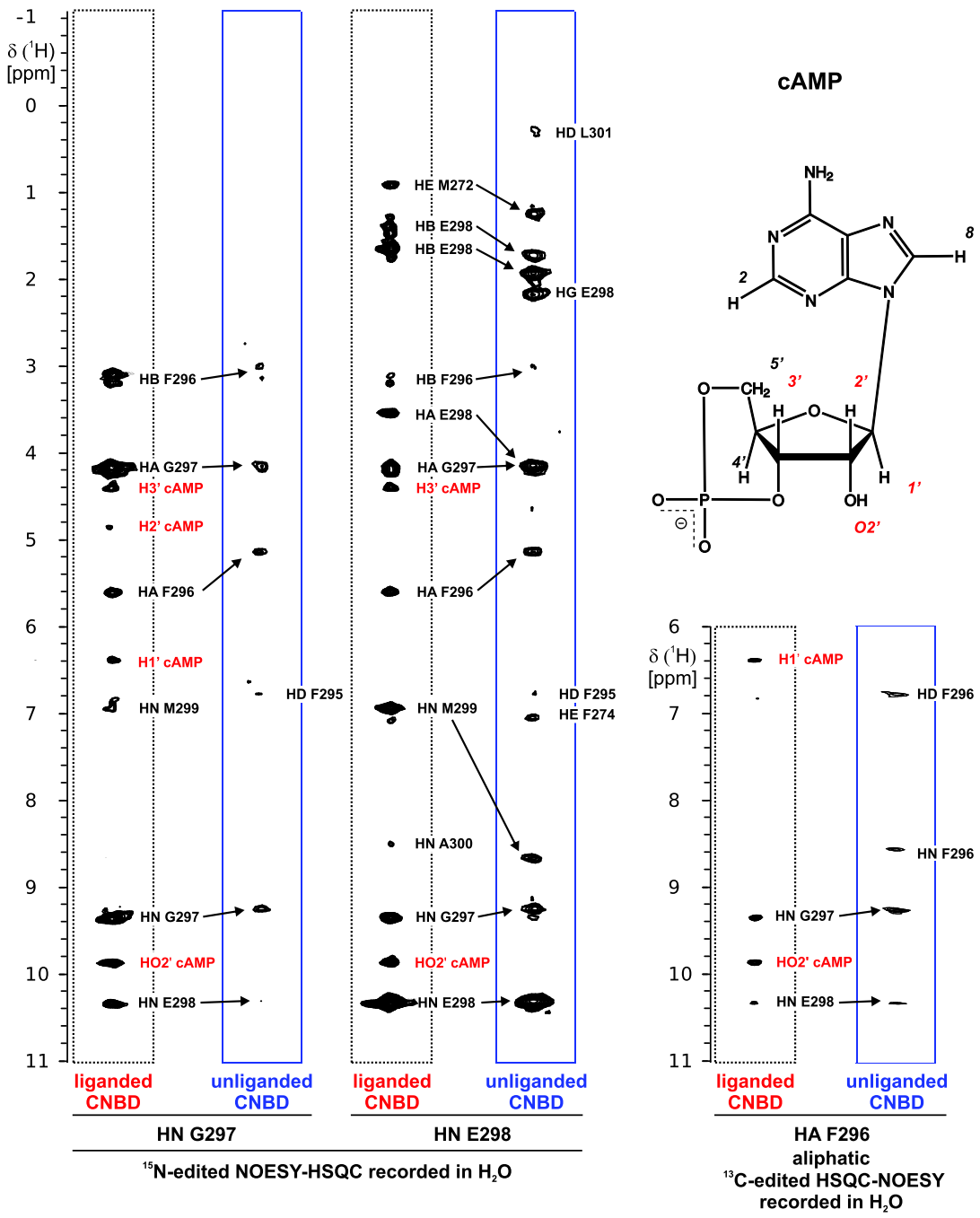

Fig. S4. Comparison of the NOE strips from ^{13}C-edited HSQC-NOESY and ^{15}N-edited NOESY-HSQC spectra of the cAMP-bound and -free CNBD. Shown are strips for the amide protons of G297, E298, and aliphatic alpha proton of F296. Strips of the cAMP-bound CNBD (1) (PDB ID code 2K0G) show intermolecular NOEs between the CNBD and cAMP (red). As compared to the cAMP-bound CNBD, NOEs to the cAMP molecule (red) are absent in all cAMP-free strips (blue). Moreover, the cAMP-free CNBD shows significant changes in chemical shifts and NOE pattern for atoms that are located in the binding site. The respective NOE is characterized by the cAMP proton labeled (scheme in the upper right corner) and CNBD proton labeled to the right of each cross resonance within the respective stripe.

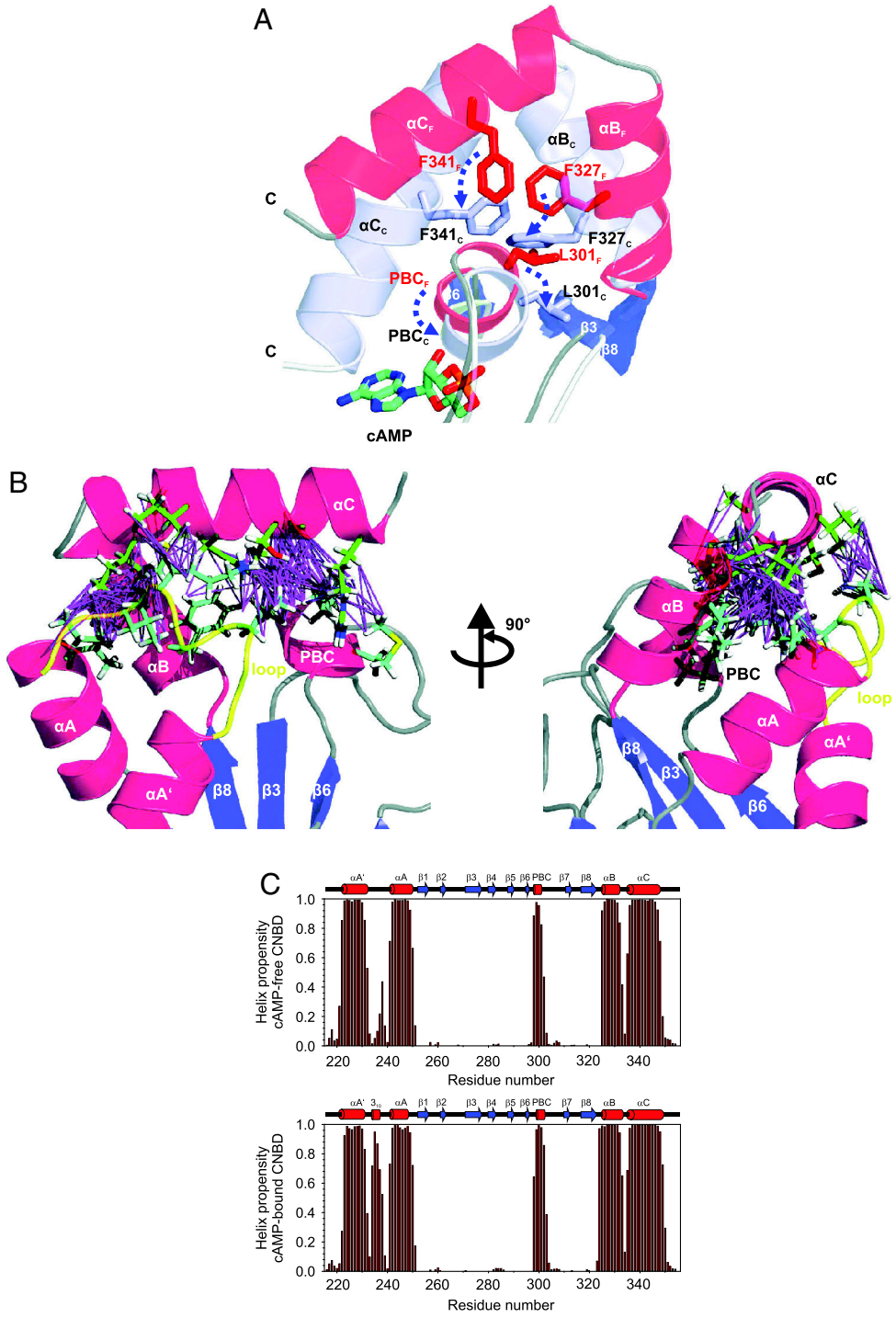

Fig. S5. Comparison of the helical portion of cAMP-free and -bound wild-type MloK1 CNBD. (*A*) A focused view into the reorientation of the C-terminal helical portion. The cAMP-free (red) and -bound (white) CNBD were superimposed. Reorientation of αB and αC helix is induced by binding of cAMP to the PBC helix region. In the cAMP-free state, residue L301 in the PBC helix occupies the space that is filled by F327 in αB helix in the cAMP-bound state, and movement of F327 would clash into L301. Binding of cAMP attracts the PBC, repositions L301, and allows that the resulting gap can be filled by F327. Residue F327 in αB is directly coupled to F341 in αC via hydrophobic interactions and repositioning of F327 leads to the repositioning of F341. Repositioning of the respective residues is shown by arrows. (*B*) Representation of all 48 long-range NOE-derived distances involving residues of helix αC. Two different views are given. (*C*) Helical propensities of cAMP-free (upper) and -bound (lower) CNBD as derived from C^{α}, C^{β}, C′, HA, H_N, and N chemical shifts using the program TALOS+ (15). β strands in both structures are shown in blue. Secondary structure elements are shown and labeled (label "$_C$" stands for "cAMP-bound state"; label "$_F$" stands for "cAMP-free state").

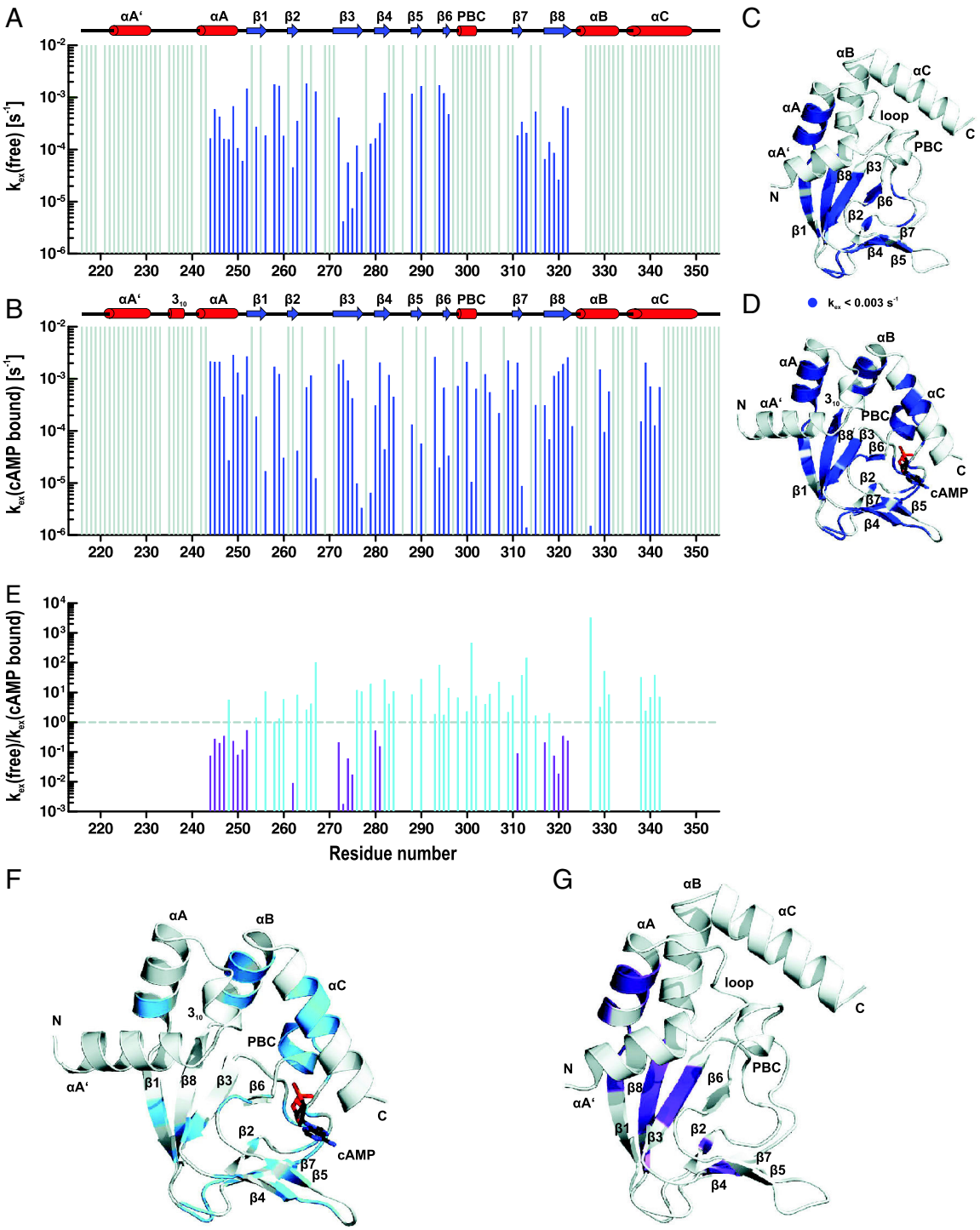

Fig. S6. Proton-deuterium exchange in the absence and presence of cAMP. Exchange rates (k_{ex}) of the respective CNBD residues in the absence (*A*) or presence (*B*) of cAMP. Residues for which the proton–deuterium exchange reaction was almost completed after 300 s are shown in gray. Secondary structure elements are shown on top of each panel. Ribbon representation of the cAMP-free (*C*) and cAMP-bound (*D*) CNBD. Residues with slower exchange rates are shown in blue. (*E*) Ratio of exchange rates of the cAMP-free and -bound CNBD. Residues with values greater than one (gray dotted line) show an enhanced protection in the cAMP-bound state compared to cAMP-free state. Residues with values less than one show an enhanced protection in the cAMP-free compared to the cAMP-bound state. Protection factors of residues for which the exchange in the absence or presence of cAMP was almost complete after 300 s are also shown. In these cases, a value for k_{ex} of 0.005 s^{-1} was assumed to calculate the underestimated ratio. Residues with an elevated protection against proton–deuterium exchange were mapped onto the solution structures of the cAMP-bound (*F*) and cAMP-free (*G*) CNBD.

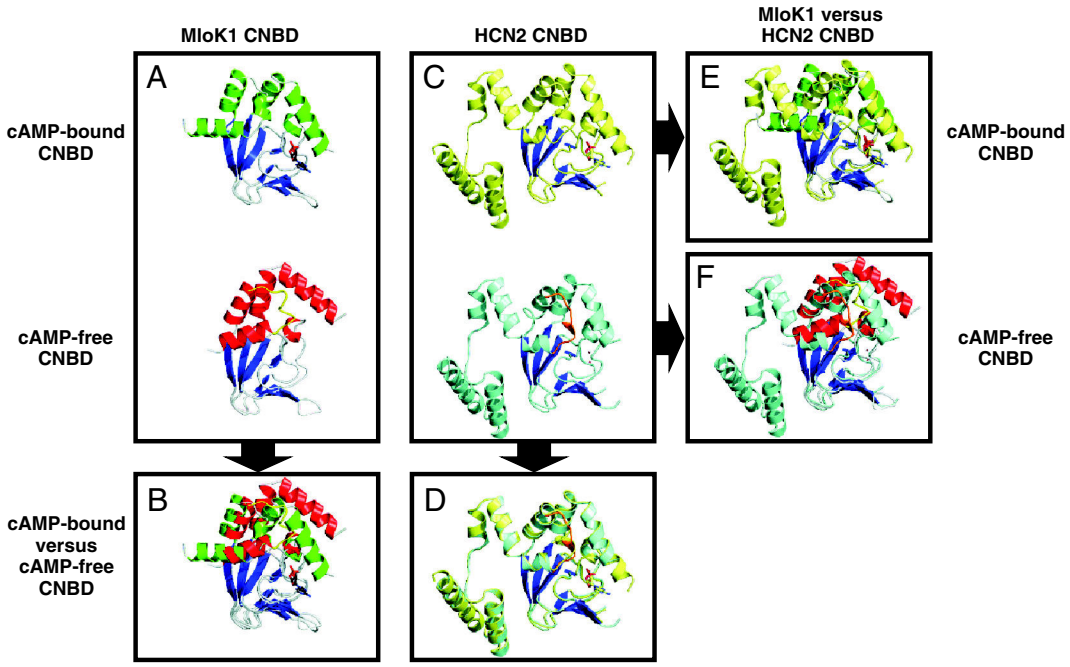

Fig. S7. Comparison of cAMP-bound and -free MloK1 CNBD solution structures and monomers of eukaryotic HCN2 CNBD crystal structures. The solution structure of the cAMP-bound and -free wild-type MloK1 CNBD (*A*) is superimposed onto each other (*B*). The cAMP-bound and -free CNBD structure of the HCN2 channel (*C*) is superimposed onto each other (*D*). The cAMP-bound and -free MloK1 CNBD solution structure is superimposed onto the cAMP-bound and -free CNBD crystal structure of the HCN2 channel (*E* and *F*). The CNBDs were taken from PDB ID codes 2K0G (MloK1 CNBD holo state (1), helices are shown in green), 1Q43 (HCN2 CNBD holo state (2), helices are shown in light yellow), 2KXL (MloK1 CNBD apo state, helices are shown in red and loop region in yellow), and 3FFQ (HCN2 CNBD apo state (3), helices are shown in light blue and loop region in orange). β strands are shown in blue and cAMP in stick model. The least-square superposition of the structures was done using the backbone atoms of the β roll forming strands. MloK1 CNBD backbone atoms of the amino- and carboxy-terminal ends (residues Q216-R220 and A351-A355) are not shown.

1 Schünke S, Stoldt M, Novak K, Kaupp UB, Willbold D (2009) Solution structure of the *Mesorhizobium loti* K1 channel cyclic nucleotide-binding domain in complex with cAMP. *EMBO Rep* 10:729–735.
2 Zagotta WN, et al. (2003) Structural basis for modulation and agonist specificity of HCN pacemaker channels. *Nature* 425:200–205.
3 Taraska JW, Puljung MC, Olivier NB, Flynn GE, Zagotta WN (2009) Mapping the structure and conformational movements of proteins with transition metal ion FRET. *Nat Methods* 6:532–537.

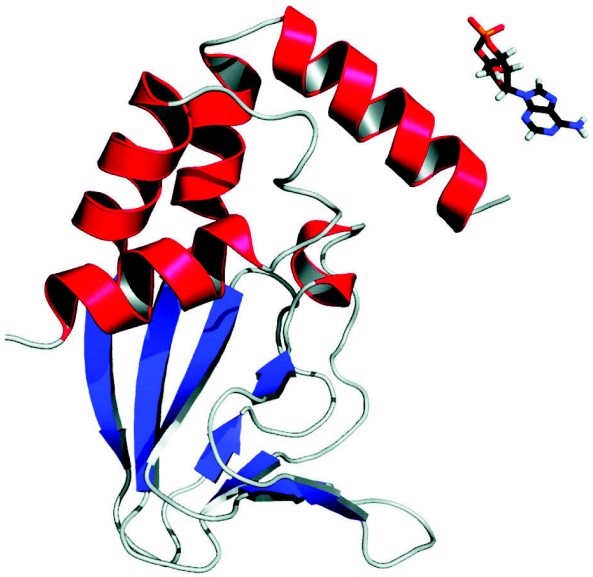

Movie S1. Structure comparison of cAMP-free and -bound wild-type MloK1 CNBD—an animation to illustrate the large conformational rearrangement on ligand binding. The CNBD is shown in ribbon representation and the cAMP molecule is shown as stick model.
Movie S1 (GIF)

Table S1. NMR constraints and structural statistics for the resulting 15 NMR structures of cAMP-free CNBD

Number of experimental NMR restraints:	
Total number of assigned NOEs	2,380
Intraresidue ($\|i-j\|=0$)	665
Interresidue sequential ($\|i-j\|=1$)	627
Interresidue medium-range ($1<\|i-j\|\leq 5$)	456
Interresidue long-range ($\|i-j\|>5$)	632
Average number of NOE constraints per residue	17
Dihedral ϕ and ψ angle constraints from TALOS*	254
CYANA structural statistics[†]:	
RMS deviations (nm) to mean structure[‡]:	
Backbone heavy atoms	0.037 ± 0.007
All heavy atoms	0.070 ± 0.007
CYANA target function (nm^2)	0.058 ± 0.005
NOE distance constraints, sum (nm)	0.28 ± 0.040
NOE distance constraints, max (nm)	0.017 ± 0.002
Dihedral angle constraints, max (°)	3.37 ± 0.460
Φ, Ψ angles consistent with Ramachandran plot[§]:	
Most favored regions (%)	89.9
Allowed regions (%)	99.2
Generously allowed regions (%)	100
Disallowed regions (%)	0

*Derived from C^{α}, C^{β}, C′, N and H^{α} chemical shifts for 127 high confidence predictions found by TALOS using the calculated range of ±10°.

[†]Average value ± standard deviation.

[‡]Superposition made for all heavy atoms (except N- and C-terminal residues Q216-G221 and R349-A355).

[§]Ramachandran analysis was determined using PROCHECK-NMR.

Chapter 4

Material and Methods

Most of the materials and methods used and applied in this study have been already mentioned in the "*Materials and Methods*" sections of the respective publications. However, the following chapter offers a combined detailed description of all materials and methods used and applied in this study.

4.1 Material

4.1.1 Chemicals, enzymes and miscellaneous materials

All chemicals used in this study and not mentioned in table 4.1 were of analytical grade. Standard chemicals were purchased from AppliChem GmbH (Darmstadt, Germany), Carl Roth GmbH (Karlsruhe, Germany) Merck KGaA (Darmstadt, Germany), and Sigma Aldrich Chemie GmbH (Steinheim, Germany). All solutions were prepared using deionized water with additional treatment by an Milli-Q-Biocell-System and subsequent filtration through a 0.22 µm Millipack-20-filter device (Millipore GmbH, Schwalbach, Germany). Buffer solutions were additionally filtered using a 0.22 µm filtermembrane (Schleicher & Schuell Bio Science GmbH, Dassel, Germany), degased, and if possible autoclaved for 20 minutes at 120 °C.

Table 4.1: Chemicals, enzymes and miscellaneous materials

Chemical	Supplier
[$^{13}C_6$, 99 %]-Glucose	Cambridge Isotope Laboratories, Andover, USA
[^{15}N, 99 %]-Ammonium chloride	Cambridge Isotope Laboratories, Andover, USA
Acrylamide 4K solution (30 %; Mix 29:1; ratio of Acrylamide 4K : Bisacrylamide 4K)	AppliChem GmbH, Darmstadt, Germany
Adenosine-3', 5'-cyclic-monophosphate	Sigma Aldrich Chemie, Steinheim, Germany
Amicon stirred system Ultracel PL-3	Millipore, Schwalbach, Germany
Ampicillin	Carl Roth GmbH, Karlsruhe, Germany
Bio-Rad protein assay dye reagent	Bio-Rad, München, Germany
β-mercaptoethanol	Carl Roth GmbH, Karlsruhe, Germany
Bovine serum albumin (BSA)	Merck KGaA, Darmstadt, Germany
Chloramphenicol	Carl Roth GmbH, Karlsruhe, Germany
Complete protease inhibitor cocktail tablet	Roche GmbH, Freiburg, Germany
Deuterium oxide (99,99 %)	Sigma Aldrich Chemie, Steinheim, Germany
Deuterium oxide (99,90 %)	Euriso-Top, Saint-Aubin Cedex, France
Dialysis tube (MWCO 3500)	Carl Roth GmbH, Karlsruhe, Germany
DNase I	Applichem GmbH, Darmstadt, Germany
Ethylenediaminetetraacetic acid (EDTA)	AppliChem, Darmstadt, Germany
Gluthathione-sepharose 4B	GE-Healthcare, München, Germany
Isopropyl-β-D-thiogalactoside (IPTG)	Boehringer, Mannheim, Germany
N,N,N',N'-Tetramethylendiamine	Merck KGaA, Darmstadt, Germany
Protease inhibitor Complete	Roche GmbH, Freiburg, Germany
Protein molecular weight marker	MBI Fermentas, St. Leon-Rot, Germany
Rotilabo filter (0.22 μm)	Sartorius AG, Göttingen, Germany
Thrombin	Merck KGaA, Darmstadt, Germany
Tris-d11/HCl	Cambridge Isotope Laboratories, Andover, USA

4.1.2 Bacterial strain

The bacterial strain *Escherichia coli* (*E. coli*) BL-21 (DE3)-pLysE was used for protein expression. Details of the *E. coli* strain genotype are shown in table 4.2.

Table 4.2: Genotype of the used *E. coli* strain

***E. coli* strain**	**Genotype**	**Reference**
BL-21 (DE3)-pLysE	F^- *ompT* *hsd*S_B($r_B^-m_B^-$) *gal dcm* λ(DE3) *ton*A pLysE (Cm^R)	Novagen, Darmstadt, Germany

DNA encoding the whole *Mesorhizobium loti* K1 channel (MloK1) was amplified from genomic DNA. The coding region for residues 216 to 355 of the MloK1 channel was cloned into the pGEX-2T (Amersham Biosciences) plasmid vector and verified by DNA sequencing. This vector was used and encodes the MloK1 cyclic nucleotide binding domain (CNBD) with an N-terminal glutathione S-transferase (GST) fusion protein gene and a thrombin cleavage site integrated in between. The vector was cloned by Dr. K. Novak of the formerly Institute for Structural Biology and Biophysics, Cellular Biophysics (ISB-1), Research Center Jülich.

4.1.3 Gel electrophoresis marker

Size estimation of proteins during sodium dodecylsufate polyacrylamide gel electrophoresis was performed using the unstained protein molecular weight marker (Fig. 4.1, Fermentas, St. Leon-Rot, Germany).

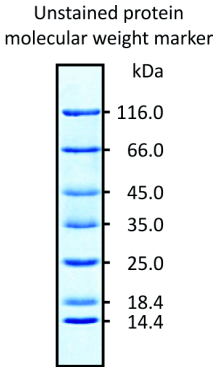

Figure 4.1: Depiction of the gel electrophoresis molecular weight marker applied in this work

4.1.4 Laboratory equipment

Glutathione-Sepharose 4B column material for affinity chromatography was obtained from GE Healthcare (Freiburg, Germany). All affinity chromatography purification steps were performed using gravity flow columns.

Table 4.3: Laboratory instruments

Instrument	Supplier
ÄKTApurifier 10	GE Healthcare, Freiburg, Germany
Aquatron incubation shaker	Infors-HT, Einsbach, Germany
Branson sonifier 250	Branson Ultrasonics Corp, Danbury, USA
Centrifuge 5417R	Eppendorf, Hamburg, Germany
Centrifuge 5804R	Eppendorf, Hamburg, Germany
Centrifuge Avanti J-20 XP	Beckman Coulter, Krefeld, Germany
GelDoc 2000	Bio-Rad, München, Germany
HEλIOS ϵ spectrophotometer	Thermo Scientific, Waltham, USA
Hoefer mighty small SE 260 vertical gel electrophoresis apparatus	Hoefer Scientific Instruments, San Francisco, USA
Lambda 25 UV/VIS spectrometer	Perkin Elmer, Waltham, USA
Lyophilizer Alpha 1-4	Christ, Osterode am Harz, Germany
Milli-Q-Biocell system	Millipore GmbH, Schwalbach, Germany
pH-Meter and pH-electrode	Mettler Toledo, Steinbach, Germany
Semi-micro balance CP225D	Sartorius, Göttingen, Germany
Unitron incubation shaker	Infors-HT, Einsbach, Germany

Table 4.4: List of laboratory and chromatographic equipment

Equipment	Supplier
Amicon 8000 stirred cells	Millipore GmbH, Schwalbach, Germany
HiPrep 26/10 desalting column	GE Healthcare, Freiburg, Germany
Mono S HR 5/5 cation-exchange column	GE Healthcare, Freiburg, Germany
Rotilabo syringe filters	Carl Roth GmbH, Karlsruhe, Germany
Spectra/Por dialysis membranes (3 kDa MWCO)	Carl Roth GmbH, Karlsruhe, Germany
Ultrafiltration membrane PLBC (3 kDa MWCO)	Millipore GmbH, Schwalbach, Germany

4.1.5 Software and Databases

The analysis of protein sequences (e.g. protein isoelectric point calculation and protein properties) was performed using the ExPASy proteomics server (http://expasy.org/tools, e.g. ProtParam). Protein sequence database enquiries were carried out using EMBL- and GenBank-database (http://www.ebi.ac.uk/embl/Access/index.html, http://www.ncbi.nlm.nih.gov/genbank). Protein structure database enquiries and depositions were carried out using RCSB Protein Data Bank (http://www.rcsb.org/pdb). Nuclear magnetic resonance assignments have been deposited at the Biological Magnetic Resonance Bank (www.bmrb.wisc.edu).

Table 4.5: Software used in this work

Software product	Version	Reference
Common Interface for NMR structure Generation (CING)	2.0	http://nmr.cmbi.ru.nl/cing
Crystallography and NMR System (CNS)	1.2.1	(Brunger 2007)
CARA	1.8.4.2	(Keller 2004)
CSI	n/a	(Wishart & Sykes 1994)
CYANA	1.1	(Güntert et al. 1997)
DSSP	n/a	(Kabsch & Sander 1983)
Molprobity	3.1.8	(Davis et al. 2007)
MOLMOL	n/a	(Koradi et al. 1996)
NMRPipe	5.5.X	(Delaglio et al. 1995)
PROCHECK-NMR	n/a	(Laskowski et al. 1993)
PyMOL	1.3.X	(DeLano 2002)
TALOS+	3.4.0	(Shen et al. 2009)
TENSOR2	n/a	(Dosset et al. 2000)
Quantity One	4.6.5	BioRad, München, Germany

4.2 Methods

4.2.1 SDS polyacrylamide gel electrophoresis (SDS-PAGE)

Sodium dodecyl sulfate polyacrylamide gel electrophoresis (SDS-PAGE) was performed as described by Laemmli (Laemmli 1970) and gels consisted of a of a 5 % stacking gel and a 15 % separating gel. Protein samples were mixed (ratio of 1:4) with loading buffer and loaded onto the gel after boiling for 5 minutes at 95 °C. SDS-PAGE was carried out in a vertical electrophoresis chamber (Mighty Small II, Hoefer/GE-Healthcare, München, Germany) at 30 to 40 mA per gel (for 1 hour) containing the SDS-running buffer. Protein gels were stained with Coomassie Brilliant Blue R-250 staining solution for 30 to 60 minutes. Fast staining was performed by heating the staining solution for 2 minutes with microwaves. Destaining of protein gels was performed with destaining solution, alternative by carefully boiling the gels in water. Documentation of the gels was done with a GelDoc 2000 system (BioRad, München, Germany). Protein sizes were determined by comparing the migration of the respective protein band to a standard protein molecular weight marker (MBI Fermentas, St. Leon-Rot, Germany).

5 % Stacking gel	**15 % Separating gel**
4.85 % (w/v) acrylamide	14.55 % (w/v) acrylamide
0.15 % (w/v) N,N'-methylenebis-acrylamide	0.45 % (w/v) N,N'-methylenebis-acrylamide
125 mM Tris/HCl, pH 6.8	375 mM Tris/HCl, pH 8.8
0.1 % (w/v) SDS	0.1 % (w/v) SDS
0.1 % (w/v) APS	0.1 % (w/v) APS
0.1 % (v/v) TEMED	0.1 % (v/v) TEMED

SDS-Running buffer	**4x Loading buffer**
50 mM Tris/HCl, pH 8.3	200 mM Tris/HCl, pH 8
385 mM Glycine	8 % (w/v) SDS
0.1 % (w/v) SDS	8 % (v/v) β-mercaptoethanol
	40 % (v/v) Glycerol
	0.05 % bromphenol blue

Coomassie Blue staining solution	**Destaining solution**
25 % (v/v) Isopropanol	25 % (v/v) Isopropanol
10 % Acetic acid	10 % Acetic acid
0.5 g/l Coomassie Brilliant Blue R-250	

4.2.2 Determination of protein concentration

UV absorption spectroscopy

Protein concentration was measured by absorbance spectroscopy using a Lamda 25 spectral photometer (Perkin Elmer, Waltham, USA) and quartz cuvettes (Hellma, Mühlheim, Germany) with 1 cm path length. The Protein concentration was determined at a wavelength of $\lambda =$ 280 nm according to Beer-Lambert law:

$$A = \varepsilon \cdot c \cdot l \tag{4.1}$$

where A is the measured absorbance, ε the wavelength-dependent molar absorption coefficient (in $cm^{-1} \cdot M^{-1}$), c the molar protein concentration, and l the path length (in cm). The molar absorption coefficient $\varepsilon = 5690\ M^{-1} \cdot cm^{-1}$ of MloK1 CNBD was calculated using contributions of aromatic and cysteine amino acids in the denatured state at a wavelength of $\lambda = 280$ nm (Gill & von Hippel 1989).

4.2.3 Bradford assay

Protein concentration was also measured by Bradford assay (Bradford 1976). Four protein dilutions (not exceeding 10 µg/ml) were prepared with double distilled water (total volume of 800 µl). The Bradford reaction was initiated by adding 200 µl of Bio-Rad protein assay dye reagent (Bio-Rad, München, Germany) to each sample. The reaction was incubated at RT for 5 minutes and the absorbance was measured at = 595 nm using a Lamda 25 spectral photometer (Perkin Elmer, Waltham, USA) against a blank sample (200 µl Bradford reagent and 800 µl double distilled water). A standard calibration curve was established each time a protein assay was performed with bovine serum albumin (BSA) dilutions of known concentrations (1.5 to 10 µg/ml). Using the calibration curve, the protein concentration of each sample was determined according to its absorbance.

4.3 Expression and purification of MloK1 CNBD

4.3.1 Transformation of *E. coli*

A tube of frozen competent cells and plasmid DNA were thawed on ice. An amount of either 1 to 10 ng of plasmid DNA was added to the cells, and then incubated on ice for 20 minutes. Afterwards, a 'heat shock' was performed at 42 °C for 45 seconds and the cells were again placed on ice for 2 minutes. LB medium was added to the cells up to a final volume of 500 µl and cells were incubated at 37 °C for 45 minutes. The cells were finally plated on LB agar plates containing ampicillin (100 µg/ml) to select pGEX-2T transformed cells. The plates were incubated overnight at 37 °C.
For long-term storage 860 µl of a bacterial culture (OD_{600}: 0.7) was mixed with 115 µl of 70 % glycerol and 25 % glucose. Storage was performed at -80 °C until further use.

Luria Bertani (LB) medium
10 g/l Tryptone
5 g/l Yeast extract
5 g/l NaCl

4.3.2 Expression of GST-MloK1 CNBD fusionprotein

Recombinant MloK1 CNBD was expressed as a fusion protein with an N-terminal glutathione S-transferase (GST) affinity tag. DNA was transformed into *E. coli* BL21 (DE3) pLysE cells. Single *E. coli* colonies were used within 24 hours of pGEX-2T/MloK1 CNBD transformation to inoculate a 10 ml preculture of LB medium containing ampicillin and chloramphenicol (final concentration of 100 µg/ml and 18 µg/ml). Cells were grown and shaken by 200 rpm at 37 °C (Unitron, Infors-HT, Einsbach, Germany) until the culture reached an optical density OD_{600}: 0.8. The cells were collected by centrifugation (2000 x g, 5 minutes, RT; centrifuge 5804R, Eppendorf, Hamburg, Germany) and inoculated in M9 medium ($[^{15}N]$-ammonium chloride and $[^{13}C]$-glucose were used as isotope sources) to an OD_{600}: 0.1 containing ampicillin and chloramphenicol (final concentration of 100 µg/ml and 18 µg/ml). Cells were shaken at 37 °C until the culture reached an OD_{600}: 0.8. Afterwards, the cells were again collected by centrifugation (2000 x g, 5 minutes, RT; centrifuge 5804R, Eppendorf, Hamburg, Germany) and a corresponding expression culture of M9 medium containing ampicillin (final concentration of 100 µg/ml) was inoculated to an OD_{600}: 0.1. The expression culture was shaken at 37 °C and protein expression was induced at OD_{600}: 0.6 to 0.7 with 1 mM IPTG (final concentration). Cells were grown over night at 20 °C and harvested by centrifugation (5000 x g,

20 minutes, 5 °C; centrifuge Avanti J-20XP, Beckmann-Coulter, Krefeld, Germany). The cell pellet was washed with PBS buffer and frozen at -20 °C or directly used. The expression was verified according to analysis by SDS-PAGE.

Trace elements solution
30 mg/l $MnCl_2{\cdot}4H_2O$
58.8 mg/l $ZnSO_4{\cdot}H_2O$
300 mg/l H_3BO_3
200 mg/l $CoCl_2{\cdot}6H_2O$
20 mg/l $NiCl_2{\cdot}6H_2O$
10 mg/l $CuCl_2{\cdot}2H_2O$
900 mg/l $Na_2MoO_4{\cdot}2H_2O$
20 mg/l Na_2SeO_3

Vitamin cocktail solution
1 mg/l d-Biotin
1 mg/l Cholin chloride
1 mg/l Folic acid
1 mg/l Nicotinamide
1 mg/l Sodium-D-Pantothenate
1 mg/l Pyridoxal HCl
0.1 mg/l Riboflavin

M9 medium
9.1 g/l $Na_2HPO_4{\cdot}2H_2O$
3 g/l KH_2PO_4
0,5 g/l NaCl
1 g/l $^{15}NH_4Cl$
100 µM $CaCl_2$
2 mM $MgSO_4$
10 µM Fe(III)-citrate
4 g/l Glucose or 2 g/l $^{13}C_6$-Glucose
0.2 % (v/v) Trace elements solution
5 mg/l Thiamin HCl
0.1 % (v/v) Vitamin cocktail solution (1000x)
pH 7.4

4.3.3 Preparation of cleared *E. coli* lysates

The cell pellet of an overnight expression containing [*U*-^{15}N, ^{13}C] or [*U*-^{15}N] isotopically labeled GST-MloK1 CNBD fusion protein was resuspended on ice in 30 ml lysis buffer. The cells were lysed on ice by sonication using a Branson sonifier 250 (6 x 30 seconds, duty cycle 50 %, output control setting 5). Lysate clarification was achieved by centrifugation (50000 x g, 30 minutes, 5 °C; centrifuge Avanti J-20XP, Beckmann-Coulter, Krefeld, Germany) and the GST-MloK1 CNBD fusion protein was found quantitatively in the supernatant of the cell lysate

according to analysis by SDS-PAGE. The supernatant was collected for further steps of protein purification.

1 x PBS buffer	**Lysis buffer**
140 mM NaCl	140 mM NaCl
2.7 mM KCl	2.7 mM KCl
10 mM Na_2HPO_4	10 mM Na_2HPO_4
1.8 mM KH_2PO_4	1.8 mM KH_2PO_4
pH 7.4	30 µg/ml DNase I
	2 mM $MgCl_2$
	1 tablet/30 ml protease
	inhibitor mix "Complete"
	pH 7.4

4.3.4 Purification of cAMP-bound MloK1 CNBD

Affinity chromatography

A gravity column (bed volume 1 ml) packed with Glutathione Sepharose 4B (GE Healthcare, Freiburg, Germany) was equilibrated with 10 column volumes of ice-cold 1x PBS binding buffer. The cell lysate after clarification by centrifugation was loaded on and the column was washed with 10 column volumes of cold 1x PBS buffer to remove non-specifically bound proteins. For enzymatic cleavage Thrombin protease (80 U/l cell pellet, Merck, Darmstadt, Germany) was dissolved in 1 column volume of 1x PBS buffer and applied to the column. The MloK1 CNBD C-terminal part of the fusion protein corresponding to amino acid residues Q216 to A355 was cleaved, comprising additional Glycine-Serine residue sequence at the N-terminus. Total time of fusion protein cleavage was at least 3 hours at room temperature. The column was allowed to empty by gravity flow and cleaved MloK1 CNBD was eluted with two and a half column volumes of 1x PBS buffer. The MloK1 CNBD containing fractions after affinity chromatography were pooled. Protein cleavage and final purity of MloK1 CNBD were evaluated by SDS-PAGE analysis.

Size exclusion chromatography

Subsequently size exclusion chromatography was utilized for further purification purpose. A Superdex 75 prep grade, Hi-Load 16/60 column (GE Healthcare, Freiburg, Germany) was equilibrated with 600 ml gel filtration buffer. The MloK1 CNBD containing fraction was loaded

on the column and the run done at 11 °C with a flow-rate of 1 ml/min and was monitored at 280 nm. The MloK1 CNBD containing fractions were pooled and the final purity of the protein was evaluated by SDS-PAGE analysis. The final yield of MloK1 CNBD was roughly 10 mg/l cell culture for [*U*-^{15}N, ^{13}C] or [*U*-^{15}N] isotopically enriched protein. Due to the high affinity of cAMP (K_D = 100 nM) to CNBD (Cukkemane et al. 2007), the CNBD copurifies with the ligand. Therefore, this purification steps yielded exclusively cAMP-bound MloK1 CNBD. The protein purification protocol of the nucleotide-free MloK1 CNBD is described in section 4.3.5.

Gel filtration buffer
10 mM KH_2PO_4
100 mM KCl
100 μM EDTA
pH 7

4.3.5 Purification of nucleotide-free MloK1 CNBD

The protein purification and preparation protocol as described in section 4.3.4 yields exclusively cAMP-bound MloK1 CNBD. Therefore, this protocol was expanded by an additional extensive washing step during the affinity chromatography and ion exchange chromatography was additionally used to separate cAMP-free and remaining cAMP-bound MloK1 CNBD protein of each other.

Affinity chromatography

A gravity column (bed volume 30 ml) packed with Glutathione Sepharose 4B (Amersham Biosciences) was equilibrated with 10 column volumes of ice-cold 1x PBS binding buffer. After the supernatant has been applied, the column was washed with 10 column volumes of cold 1x PBS binding buffer to remove non-specifically bound proteins. 8 liter washing buffer (50 mM MES, pH 6.5, 100 μM EDTA, 50 mM NaCl) was continuously pumped through the column with a flow rate of 7.5 ml/min. This step was meant to constantly remove cAMP from the column-immobilized MloK1 CNBD/GST fusion protein.

Enzymatic cleavage of fusion protein and elution

After the washing step, the column was washed with 10 column volumes of 1x PBS buffer. For enzymatic cleavage, Thrombin protease (160 U/l cell pellet, Merck, Darmstadt, Germany) was dissolved in 1 column volume of 1x PBS and applied to the column. The C-terminal

MloK1 CNBD corresponding to amino acid residues Q216 to A355 was released from GST, comprising additional Glycine-Serine residue sequence at the N-terminus. Total time of fusion protein cleavage was at least 3 hours at room temperature. Cleaved MloK1 CNBD protein was eluted with two and a half column volumes of 1x PBS buffer. Cleavage and final purity of MloK1 CNBD protein after affinity chromatography were evaluated by SDS-PAGE analysis.

Ion exchange chromatography

The buffer was immediately exchanged to buffer A on a HiPrep 26/10 desalting column mounted on an Äkta purifier system (GE Healthcare, Freiburg, Germany). The system was operated at 11 °C. A flow rate of 4.5 ml/min was applied and the desalting step was monitored at 280 nm and 260 nm. Performance of the desalting step was observed by measuring the conductivity. The MloK1 CNBD protein containing fractions were pooled.

Ion exchange chromatography

Buffer A	**Buffer B**
10 mM MES	10 mM MES
100 μM EDTA	100 μM EDTA
pH 6	pH 6
	1 M NaCl

Subsequently ion exchange chromatography was used to separate cAMP-free from residual cAMP-bound MloK1 CNBD. A cation exchange chromatography column Mono S HR 5/5 (GE Healthcare, Freiburg, Germany) was operated with a flow rate of 1 ml/min, the absorption was monitored at 260 nm and 280 nm. Buffer A was used as binding buffer and elution was directed with buffer B. The CNBD protein was loaded on the column followed by 6 column volumes of buffer A. The cAMP-free and cAMP-bound CNBD protein was clearly, separately eluted at 6.92 mS/cm and 9.22 mS/cm, respectively, using a high ionic strength gradient from 0 % to 17 % of buffer B in 20 column volumes. Finally, the column was re-equilibrated using a gradient to 100 % buffer B. Ion exchange chromatography runs were done at 11 °C, which was required for best performance. The cAMP-free and cAMP-bound CNBD fractions were pooled separatively and dialyzed against buffer C and D, respectively. The identity of the CNBD protein fractions was established by SDS-PAGE analysis and mass spectroscopy. The final yield of CNBD was roughly 10 mg/l culture for [U-^{15}N, ^{13}C] or [U-^{15}N] isotopically enriched protein.

Dialysis buffer

Buffer C	**Buffer D**
10 mM KH_2PO_4	10 mM Tris/HCl
100 mM KCl	100 mM NaCl
100 μM EDTA	200 μM EDTA
0.02 % (w/v) sodium azide	0.02 % (w/v) sodium azide
pH 7	pH 7

Two dialysis steps with a ratio of 1:100 (sample:dialysis buffer) were performed (three hours and over night). In the final step MloK1 CNBD was concentrated with an Amicon stirred system (Ultracel PLBC, 3 kDa molecular weight cutoff, Millipore, Schwalbach, Germany). During the final concentration steps the buffer was exchanged by four volumes of the respective NMR buffer including 5 % (v/v) ^2H_2O and deuterated Tris-d11 (98 %, Cambridge Isotope Laboratories, Andover, USA)/HCl. The protein concentration was determined with Bradford assay (Bio-Rad, München, Germany).

4.4 NMR spectroscopy and data analysis

4.4.1 Sample preparation of cAMP-bound MloK1 CNBD

The cAMP-bound MloK1 CNBD fractions after size-exclusion chromatography were pooled and concentrated at 11 °C with an Amicon (GE-Healthcare, Freiburg, Germany) stirred system (Ultracel PLBC , 3 kDa molecular weight cutoff, Millipore, Schwalbach, Germany). During the final concentration steps the buffer was exchanged by four volumes of NMR buffer. The protein concentration was determined with Bradford assay (Bio-Rad, München, Germany). NMR samples used to perform all NMR experiments contained 300 µl of 0.5 mM [*U*-^{15}N, ^{13}C] or [*U*-^{15}N] isotopically labeled MloK1 CNBD in 5 mm Shigemi BMS-005V NMR tubes (Shigemi, Tokio, Japan) with an equivalent amount of cAMP in aqueous solution. For protein storage NMR samples were frozen in liquid nitrogen, lyophyllized (Alpha 1-4 lyophyllizer, Martin Christ, Osterade, Germany) and finally stored at RT. Sample preparation in D_2O was carried out by resuspending a lyophyllized sample in 99.996 % D_2O (Cambridge Isotope Laboratories, Andover, USA).

NMR buffer of cAMP-bound MloK1 CNBD
10 mM KH_2PO_4
100 mM KCl
100 µM EDTA
5 % (v/v) D_2O
0.02 % (w/v) NaN_3
pH 7

4.4.2 Sample preparation of nucleotide-free MloK1 CNBD

The NMR sample used to perform experiments for resonance assignments contained 0.5 mM [*U*-^{15}N, ^{13}C] or [*U*-^{15}N] isotopically labeled nucleotide-free MloK1 CNBD in aqueous solution (NMR buffer). For protein storage NMR samples were frozen in liquid nitrogen, lyophyllized (Alpha 1-4 lyophyllizer, Martin Christ, Osterade, Germany) and finally stored at RT. Sample preparation in deuterium oxide was carried out by resuspending a lyophyllized sample carefully in 99.996 % deuterium oxide (Cambridge Isotope Laboratories, Andover, USA).

NMR buffer of unliganded MloK1 CNBD
10 mM deuterated Tris-d11/HCl
100 mM NaCl
100 µM EDTA
5 % (v/v) D_2O
0.02 % (w/v) NaN_3
pH 7

4.4.3 NMR experiments

All NMR experiments using cAMP-bound MloK1 CNBD were carried out at 25 °C on a Varian ^{Unity}INOVA instrument, equipped with a 5 mm cryogenic Z-axis pulse-field-gradient (PFG) $^{1}H[^{13}C, ^{15}N]$ triple resonance probe at a proton frequency of 800 MHz.

NMR experiments using nucleotide-free MloK1 CNBD were performed at 25 °C on Varian ^{Unity}INOVA and VNMRS instruments, equipped with a 5 mm cryogenic Z-axis PFG triple resonance probe at proton frequencies of 800 MHz and 600 MHz.

Decoupling of ^{15}N and ^{13}C nuclei during proton aquisition has been performed by application of GARP (Shaka & Keeler 1987) and adiabatically by WURST (Kupce & Freeman 1995) sequences. DIPSI-2 (Rucker & Shaka 1989) isotropic mixing scheme was used during TOCSY-^{13}C spin lock periods. Solvent suppression was achieved by WATERGATE (Piotto et al. 1992) technique. ^{1}H chemical shifts were referenced directly to the methyl resonance of DSS ($\delta_{DSS} = 0$ ppm), ^{13}C and ^{15}N chemical shifts were referenced indirectly to DSS (Wishart et al. 1995) using the absolute frequency ratios $\upsilon(^{13}C)/\upsilon(^{1}H) = 0.25144953$ and $\upsilon(^{15}N)/\upsilon(^{1}H) = 0.101329118$.

All NMR data were processed using NMRPipe (Delaglio et al. 1995) and evaluated with CARA (Keller 2004) software. NMR acquisition and data processing parameter of performed NMR experiments for the liganded and unliganded MloK1 CNBD are shown in table 4.6 on page 60 and table 4.7 on page 61, respectively.

Table 4.6: NMR acquisition and data processing parameter of performed NMR experiments on cAMP-bound MloK1 CNBD

Experiment	sw1[$] [ppm]	t1[#] [pts]	sw2[$] [ppm]	t2[#] [pts]	sw3[$] [ppm]	t3[#] [pts]	nt*	d1[§] [s]	mix[¶] [ms]	^{15}N[◇] [ppm]	^{13}C[◇] [ppm]	ω1[∃] [pts]	ω2[∃] [pts]	ω3[∃] [pts]
2D (^{15}N-^{1}H)-HSQC	30.8	200	17.5	1536	-	-	4-8	1-1.5	-	119.4	-	1024	2340	-
2D SOFAST (^{15}N-^{1}H)-HSQC	28.8	200	20.0	1202	-	-	4	0.4	-	119.5	-	1024	1024	-
2D ct-(^{13}C-^{1}H)-HSQC (aliphatic)	68.1	738	15.0	1536	-	-	32	1.7	-	-	40.9	2048	1024	-
2D (^{13}C-^{1}H)-HSQC (aliphatic)	68.1	738	15.0	1536	-	-	32	1.5	-	-	40.9	2048	1024	-
2D (^{13}C-^{1}H)-HSQC (aromatic)	41.0	500	12.5	1280	-	-	128	1.5	-	-	145.7	2048	722	-
3D HNCO	30.8	70	12.7	76	15.0	1536	8	1.0	-	119.4	176.1	256	512	615
3D HNCACB	30.8	92	59.7	240	15.0	1536	16	1.0	-	119.4	45.1	256	1024	533
3D HNHA	30.8	68	7.5	190	15.0	1536	16	1.0	-	119.4	-	256	1024	615
3D H(C)CH-COSY	38.3	174	6.6	230	15.0	1280	8	1.25	-	-	29.2	512	512	903
3D H(C)CH-TOCSY	38.3	152	6.6	180	15.0	1200	16	1.0	14	-	31.3	512	512	903
3D (^{1}H-^{13}C-^{1}H)-HSQC-NOESY (aliphatic)	38.3	168	6.6	172	15.0	1500	16	1.0	100	-	29.2	512	1024	1764
3D (^{1}H-^{13}C-^{1}H)-HSQC-NOESY (aromatic)	19.1	100	2.4	72	16.3	1626	32	1.45	140	-	126.7	256	512	1449
3D (^{1}H-^{1}H-^{15}N)-NOESY-HSQC	28.4	92	11.9	384	15.0	1510	8	1.5	120	119.7	-	512	1024	684
^{15}N (R_1) relaxation	29.1	260	15.0	1536	-	-	64	2.25	-	119.4	-	1024	2727	-
^{15}N (R_2) relaxation	29.1	260	15.0	1536	-	-	64	2.0	-	119.4	-	1024	2727	-
2D {^{1}H}^{15}N-NOE-TROSY	28.4	346	15.0	1500	-	-	128	2.5	-	119.7	-	1024	2731	-

[$] acquired spectral width in the respective dimension
[§] delay time in seconds between two single experiments
[◇] ^{15}N or ^{13}C carrier frequency in ppm after Fourier transform and reduced spectral width
[#] acquired complex data points in the respective dimension
[¶] NOESY or TOCSY mixing time in milliseconds
[∃] number of real data points in the respective dimension
* number of transients for each time increment

4.4.4 Resonance assignments and NOE spectroscopy

A combined set of heteronuclear multidimensional NMR experiments were used for sequential resonance assignments of ^{1}H, ^{13}C, and ^{15}N chemical shifts of [*U*-^{15}N, ^{13}C] or [*U*-^{15}N] isotopically labeled MloK1 CNBD. The assignment strategy comprised the concerted use of the following experiments: 2D (^{15}N-^{1}H)-HSQC (Bodenhausen & Ruben 1980; Grzesiek & A. 1993), 2D (^{13}C-^{1}H)-HSQC (Kay et al. 1992), 2D ct-(^{13}C-^{1}H)-HSQC (Santoro & King 1992), 3D HNCACB (Wittekind & Mueller 1993), HNCO (Ikura et al. 1990), HNHA (Vuister & Bax 1993), H(C)CH-COSY (Bax et al. 1990), H(C)CH-TOCSY (14 ms mixing time; Bax et al. 1990), (^{1}H-^{13}C-^{1}H)-HSQC-NOESY (100 ms mixing time; Norwood et al. 1990) and (^{1}H-^{1}H-^{15}N)-NOESY-HSQC (120 ms mixing time; Zuiderweg & Fesik 1989). Aromatic side chain resonances of the liganded MloK1 CNBD were assigned using aromatic 2D (^{13}C-^{1}H)-

Table 4.7: NMR acquisition and data processing parameter of performed NMR experiments on nucleotide-free MloK1 CNBD

Experiment	sw1[$] [ppm]	t1[#] [pts]	sw2[$] [ppm]	t2[#] [pts]	sw3[$] [ppm]	t3[#] [pts]	nt*	d1[§] [s]	mix[¶] [ms]	^{15}N[◇] [ppm]	^{13}C[◇] [ppm]	ω1[ǂ] [pts]	ω2[ǂ] [pts]	ω3[ǂ] [pts]
2D (^{15}N-^{1}H)-HSQC	28.4	250	15.0	1316	-	-	4-8	1.0-1.5	-	119.6	-	1024	2733	-
2D SOFAST (^{15}N-^{1}H)-HSQC	28.8	200	20.0	1418	-	-	8	0.3	-	119.5	-	1024	1024	-
2D ct-(^{13}C-^{1}H)-HSQC (aliphatic)	66.0	760	15.0	1536	-	-	32	1.0	-	-	40.4	2048	1777	-
2D (^{13}C-^{1}H)-HSQC (aliphatic)	66.1	718	15.0	1536	-	-	32	1.0	-	-	40.4	2048	1777	-
2D (^{13}C-^{1}H)-HSQC (aromatic)	30.3	303	15.0	1536	-	-	32	1.8	-	-	128.2	2048	438	-
2D ct-(^{13}C-^{1}H)-HSQC (aromatic)	30.2	308	15.0	1536	-	-	32	1.8	-	-	128.2	2048	438	-
3D HNCO	28.8	70	12.2	74	20.0	2036	8	1.7	-	119.5	175.6	256	256	462
3D HNCACB	28.4	80	58.7	276	15.0	1536	16	1.13	-	119.4	45.1	256	1024	574
3D HNHA	28.4	66	7.3	180	15.0	1558	16	1.0	-	119.4	-	256	1024	615
3D H(C)CH-COSY	39.0	156	6.4	178	15.0	1280	16	1.0	-	-	28.4	512	512	958
3D H(C)CH-TOCSY	39.0	190	6.4	172	15.0	1200	16	1.0	14	-	30.3	512	512	958
3D (^{1}H-^{13}C-^{1}H)-HSQC-NOESY (aliphatic)	39.0	160	6.0	170	15.0	1500	16	1.2	100	-	28.4	512	1024	1641
3D (^{1}H-^{13}C-^{1}H)-HSQC-NOESY (aromatic)	15.9	96	1.4	44	15.0	1626	32	1.5	140	-	127.1	512	256	1449
3D (^{1}H-^{1}H-^{15}N)-NOESY-HSQC	27.1	96	11.5	380	15.0	1562	8	1.8	120	119.5	-	512	1024	547
2D (^{1}H-^{13}C-^{1}H)-HSQC-NOESY (aromatic)	1.5	248	15.0	1418	-	-	408	2.0	100	-	-	1024	1501	-
^{15}N (R_1) relaxation	28.8	240	20.0	1438	-	-	64	2.25	-	119.5	-	1024	2050	-
^{15}N (R_2) relaxation	28.8	240	20.0	1438	-	-	96	1.5	-	119.5	-	1024	2050	-
2D {^{1}H}^{15}N-NOE-TROSY	28.4	346	15.0	1536	-	-	128	2.5	-	119.5	-	1024	2731	-

[$] acquired spectral width in the respective dimension
[§] delay time in seconds between two single experiments
[◇] ^{15}N or ^{13}C carrier frequency in ppm after Fourier transform and reduced spectral width
[#] acquired complex data points in the respective dimension
[¶] NOESY or TOCSY mixing time in milliseconds
[ǂ] number of real data points in the respective dimension
[*] number of transients for each time increment

HSQC and 3D (^{1}H-^{13}C-^{1}H)-HSQC-NOESY (140 ms mixing time) experiments. Aromatic 2D ct-(^{13}C-^{1}H)-HSQC and 2D (^{1}H-^{13}C-^{1}H)-HSQC-NOESY (100 ms mixing time) experiments were additionally used for aromatic side chain resonance assignments of the nucleotide-free MloK1 CNBD. Resonances of cAMP were identified and assigned using a combination of the following experiments: aliphatic and aromatic 2D (^{13}C-^{1}H)-HSQC, 2D ct-(^{13}C-^{1}H)-HSQC, 3D aliphatic ^{13}C-edited HSQC-NOESY (100 ms mixing time), 3D aromatic ^{13}C-edited HSQC-NOESY (140 ms mixing time) and ^{15}N-edited NOESY-HSQC (120 ms mixing time). Adenine H2 resonance was distinguished from other aromatic resonances and assigned by the unique chemical shift of the attached C2 carbon, and the H8 resonance was respectively assigned. Proton resonances of the ribose were successively identified by using the unique H1' reso-

nance as a starting point for interpretation of the NOE experiments. Nuclear Overhauser Effect (NOE) distance constraints for structure calculations were derived from 3D ^{15}N-edited NOESY-HSQC (120 ms mixing time), aliphatic ^{13}C-edited HSQC-NOESY (100 ms mixing time) and aromatic ^{13}C-edited HSQC-NOESY (140 ms mixing time) experiments. Additional NOE distance constraints were derived from a 2D aromatic ^{13}C-edited HSQC-NOESY experiment (100 ms mixing time) on the unliganded MloK1 CNBD. Furthermore, aliphatic ^{13}C-edited HSQC-NOESY and aromatic ^{13}C-edited HSQC-NOESY experiments were used for structural constraints with cAMP-bound MloK1 CNBD in buffer after exchange of H_2O by deuterium oxide. On the basis of almost complete assignments of ^{1}H, ^{13}C and ^{15}N resonances of liganded and unliganded MloK1 CNBD, NOE cross-peak assignments were obtained by an iterative procedure using a combination of manual and automatic steps. As an initial step, the program CARA was used to evaluate NOE spectra and to manually assign nearly all of the apparently unambiguous NOE distance constraints. NOE cross peak intensities were classified as strong, medium or weak, corresponding to upper limit distance constraints of 2.7, 3.8 and 5.5 Å, respectively. Cross peak intensities of NOEs between protons of known distances were used for calibration. For NOEs involving methyl groups, upper limit distance constraints of 2.9, 4.0 and 5.7 Å for strong, medium or weak interactions, respectively, were used.

4.4.5 NMR structure calculation

Structure calculations were performed using the program CYANA 1.1 (Güntert et al. 1997). CYANA runs were performed according to the protocol for simulated annealing with 100 randomly generated starting conformations, 25000 steps torsion angle dynamics and subsequent 2000 conjugate gradients minimization steps. 25 intermolecular NOEs between the protein and cAMP were manually assigned. According to all manually assigned NOEs, an initial fold of the protein was calculated. Additional NOEs were automatically assigned in an iterative approach using ATNOS/CANDID (Herrmann et al. 2002b; Herrmann et al. 2002a) algorithms in combination with CYANA, providing the resonance assignments, all manually assigned NOEs and corresponding NOESY spectra as input.

The standard protocol with seven cycles of peak picking, NOE assignment and subsequent structural calculation with CYANA was applied. In the final step, dihedral angle restraints for backbone ϕ and ψ angles were derived from $^{1}H^{\alpha}$, $^{13}C^{\alpha}$, $^{13}C^{\beta}$, $^{13}C'$, and ^{15}N chemical shifts using the program TALOS (Cornilescu et al. 1999). For further refinement CYANA runs were performed according to the protocol for simulated annealing with 100 randomly generated starting conformations, 35000 steps torsion angle dynamics and subsequent 2000 conjugate gradients minimization steps. A final bundle of 15 NMR structures with the lowest CYANA

target function that did not show any distance constraint violations of more than 0.019 nm were used for further analysis.

Geometry of the structures, structural parameters, and secondary structural elements were analysed and visualised using the following programs: MOLMOL (Koradi et al. 1996), PyMOL (DeLano 2002), WHATIF (Vriend 1990), MolProbity (Davis et al. 2007), and PROCHECK-NMR (Laskowski et al. 1993; Laskowski et al. 1996). Electrostatic properties were evaluated with APBS (Baker et al. 2001).

4.4.6 Heteronuclear $\{^1H\}$-^{15}N-NOE, longitudinal and transverse relaxation rate experiments

For the characterization of overall and internal motions, ^{15}N longitudinal (R_1) and transverse (R_2) relaxation rates, together with the steady-state $\{^1H\}$-^{15}N-NOE, were recorded at 25 °C on 0.5 mM [*U*-^{15}N] isotopically labeled MloK1 CNBD using standard methods (Farrow et al. 1994; Pervushin et al. 1997; Zhu et al. 2000) at 800 MHz and 600 MHz proton frequencies. $\{^1H\}^{15}N$-NOE-TROSY spectra were acquired with 2.5 seconds proton saturation.

For ^{15}N-R_1 experiments the following relaxation delays were applied: 11, 60, 140, 240, 360, 530, 750, and 1150 ms were used for the liganded and 11, 65, 141, 249, 380, 542, 758, and 1192 ms for the unliganded state.

For ^{15}N-R_2 experiments the following relaxation delays were applied: 10, 30, 50, 70, 90, and 110 ms were used for the liganded and 10, 30, 50, 70, 90, 110, and 150 ms for the unliganded state.

Peak integral values were obtained by fitting signals to an adjustable 'peak model' shape using the program CARA. A superposition of Gauss and Lorentz functions was employed, adjusted manually and independently for both spectral dimensions. Data of R_1 and R_2 relaxation experiments were fitted to a mono-exponential decay using the program CurveFit (A.G. Palmer, Columbia University, USA). The correlation time was determined for an isotropic tumbling model using the TENSOR2 package (Dosset et al. 2000).

4.4.7 NMR titration experiment

NMR titration experiments were carried out to 0.2 mM [*U*-^{15}N] isotopically labeled nucleotide-free MloK1 CNBD by stepwise addition of small aliquots of concentrated cAMP (Sigma-Aldrich, München, Germany) stock solutions. The experiments were performed at 25 °C on a Varian ^{Unity}INOVA instrument, equipped with a 5 mm cryogenic Z-axis PFG triple resonance

probe at a proton frequency of 600 MHz. Eight 2D (^{15}N-^{1}H)-HSQC spectra were recorded with increasing ligand concentrations of 5, 10, 25, 50, 75, 100, 250, and 500 μM cAMP.

4.4.8 Proton-deuterium exchange experiment

Slowly exchanging amide protons were identified by sequently recording a set of 2D SOFAST (^{15}N-^{1}H)-HSQC (Schanda & Brutscher 2005) spectra using 0.5 mM [*U*-^{15}N] isotypically labeled MloK1 CNBD samples, either in the absence or presence of cAMP, which were lyophilized and dissolved in deuterium oxide. Proton-deuterium exchange experiments were performed at 25 °C on a Varian $^{\text{Unity}}$INOVA instrument, equipped with a 5 mm cryogenic Z-axis PFG triple resonance probe at a proton frequency of 600 MHz. The first 2D (^{15}N-^{1}H)-HSQC data points were obtained after a delay of roughly 5 minutes, the last spectrum was recorded after 14 hours for the unliganded and 24 hours for the liganded MloK1 CNBD. Total measuring time of each experiment was 10.83 and 6.67 minutes for the nucleotide-free and cAMP-bound MloK1 CNBD, respectively. Relative cross peak intensities were extracted and fitted using a single exponential decay to determine the exchange rate (k_{ex}).

4.4.9 Deposition of NMR assignments and solution structures

Backbone and side chain ^{1}H, ^{13}C, ^{15}N resonance assignments of liganded and unliganded MloK1 CNBD have been deposited at the Biological Magnetic Resonance Bank under accession number **15249** and **16628**, respectively. The atomic coordinates for the resulting 15 NMR structures of cAMP-bound and cAMP-free MloK1 with the lowest CYANA target function have been deposited at the RCSB Protein Data Bank under accession code **2K0G** and **2KXL**, respectively.

Summary

Ion channels activated by cyclic nucleotides play crucial roles in neuronal excitability and sensory signaling. These channels are activated by binding of cyclic nucleotides to their intracellular cyclic nucleotide-binding domain (CNBD). Ligand binding to the CNBD promotes the opening of the channel, most probably by propagating a conformational change from the CNBD to the pore. However, the mechanism underlying the channel activation is only poorly understood. To elucidate the mechanism of channel gating knowledge of the structure of ligand-free and ligand-bound CNBDs is required. One member of ion channels activated by cyclic nucleotides represents the prokaryotic K^+-selective MloK1 channel, that has been identified in *Mesorhizobium loti*. The MloK1 channel forms homotetramers. Each subunit encompasses six transmembrane segments, a signature sequence for potassium selectivity, and a C-terminal intracellular located CNBD.

In this study, the three-dimensional structure of the 15 kDa MloK1 CNBD in complex with cAMP was determined by NMR spectroscopy in solution. The root-mean-squared (r.m.s.) displacement of the NMR structure ensemble compared to the average structure is 0.025 nm and 0.068 nm for backbone and for all heavy atoms, respectively. The NMR structure of the CNBD in complex with cAMP features an antiparallel β roll with a short internal α helix, known as phosphate binding cassette (PBC), similar to other CNBDs, the cAMP-dependent protein kinase A (PKA), the catabolite activator protein (CAP), and the exchange protein directly activated by cAMP (Epac). The β roll is topped by a region of four α helices. The binding site is formed by parts of the β roll and the PBC helix that provide interactions to the phosphate and ribose moieties of cAMP. The C-terminal helix is placed like a 'lid' above the binding pocket and stabilizes the complex. Side chain R348 of this helix reaches across and interacts with the purine base.

Structure determination of the wildtype cAMP-free CNBD was principally impossible, because cAMP co-purifies with the protein and even extensive dialysis fails to remove the ligand to obtain pure cAMP-free protein samples. Therefore, in the present work a procedure was developed that allows preparation of cAMP-free protein for structure determination. It is based on an extensive washing step of matrix-bound CNBD-GST fusion protein. The present work reports for the first time the three-dimensional structure of the wildtype cAMP-free MloK1 CNBD. The NMR structure could be obtained with an ensemble r.m.s. displacement of 0.037 nm and 0.070 nm for backbone and all heavy atoms, respectively. Superposition of cAMP-bound and -free CNBD solution structures show that the β roll is virtually identical. In contrast, the helical portion shows substantial rearrangements between the two CNBDs. The orientation of each helix with respect to the β roll differs remarkably in the two structures. The movement

of the C-terminal helix is coupled to a substantial displacement of the N-terminal helix, which is directly connected to the last transmembrane segment of the MloK1 channel.

In previous studies, crystal structures of ligand-free MloK1 CNBDs were obtained from R348A and R307W mutants. Both arginine residues are essential for and directly involved in cAMP binding. Mutation of either one of these residues severely impairs cAMP binding affinity and thereby allowed the preparation of cAMP-free CNBD. The crystal structures of the mutants and a crystal structure of CNBD in complex with cAMP are similar to the solution structures. However, a dimeric arrangement was observed only in the crystal structures, and the dimer interface formed by the N-terminus has been proposed to be involved in channel gating (Clayton et al. 2004; Altieri et al. 2008). In contrast to these observations the MloK1 CNBD exists as a monomer in solution, even at high concentrations required for NMR measurements (0.5 mM in this case). This is supported by ^{15}N relaxation experiments that reveal an isotropic rotational correlation time of 8.4 ns and 8.5 ns for the cAMP-free and cAMP-bound CNBD, respectively. These data are consistent with a monomeric CNBD in solution and are clearly below the value expected for a dimer. There is a striking difference between the crystal and solution structures: The N-terminal helix is straight in the solution structures rather than bent. Additionally, in a structure revealed by electron microscopy of the full-length MloK1 channel the CNBDs appear as independent domains separated by discrete gaps, suggesting that CNBDs are not interacting with each other (Chiu et al. 2007). NMR structures of the wildtype cAMP-free and -bound MloK1 CNBD provide for the first time insights on conformational events that accompany gating within the ligand-binding site. A comparison of both structures allows to speculate that pulling a single 'leash' on one subunit could be sufficient enough to activate the channel.

Zusammenfassung

Zyklische Nukleotid-gesteuerte Ionenkanäle spielen eine entscheidende Rolle in der neuronalen Erregbarkeit und in der Signaltransduktion primärer Sinneszellen. Die Kanäle werden durch die Bindung zyklischer Nukleotide an eine intrazelluläre zyklische Nukleotid-Bindedomäne (CNBD) aktiviert. Die direkte Bindung zyklischer Nukleotide an die CNBD begünstigt die Öffnung des Kanals, vermutlich werden fortlaufende Konformationsänderungen beginnend von der CNBD bis zur Kanalpore übertragen. Der grundlegende Mechanismus der zur Aktivierung des Kanals führt ist weitgehend unbekannt. Um den Mechanismus der Kanalaktivierung verstehen zu können, sind Informationen über die Raumstruktur der CNBD im zyklischen-Nukleotid gebundenen und im freien Zustand nötig. Der K^+-selektive MloK1 Kanal ist ein Mitglied der zyklischen Nukleotid-gesteuerten Ionenkanäle und wurde in dem Bakterium *Mesorhizobium loti* entdeckt. Der MloK1 Kanal setzt sich aus vier gleichen Untereinheiten zusammen, die zusammen ein Tetramer bilden. Jede Untereinheit enthält sechs Transmembransegmente, eine charakteristische Sequenz für die Selektivität von Kaliumionen und eine C-terminale, intrazellulär vorliegende CNBD.

In der vorliegenden Arbeit wurde die Raumstruktur der CNBD des MloK1 Kanals im Komplex mit cAMP mittels mehrdimensionaler NMR-Spektroskopie bestimmt. Die Lösungsstruktur des cAMP-gebundenen Proteins wurde mit einer Präzision von 0.025 nm und 0.068 nm r.m.s.-Abweichung der Proteinrückgrat- und aller Schweratom-Positionen in einer Konformerenschar bestimmt. Ähnlich zu bereits strukturell charakterisierten Bindedomänen für zyklische Nukleotide wie der Proteinkinase A (PKA), dem Katabolit-Aktivatorprotein (CAP) und dem Guaninnukleotid-Austauschfaktor Protein (Epac) besteht die Raumstruktur aus einer β Faltblattrolle und einer kurzen internen α Helix. Letztere ist auch bekannt als Phosphatbindekassette (PBC). Über der β Faltblattrolle positioniert befinden sich vier zusätzliche α Helices. Ein Teilbereich der β Faltblattrolle sowie die Phosphatbindekassette bilden die Bindestelle für zyklische Nukleotide. Dieser Bereich zeigt direkte Wechselwirkungen zum Phosphat und dem Ribosering des zyklischen Nukleotids. Die C-terminale Helix ist über der cAMP-Bindestelle positioniert und stabilisiert diesen Komplex indem die Seitenkette von R348 über der Purinbase liegt und mit dieser interagiert.

Bisher war es nicht gelungen die Struktur der wildtyp cAMP-freien CNBD zu lösen. Nach der Proteinexpression liegt die CNBD weitgehend im cAMP-gebundenen Zustand vor und cAMP kann selbst durch intensive Dialyse nicht vom Protein entfernt werden. Im Rahmen dieser Arbeit wurde daher ein Protokoll entwickelt, um cAMP-freies CNBD Protein in ausreichender Menge für NMR-spektroskopische Untersuchungen herzustellen. Der wesentliche Bestandteil des Protokolls ist ein intensiver Waschschritt des Matrix-gebundenen GST-CNBD Fusions-

proteins. So gelang es die NMR Struktur der Nukleotid-freien CNBD mit einer Präzision von 0.037 nm und 0.070 nm r.m.s.-Abweichung der Proteinrückgrat- und aller Schweratom-Positionen in einer Konformerenschar zu bestimmen. Eine Überlagerung der NMR Strukturen der cAMP-gebundenen und -freien CNBD zeigt dass die Strukturbereiche der β Faltblattrolle in beiden Strukturen nahezu identisch sind. Im Gegensatz dazu zeigen die α helikalen Bereiche erhebliche Unterschiede. Die jeweiligen Positionen der Helices sind sehr unterschiedlich im Vergleich zur β Faltblattrolle. Die Positionsänderung der C-terminalen Helix führt zu einer erheblichen Positionsverschiebung der N-terminalen Helix. Diese Helix ist im Kanal direkt mit dem letzten Transmembransegment verbunden.

In bisherigen Studien konnten Kristallstrukturen der cAMP-freien CNBD durch die Einführung von Punktmutationen der Aminosäurereste R348A und R307W gelöst werden. Beide Argininreste sind direkt an der Bindung von cAMP an die CNBD beteiligt. Durch die Einführung der jeweiligen Punktmutation, wurde die Affinität der cAMP-Bindung erheblich vermindert, was die Preparation der cAMP-freien CNBD ermöglichte. Die Kristallstrukturen der cAMP-freien und cAMP-gebundenen CNBD sind den entsprechenden Lösungsstrukturen recht ähnlich. In allen Kristallstrukturen wurde jedoch eine dimere Anordnung der CNBDs zueinander festgestellt. Die dimere Grenzfläche setzt sich aus der Interaktion der ersten beiden N-terminalen α Helices einer CNBD mit den ersten beiden N-terminalen α Helices einer weiteren CNBD zusammen. Diese Beobachtung führte zu dem Vorschlag, dass die dimere Anordnung der CNBDs untereinander bei der Aktivierung des Kanals eine wichtige Rolle spielt (Clayton et al. 2004; Altieri et al. 2008). Im Gegensatz dazu ist die MloK1 CNBD in Lösung ein monomeres Protein und eine dimere Anordnung der CNBDs konnte in den NMR Strukturen nicht beobachtet werden, selbst bei der für die Strukturaufklärung benötigten hohen Proteinkonzentration (in diesem Fall 0.5 mM). Die Durchführung von ^{15}N Relaxationsexperimenten bestätigt die Beobachtung des monomeren Proteins in Lösung. Isotrope Rotationskorrelationszeiten von 8.4 ns und 8.5 ns wurden für die cAMP-freie und cAMP-gebundene CNBD gemessen. Diese Werte liegen eindeutig unterhalb des Erwartungswertes für ein dimeres Protein in Lösung. Der größte Unterschied der NMR Strukturen im Vergleich zu den Kristallstrukturen liegt im Bereich der N-terminalen Helix: In den Lösungsstrukturen ist die Helix eher geradlinig als gekrümmt ausgeprägt. Zusätzlich konnten in einer elektronenmikroskopischen Struktur des ganzen MloK1 Kanals einzelne CNBDs getrennt beobachtet werden (Chiu et al. 2007). Zusammengenommen deuten diese Beobachtungen darauf hin, dass die CNBDs vermutlich nicht miteinander interagieren.

List of abbreviations

[*U*-^{15}N]	uniform isotope labeling with nuclide ^{15}N
[*U*-^{15}N, ^{13}C]	uniform isotope labeling with nuclide ^{15}N and ^{13}C
°C	degree celsius
λ	wavelength
µ	micro
2D, 3D	two-dimensional, three-dimensional
Å	Angstrom
A_{xxx}	absorbance at xxx nm
a	Ampere
AMP	adenosine monophosphate
APS	ammonium persulfate
AU	absorbance units
cAMP	adenosine-3',5'-cyclic-monophosphate
CAP	catabolite activator protein
cm	centimeter
CNBD	cyclic nucleotide-binding domain
CNG	cyclic nucleotide-gated
COSY	correlated spectroscopy
ct	constant time
D_2O	deuterium-oxide; ^2H_2O
Da	Dalton (molecular mass unit for biopolymers)
DNA	deoxyribonucleic acid
DIPSI-2	decoupling in the presence of scalar interactions
DNase	deoxyribonuclease
DSS	2,2-dimethyl-2-silapentane-5-sulfonate
ε	wavelength-dependent molar absorption coefficient
E. coli	*Escherichia coli*
e. g.	for example

EDTA	ethylenediaminetetraacetic acid
Epac	exchange protein directly activated by cAMP
et al.	*et alii* (and others)
g	gravitational acceleration
GARP	globally optimized, alternating-phase rectangular pulses
GST	gluthatione S-transferase
HCN	hyperpolarization-activated and cyclic nucleotide-gated
HSQC	heteronuclear single quantum coherence
Hz	Hertz
IPTG	isopropyl-β-D-thiogalactopyranoside
K	kelvin
k	kilo
K_D	dissociation constant
k_{ex}	exchange rate
l	liter
λ	wavelength
LB medium	Luria Bertani medium
M9 medium	synthetic minimal medium for isotope labeling
M	molar (Mol/Liter)
m	milli
mg	unit Milligramm
min	minute
mS/cm	conductivity measured in milli Siemens per cm
MES	2-(N-morpholino)ethanesulfonic acid
MHz	Megahertz
MloK1	*Mesorhizobium loti* K1
M. loti	*Mesorhizobium loti*
MWCO	molecular weight cutoff
n	nano
NMR	nuclear magnetic resonance
NOE	Nuclear Overhauser enhancement
NOESY	NOE spectroscopy
OD_{xxx}	optical density at a wavelength of xxx nm
PAGE	polyacrylamide gel electrophoresis
PBC	phosphate binding cassette
PBS	phosphate buffered saline

PDB	Protein Data Bank
PFG	pulse field gradient
PKA	cAMP-dependent protein kinase A
ppm	parts per million
R_1	longitudinal relaxation rate
R_2	transverse relaxation rate
r.m.s.	root-mean-squared
RT	room temperature
s	seconds
SDS	sodium dodecyl sulfate
SDS-PAGE	SDS-polyacrylamide gel electrophoresis
TEMED	N, N, N', N'-tetramethylethylenediamine
TOCSY	total correlated spectroscopy
Tris	tris(hydroxymethyl)-aminomethane
TROSY	transverse relaxation optimized spectroscopy
UV	ultraviolet
v/v	volume per volume
w/v	weight per volume
WURST	wideband, uniform rate, and smooth truncation

Abbreviation of amino acid residues

A	Ala	Alanine
C	Cys	Cysteine
D	Asp	Aspartate
E	Glu	Glutamate
F	Phe	Phenylalanine
G	Gly	Glycine
H	His	Histidine
I	Ile	Isoleucine
K	Lys	Lysine
L	Leu	Leucine
M	Met	Methionine
N	Asn	Asparagine
P	Pro	Proline
Q	Gln	Glutamine
R	Arg	Arginine
S	Ser	Serine
T	Thr	Threonine
V	Val	Valine
W	Trp	Tryptophane
Y	Tyr	Tyrosine

References

Altenbach, C., A. K. Kusnetzow, O. P. Ernst, K. P. Hofmann, & W. L. Hubbell (2008). High-resolution distance mapping in rhodopsin reveals the pattern of helix movement due to activation. *Proc. Natl. Acad. Sci. USA 105*, 7439–7444.

Altieri, S. L., G. M. Clayton, W. R. Silverman, A. O. Olivares, E. M. De la Cruz, L. R. Thomas, & J. H. Morais-Cabral (2008). Structural and energetic analysis of activation by a cyclic nucleotide binding domain. *J. Mol. Biol. 381*(3), 655–669.

Altomare, C., B. Terragni, C. Brioschi, R. Milanesi, C. Pagliuca, C. Viscomi, A. Moroni, M. Baruscotti, & D. DiFrancesco (2003). Heteromeric HCN1-HCN4 channels: a comparison with native pacemaker channels from the rabbit sinoatrial node. *J. Physiol. 549*(Pt 2), 347–359.

Baker, N. A., D. Sept, S. Joseph, M. J. Holst, & J. A. McCammon (2001). Electrostatics of nanosystems: application to microtubules and the ribosome. *Proc. Natl. Acad. Sci. USA 98*(18), 10037–10041.

Bax, A., G. M. Clore, P. C. Driscoll, A. M. Groneborn, M. Ikura, & L. E. Kay (1990). Practical aspects of proton-carbon-carbon-proton three-dimensional correlation spectroscopy of ^{13}C-labeled proteins. *J. Magn. Reson. 87*, 620–627.

Bodenhausen, G. & D. J. Ruben (1980). Natural abundance nitrogen-15 NMR by enhanced heteronuclear spectroscopy. *Chem. Phys. Lett. 69*, 185.

Bönigk, W., A. Loogen, R. Seifert, N. Kashikar, C. Klemm, E. Krause, V. Hagen, E. Kremmer, T. Strünker, & U. B. Kaupp (2009). An atypical CNG channel activated by a single cGMP molecule controls sperm chemotaxis. *Sci. Signal. 2*, ra68.

Bradford, M. M. (1976). A rapid and sensitive method for quantitation of microgram quantities of protein utilizing the principle of protein-dye-binding. *Anal. Biochem. 72*, 248–254.

Brunger, A. T. (2007). Version 1.2 of the Crystallography and NMR system. *Nat. Protoc. 2*, 2728–2733.

Chen, S., J. Wang, & S. A. Siegelbaum (2001). Properties of hyperpolarization-activated pacemaker current defined by coassembly of HCN1 and HCN2 subunits and basal modulation by cyclic nucleotide. *J. Gen. Physiol. 117*(5), 491–504.

Chiu, P. L., M. D. Pagel, J. Evans, H. T. Chou, X. Zeng, B. Gipson, H. Stahlberg, & C. M. Nimigean (2007). The structure of the prokaryotic cyclic nucleotide-modulated potassium channel MloK1 at 16 A resolution. *Structure 15*(9), 1053–1064.

Clayton, G. M., S. Altieri, L. Heginbotham, V. M. Unger, & J. H. Morais-Cabral (2008). Structure of the transmembrane regions of a bacterial cyclic nucleotide-regulated channel. *Proc. Natl. Acad. Sci. USA 105*(5), 1511–1515.

Clayton, G. M., W. R. Silverman, L. Heginbotham, & J. H. Morais-Cabral (2004). Structural basis of ligand activation in a cyclic nucleotide regulated potassium channel. *Cell 119*(5), 615–627.

Cornilescu, G., F. Delaglio, & A. Bax (1999). Protein backbone angle restraints from searching a database for chemical shift and sequence homology. *J. Biomol. NMR 13*(3), 289–302.

Craven, K. B. & W. N. Zagotta (2006). CNG and HCN channels: two peas, one pod. *Annu. Rev. Physiol. 68*, 375–401.

Cukkemane, A., B. Grüter, K. Novak, T. Gensch, W. Bönigk, T. Gerharz, U. B. Kaupp, & R. Seifert (2007). Subunits act independently in a cyclic nucleotide-activated K(+) channel. *EMBO Rep. 8*(8), 749–755.

Cukkemane, A., R. Seifert, & U. B. Kaupp (2011). Cooperative and uncooperative cyclic-nucleotide-gated ion channels. *Trends Biochem. Sci. 36*, 55–64.

Davis, I. W., A. Leaver-Fay, V. B. Chen, J. N. Block, G. J. Kapral, X. Wang, L. W. Murray, W. B. Arendall, J. Snoeyink, J. S. Richardson, & D. C. Richardson (2007). MolProbity: All-atom contacts and structure validation for proteins and nucleic acids. *Nucleic Acids Res. 35*(Web Server issue), W375–383.

Delaglio, F., S. Grzesiek, G. W. Vuister, G. Zhu, J. Pfeifer, & A. Bax (1995). NMRPipe: a multidimensional spectral processing system based on UNIX pipes. *J. Biomol. NMR 6*(3), 277–293.

DeLano, W. (2002). The PyMOL Molecular Graphics System. DeLano Scientific LLC, San Carlos, CA, USA.

DiFrancesco, D. & P. Tortora (1991). Direct activation of cardiac pacemaker channels by intracellular cyclic AMP. *Nature 351*(6322), 145–147.

Diller, T. C., Madhusudan, N. H. Xuong, & S. S. Taylor (2001). Molecular basis for regulatory subunit diversity in cAMP-dependent protein kinase: crystal structure of the type II beta regulatory subunit. *Structure 9*(1), 73–82.

Dosset, P., J. C. Hus, M. Blackledge, & D. Marion (2000). Efficient analysis of macromolecular rotational diffusion from heteronuclear relaxation data. *J. Biomol. NMR 16*(1), 23–28.

Farrow, N. A., R. Muhandiram, A. U. Singer, S. M. Pascal, C. M. Kay, G. Gish, S. E. Shoelson, T. Pawson, J. D. Forman-Kay, & L. E. Kay (1994). Backbone dynamics of a free and phosphopeptide-complexed Src homology 2 domain studied by 15N NMR relaxation. *Biochemistry 33*(19), 5984–6003.

Fleissner, M. R., E. M. Brustad, T. Kálai, C. Altenbach, D. Cascio, F. B. Peters, K. Hideg, S. Peuker, P. G. Schultz, & W. L. Hubbell (2009). Site-directed spin labeling of a genetically encoded unnatural amino acid. *Proc. Natl. Acad. Sci. USA 106*, 21637–21642.

Flynn, G. E., K. D. Black, L. D. Islas, B. Sankaran, & W. N. Zagotta (2007). Structure and rearrangements in the carboxy-terminal region of SpIH channels. *Structure 15*(6), 671–682.

Gill, S. C. & P. H. von Hippel (1989). Calculation of protein extinction coefficients from amino acid sequence data. *Anal Biochem 182*(2), 319–326.

Gordon, S. E. & W. N. Zagotta (1995). Localization of regions affecting an allosteric transition in cyclic nucleotide-activated channels. *Neuron 14*(4), 857–864.

Grzesiek, S. & B. A. (1993). The importance of not saturating H_2O in protein NMR. Application to sensitivity enhancement and NOE measurements. *J. Am. Chem. Soc. 115*, 12593–12594.

Güntert, P., C. Mumenthaler, & K. Wüthrich (1997). Torsion angle dynamics for NMR structure calculation with the new program DYANA. *J. Mol. Biol. 273*(1), 283–298.

Heginbotham, L., Z. Lu, T. Abramson, & R. MacKinnon (1994). Mutations in the K+ channel signature sequence. *Biophys. J. 66*(4), 1061–1067.

Herrmann, T., P. Güntert, & K. Wüthrich (2002a). Protein NMR structure determination with automated NOE assignment using the new software CANDID and the torsion angle dynamics algorithm DYANA. *J. Mol. Biol. 319*(1), 209–227.

Herrmann, T., P. Güntert, & K. Wüthrich (2002b). Protein NMR structure determination with automated NOE-identification in the NOESY spectra using the new software ATNOS. *J. Biomol. NMR 24*(3), 171–189.

Hvidt, A. & S. O. Nielsen (1966). Hydrogen exchange in proteins. *Adv. Protein. Chem. 21*, 287–386.

Ikura, M., L. E. Kay, & A. Bax (1990). A novel approach for sequential assignment of ^{1}H, ^{13}C and ^{15}N spectra of proteins: heteronuclear triple-resonance three-dimensional NMR spectroscopy. Application to Calmodulin. *Biochemistry 29*, 4659–4667.

Jeng, M. F. & H. J. Dyson (1995). Comparison of the hydrogen-exchange behavior of reduced and oxidized *Escherichia coli* thioredoxin. *Biochemistry 34*(2), 611–619.

Johnson, J. P., J. & W. N. Zagotta (2001). Rotational movement during cyclic nucleotide-gated channel opening. *Nature 412*(6850), 917–921.

Kabsch, W. & C. Sander (1983). Dictionary of protein secondary structure: pattern recognition of hydrogen-bonded and geometrical features. *Biopolymers 22*, 2577–2637.

Kaupp, U. B., T. Niidome, T. Tanabe, S. Terada, W. Bonigk, W. Stuhmer, N. J. Cook, K. Kangawa, H. Matsuo, T. Hirose, & et al. (1989). Primary structure and functional expression from complementary DNA of the rod photoreceptor cyclic GMP-gated channel. *Nature 342*(6251), 762–766.

Kaupp, U. B. & R. Seifert (2001). Molecular diversity of pacemaker ion channels. *Annu. Rev. Physiol. 63*, 235–257.

Kaupp, U. B. & R. Seifert (2002). Cyclic nucleotide-gated ion channels. *Physiol. Rev. 82*(3), 769–824.

Kay, L. E., P. Keifer, & T. Saarinen (1992). Pure absorption gradient enhanced heteronuclear single quantum correlation spectroscopy with improved sensitivity. *J. Am. Chem. Soc. 114*, 10663–10665.

Kay, L. E., D. A. Torchia, & A. Bax (1989). Backbone dynamics of proteins as studied by 15N inverse detected heteronuclear NMR spectroscopy: application to staphylococcal nuclease. *Biochemistry 28*(23), 8972–8979.

Keller, R. (2004). *The Computer Aided Resonance Assignment Tutorial*. Zurich, Switzerland: Cantina Verlag.

Kim, C., N. H. Xuong, & S. S. Taylor (2005). Crystal structure of a complex between the catalytic and regulatory (RIα) subunits of PKA. *Science 307*(5710), 690–696.

Koradi, R., M. Billeter, & K. Wüthrich (1996). MOLMOL: a program for display and analysis of macromolecular structures. *J. Mol. Graph. 14*(1), 51–55, 29–32.

Kupce, E. & R. Freeman (1995). Adiabatic pulses for wideband inversion and broadband decoupling. *J. Magn. Reson. A 115*, 273–276.

Laemmli, U. K. (1970). Cleavage of structural proteins during the assembly of the head of bacteriophage T4. *Nature 227*(5259), 680–685.

Laskowski, R. A., M. W. MacArthur, D. S. Moss, & J. M. Thornton (1993). PROCHECK: A program to check the stereochemical quality of protein structures. *J. Appl. Crystallogr. 26*, 283–291.

Laskowski, R. A., J. A. Rullmannn, M. W. MacArthur, R. Kaptein, & J. M. Thornton (1996). AQUA and PROCHECK-NMR: programs for checking the quality of protein structures solved by NMR. *J. Biomol. NMR 8*(4), 477–486.

McKay, D. B. & T. A. Steitz (1981). Structure of catabolite gene activator protein at 2.9 Å resolution suggests binding to left-handed B-DNA. *Nature 290*(5809), 744–749.

Much, B., C. Wahl-Schott, X. Zong, A. Schneider, L. Baumann, S. Moosmang, A. Ludwig, & M. Biel (2003). Role of subunit heteromerization and N-linked glycosylation in the formation of functional hyperpolarization-activated cyclic nucleotide-gated channels. *J. Biol. Chem. 278*(44), 43781–43786.

Nimigean, C. M. & M. D. Pagel (2007). Ligand binding and activation in a prokaryotic cyclic nucleotide-modulated channel. *J. Mol. Biol. 371*(5), 1325–1337.

Nimigean, C. M., T. Shane, & C. Miller (2004). A cyclic nucleotide modulated prokaryotic K+ channel. *J. Gen. Physiol. 124*(3), 203–210.

Norwood, T. J., J. Boyd, J. E. Heritage, N. Soffe, & I. D. Campbell (1990). Comparison of techniques for ^{1}H-detected heteronuclear ^{1}H-^{15}N spectroscopy. *J. Magn. Reson. 87*(3), 488–501.

Paoletti, P., E. C. Young, & S. A. Siegelbaum (1999). C-Linker of cyclic nucleotide-gated channels controls coupling of ligand binding to channel gating. *J. Gen. Physiol. 113*(1), 17–34.

Peng, C., E. D. Rich, & M. D. Varnum (2004). Subunit configuration of heteromeric cone cyclic nucleotide-gated channels. *Neuron 42*(3), 401–410.

Pervushin, K., R. Riek, G. Wider, & K. Wüthrich (1997). Attenuated T2 relaxation by mutual cancellation of dipole-dipole coupling and chemical shift anisotropy indicates an avenue to NMR structures of very large biological macromolecules in solution. *Proc. Natl. Acad. Sci. USA 94*(23), 12366–12371.

Piotto, M., V. Saudek, & V. Sklenar (1992). Gradient-tailored excitation for single-quantum NMR spectroscopy of aqueous solutions. *J. Biomol. NMR 2*(6), 661–665.

Popovych, N., S.-R. Tzeng, M. Tonelli, R. H. Ebright, & D. G. Kalodimos (2009). Structural basis for cAMP-mediated allosteric control of the catabolite activator protein. *Proc. Natl. Acad. Sci. USA 106*, 6927–6932.

Rehmann, H., J. Das, P. Knipscheer, A. Wittinghofer, & J. L. Bos (2006). Structure of the cyclic-AMP-responsive exchange factor Epac2 in its auto-inhibited state. *Nature 439*(7076), 625–8.

Rehmann, H., B. Prakash, E. Wolf, A. Rueppel, J. de Rooij, J. L. Bos, & A. Wittinghofer (2003). Structure and regulation of the cAMP-binding domains of Epac2. *Nat. Struct. Biol. 10*(1), 26–32.

Rehmann, H., A. Wittinghofer, & J. L. Bos (2007). Capturing cyclic nucleotides in action: snapshots from crystallographic studies. *Nat. Rev. Mol. Cell Biol. 8*, 63–73.

Robinson, R. B. & S. A. Siegelbaum (2003). Hyperpolarization-activated cation currents: from molecules to physiological function. *Annu. Rev. Physiol. 65*, 453–480.

Rucker, S. P. & A. J. Shaka (1989). Broad-band homonuclear cross polarization in 2D NMR using DIPSI-2. *Molecular Physics 68*(2), 509–517.

Santoro, J. & G. C. King (1992). A constant-time 2D overbodenhausen experiment for inverse correlation of isotopically enriched species. *J. Magn. Reson. 97*, 202–207.

Schanda, P. & B. Brutscher (2005). Very fast two-dimensional NMR spectroscopy for real-time investigation of dynamic events in proteins on the time scale of seconds. *J. Am. Chem. Soc. 127*(22), 8014–8015.

Schünke, S., J. Lecher, M. Stoldt, U. B. Kaupp, & D. Willbold (2010). Resonance assignment of the nucleotide-free wildtype MloK1 cyclic nucleotide-binding domain. *Biomol. NMR Assign. 4*(2), 147–150.

Schünke, S., K. Novak, M. Stoldt, U. B. Kaupp, & D. Willbold (2007). Resonance assignment of the cyclic nucleotide binding domain from a cyclic nucleotide-gated K(+) channel in complex with cAMP. *Biomol. NMR Assign. 1*(2), 179–181.

Schünke, S., M. Stoldt, K. Novak, U. B. Kaupp, & D. Willbold (2009). Solution structure of the *Mesorhizobium loti* K1 channel cyclic nucleotide-binding domain in complex with cAMP. *EMBO Rep. 10*(7), 729–735.

Shaka, A. J. & J. Keeler (1987). Broadband spin decoupling in isotropic lipids. *Progr. NMR Spectr. 19*, 49–192.

Shen, Y., F. Delaglio, G. Cornilescu, & A. Bax (2009). TALOS+: A hybrid method for predicting protein backbone torsion angles from NMR chemical shifts. *J. Biomol. NMR 44*, 213–223.

Su, Y., W. R. Dostmann, F. W. Herberg, K. Durick, N. H. Xuong, L. Ten Eyck, S. S. Taylor, & K. I. Varughese (1995). Regulatory subunit of protein kinase A: structure of deletion mutant with cAMP binding domains. *Science 269*(5225), 807–813.

Taraska, J. W., M. C. Puljung, N. B. Olivier, G. E. Flynn, & W. N. Zagotta (2009). Mapping the structure and conformational movements of proteins with transition metal ion FRET. *Nat. Methods 6*(7), 532–537.

Taraska, J. W. & W. N. Zagotta (2007). Cyclic nucleotide-regulated ion channels: spotlight on symmetry. *Structure 15*, 1023–1024.

Taylor, S. S., J. Yang, J. Wu, N. M. Haste, E. Radzio-Andzelm, & G. Anand (2004). PKA: a portrait of protein kinase dynamics. *Biochim. Biophys. Acta 1697*, 259–269.

Ulens, C. & J. Tytgat (2001). Functional heteromerization of HCN1 and HCN2 pacemaker channels. *J. Biol. Chem. 276*(9), 6069–6072.

Vriend, G. (1990). WHAT IF: a molecular modeling and drug design program. *J. Mol. Graph. 8*(1), 52–56, 29.

Vuister, G. W. & A. Bax (1992). Resolution enhancement and spectral editing of uniformly ^{13}C-enriched proteins by homonuclear ^{13}C broadband decoupling. *J. Magn. Reson. 98*, 428–435.

Vuister, G. W. & A. Bax (1993). Quantitative *J* correlation: a new approach for measuring homonuclear three-bond $J(H^NH^\alpha)$ coupling constants in ^{15}N-enriched proteins. *J. Am. Chem. Soc. 115*, 7772–7777.

Wagner, G. & K. Wüthrich (1982). Amide proton exchange and surface conformation of the basic pancreatic trypsin inhibitor in solution: Studies with two-dimensional nuclear magnetic resonance. *J. Mol. Biol. 160*(2), 343–361.

Wang, J., S. Chen, & S. A. Siegelbaum (2001). Regulation of hyperpolarization-activated HCN channel gating and cAMP modulation due to interactions of COOH terminus and core transmembrane regions. *J. Gen. Physiol. 118*(3), 237–250.

Weber, I. T. & T. A. Steitz (1987). Structure of a complex of catabolite gene activator protein and cyclic AMP refined at 2.5 A resolution. *J. Mol. Biol. 198*(2), 311–326.

Weitz, D., N. Ficek, E. Kremmer, P. J. Bauer, & U. B. Kaupp (2002). Subunit stoichiometry of the CNG channel of rod photoreceptors. *Neuron 36*(5), 881–889.

Whitaker, G. M., D. Angoli, H. Nazzari, R. Shigemoto, & E. A. Accili (2007). HCN2 and HCN4 isoforms self-assemble and co-assemble with equal preference to form functional pacemaker channels. *J. Biol. Chem. 282*(31), 22900–22909.

Wishart, D. S., C. G. Bigam, J. Yao, F. Abildgaard, H. J. Dyson, E. Oldfield, J. L. Markley, & B. D. Sykes (1995). ^{1}H, ^{13}C and ^{15}N chemical shift referencing in biomolecular NMR. *J. Biomol. NMR 6*, 135–140.

Wishart, D. S. & B. D. Sykes (1994). The 13C chemical-shift index: a simple method for the identification of protein secondary structure using 13C chemical-shift data. *J. Biomol. NMR 4*, 171–180.

Wittekind, M. & L. Mueller (1993). HNCACB, a high-sensitivity 3D NMR experiment to correlate amide-proton and nitrogen resonances with the α- and β-carbon resonances in proteins. *J. Magn. Reson. 101*, 201–205.

Yao, J., J. Chung, D. Eliezer, P. E. Wright, & H. J. Dyson (2001). NMR structural and dynamic characterization of the acid-unfolded state of apomyoglobin provides insights into the early events in protein folding. *Biochemistry 40*(12), 3561–3571.

Zagotta, W. N., N. B. Olivier, K. D. Black, E. C. Young, R. Olson, & E. Gouaux (2003). Structural basis for modulation and agonist specificity of HCN pacemaker channels. *Nature 425*(6954), 200–205.

Zheng, J. & W. N. Zagotta (2004). Stoichiometry and assembly of olfactory cyclic nucleotide-gated channels. *Neuron 42*(3), 411–421.

Zhou, L., N. B. Olivier, H. Yao, E. C. Young, & S. A. Siegelbaum (2004). A conserved tripeptide in CNG and HCN channels regulates ligand gating by controlling C-terminal oligomerization. *Neuron 44*(5), 823–834.

Zhou, L. & S. A. Siegelbaum (2007). Gating of HCN channels by cyclic nucleotides: residue contacts that underlie ligand binding, selectivity, and efficacy. *Structure 15*(6), 655–670.

Zhu, G., Y. Xia, L. K. Nicholson, & K. H. Sze (2000). Protein dynamics measurements by TROSY-based NMR experiments. *J. Magn. Reson. 143*(2), 423–426.

Zong, X., H. Zucker, F. Hofmann, & M. Biel (1998). Three amino acids in the C-linker are major determinants of gating in cyclic nucleotide-gated channels. *EMBO J. 17*(2), 353–362.

Zuiderweg, E. R. P. & S. W. Fesik (1989). Heteronuclear three-dimensional NMR-spectroscopy of the inflammatory protein C5a. *Biochemistry 28*(6), 2387–2391.

Danksagung

Ich habe vielen Personen für ihre Beiträge zum Gelingen dieser Doktorarbeit zu danken:

Prof. Dr. Dieter Willbold danke ich für die herzliche Aufnahme in seiner Arbeitsgruppe und für die Vergabe des überaus interessanten und aktuellen Forschungsthemas. Besonders bedanken möchte ich mich für seine gewissenhafte wissenschaftliche Betreuung, seine stets motivierende Art und seine erfrischend optimistische und inspirierende Haltung bei allen wissenschaftlichen Fragestellungen. Insbesondere danke ich ihm für die Bereitstellung der exzellenten interdisziplinären Forschungsbedingungen im Forschungszentrum Jülich, die mir während meiner Arbeit unerlässlich waren. Darüber hinaus möchte ich seine fachliche und finanzielle Unterstützung besonders hervorheben, die mir die Möglichkeit gaben, die wissenschaftlichen Ergebnisse auch international auf wissenschaftlichen Konferenzen und Fortbildungen zu präsentieren.

Herrn Prof. Dr. Benjamin Kaupp habe ich für seinen wissenschaftlichen Weitblick, seine inspirierende, motivierende und diskussionsfreudige Hilfe, sowie seine hervorragende wissenschaftliche Unterstützung zu danken. Mit seiner Hilfe ist das Projekt in Zusammenarbeit mit dem Forschungszentrum caesar entstanden.

Mein Dank gilt auch der Graduiertenschule "BioStruct" (gefördert durch das Ministerium für Innovation, Wissenschaft, Forschung und Technologie des Landes NRW, die Heinrich-Heine-Universität Düsseldorf und der Gründerstiftung zur Förderung von Forschung und wissenschaftlichen Nachwuchs an der Heinrich-Heine Universität), die mir ein Stipendium und zusätzliche Sachmittel für meine Forschungen gewährten. Darüber hinaus war die interdisziplinäre Zusammenarbeit aller Fachbereiche der Strukturbiologie und das exzellente Angebot an Fortbildungsmaßnahmen eine sehr große Bereicherung für mich. An dieser Stelle möchte ich mich besonders bei Leonie Oberbarnscheidt, Mariana Grieben, Simon Sindbert und allen anderen Stipendiaten für den gemeinsamen Wissensaustausch und die privaten Diskussionsrunden bedanken. Dr. Cordula Kruse und Dr. Christian Dumpitak danke ich für die unkomplizierte Koordination und das stets "offene Ohr" für alle Belange innerhalb "BioStruct".

Mein besonderer Dank gilt Dr. Matthias Stoldt für seine gewissenhafte und wissenschaftliche Betreuung während der gesamten Promotionszeit. Seine Hilfsbereitschaft und seine Bereicherung an fachlichen Ratschlägen und Ideen waren mir eine große Hilfe. Ferner möchte ich mich bei ihm für seine stets exzellente Unterstützung und Begeisterung zu allen Fragen rund um die NMR-Spektroskopie bedanken. Sein Engagement hat meinerseits maßgeblich zu dem großen Interesse an der faszinierenden und vielseitigen Methode der NMR-Spektroskopie beigetragen. Sein "offenes Ohr" für alle Belange sowie die gemeinsamen Unternehmungen sind eine große, abwechselungsreiche Hilfe und Bereicherung gewesen.

Danken möchte ich auch Dr. Rudolf Hartmann, der mit seinem fachlichen Rat und seiner ruhigen, besonnenen Hilfe für zusätzliche Unterstützung rund um die NMR-Spektroskopie gesorgt hat.

Bei Justin Lecher möchte ich mich für sein außerordentliches Engagement und sein großes Interesse an dem Projekt während seines Fortgeschrittenenpraktikums bedanken. Seine Betreuung mitsamt den motivierenden und fachlichen Diskussionen hat mich begeistert.

Meinen Bürokollegen Dr. Dirk Bartnik, Dr. Julian Glück und Dr. Marc Wittlich möchte ich für die äußerst angenehmen Jahre mit ihnen, für ihre Unterstützung und für die bereichernden

fachlichen, politischen und moralischen Diskussionsrunden danken. Nicht zu vergessen sind in diesem Zusammenhang die gemeinsamen Unternehmungen am “Drehspinsimulator”.

Nicht vergessen und herzlich danken möchte ich Dr. Sophie Feuerstein und Dr. Melanie Schwarten für ihre Hilfsbereitschaft und Ratschläge sowie für die gemeinsamen Unternehmungen mitsamt abwechselungsreichen Diskussionsrunden.

Bei Dr. Rutger Leliveld möchte ich mich für stetige fachliche Hilfsbereitschaft und für viele kleine Ratschläge im Labor und bei Dr. Gunnar Schröder für seine Hilfsbereitschaft rund um die Proteinstrukturrechnung bedanken. Bei Prof. Dr. Henrike Heise bedanke ich mich für ihren Einsatz und ihre außergewöhnliche Hilfsbereitschaft zu jeglichen Fragen über “die Welt” der NMR-Spektroskopie. Dr. Joachim Granzin danke ich für seine fachliche Meinung rund um die Röntgenkristallstrukturanalyse. Bei Dr. Thomas Stangler bedanke ich mich für seine Hilfsbereitschaft mir das Betriebssystem-Linux näher zu bringen und für seine interessanten Diskussionsbeiträge und Denkansätze zu unserem Wissenschaftsbereich innerhalb der gesamten Arbeitsgruppe.

Esther Jonas möchte ich mich für ihre hilfsbereite Art sowie die reibungslose Koordination der Abläufe im Labor danken. Allen anderen Kollegen aus der Arbeitsgruppe danke ich für das außergewöhnlich angenehme Arbeitsklima, sowie die in der Freizeit gemeinsam verbrachten Grillabende und Bowlingausflüge.

Unendlich dankbar bin ich meiner Familie, meinen Freunden und Bekannten, die mir jeweils durch ihre individuelle Art die Motivation, Kraft und Harmonie für die Fertigstellung dieser Arbeit gegeben haben.

Ganz besonders danke ich an dieser Stelle meinen lieben Eltern, sowie meiner Schwester Simone für die Unterstützung in jeglicher Hinsicht. Ihre Geduld und die ruhige Ausstrahlung waren mir eine große Hilfe.

Meinem Cousin Marco Selhorst, Danni, Max und Leo möchte ich für die zahlreichen gemeinsamen Grillabende und Unternehmungen danken, die mir die zwischenzeitlich notwendige Abwechselung boten.

Meiner Freundin Lorena Mañoso-Muzac danke ich mit Liebe für ihr Verständnis, ihre Geduld und so vieles mehr. Ihr Humor und ihr sonniges Gemüt haben mich stets aufs Neue motiviert.

Die hier vorgelegte Dissertation habe ich eigenständig und ohne unerlaubte Hilfe angefertigt. Die Dissertation wurde in der vorgelegten oder in ähnlicher Form noch bei keiner anderen Institution eingereicht. Ich habe bisher keine erfolglosen Promotionsversuche unternommen.

Düsseldorf, den 04.06.2010